Climatic Stress in the Acadian Forest:

History, Triggers and Evolution of Radial Growth Forecasting

Benjamin E. Phillips and Colin P. Laroque

MAD Lab Report 2010-14

Mount Allison Dendrochronology Laboratory
Department of Geography and Environment
Mount Allison University

Table of Contents

Table of Contents ii
List of Tables v
List of Figures ix
Abstract xiii
Acknowledgements xv

1. Establishing the Framework 1
1.1. Introduction 1
1.2. Objectives 3
2. Climatically Forced Suppression and Dieback 5
2.1. Climatic Dieback Defined 5
2.2. Dieback Research 6
2.3. Experimental Research 7
2.4. Potential Connections to Ocean Conditions 8
3. Study Area 9
3.1. Study Sites 9
3.2. Climate 10
3.3. Biota 12
3.4. Individual Site Ecodistrict Descriptions 13
4. Data Composition and Analysis Procedures 25
4.1. Instrumental Climate Data 25
4.2. Coupled Global Climate Model Data 26
4.3. Climate Change Scenarios 27
4.4. Coupled Global Climate Model Calibration 28
4.5. Climate Variables 29
4.6. Global Coupled Ocean-atmosphere Interactions 32
4.7. Tree-ring Data 33

4.8. Tree-ring Chronology Analysis 34
4.10. Radial Growth-climate Analysis 35
5. Results and Discussion 37
5.1. Tree-ring Chronologies 37
5.2. Tree-ring Chronology Observations 47
5.3. Relationships to Ocean-atmosphere Interactions 50
5.4. Modulation of Radial Tree Growth through GCOAIs 58
5.5. Regional Climatic Links to GCOAIs 60
5.6. Radial Growth Future Forecasts 61
5.7. Sugar Maple Model Interpretation for SRES B1 Scenario 67
5.8. Sugar Maple Model Interpretation for SRES A1b Scenario 69
5.9. Yellow Birch Model Interpretation for SRES B1 Scenario 71
5.10. Yellow Birch Model Interpretation for SRES A1b Scenario 73
5.11. Eastern Hemlock Model Interpretation for SRES B1 Scenario 75
5.12. Eastern Hemlock Model Interpretation for SRES A1b Scenario 77
5.13. Red Spruce Model Interpretation for SRES B1 Scenario 79
5.14. Red Spruce Model Interpretation for SRES A1b Scenario 81
5.15. Eastern White Cedar Model Interpretation for SRES B1 Scenario 83
5.16. Eastern White Cedar Model Interpretation for SRES A1b Scenario 85
5.17. White Pine Model Interpretation for SRES B1 Scenario 87
5.18. White Pine Model Interpretation for SRES A1b Scenario 89
5.19. Model Credibility 90
5.19.1. *Application of Linear Models in Oscillating Climate Conditions* 91
5.19.2. *Critical Exclusions in the Future Climate Data* 92
5.19.3. *Prospective Future Biological Thresholds* 94
5.19.4. *Non-Climatic Disturbance* 95
5.19.5. *Application of Linear Models in Oscillating Climate Conditions* 91
5.20. AMO Direction and Trends 96
5.21. NAO Direction and Trends 97
6. Conclusion 98
References 100

List of Tables

Table 3.1. Tree-ring sample sites including the species, site elevation (m), geographic position (latitude and longitude in degrees and minutes), distance from the nearest climate station (km), and the elevation difference (m), abbreviated as Elv., between the site and climate station for each of the 36 sample sites.

Table 4.1. Environment Canada climate station information for the main station used for each sample site. Climate station identification including, the station ID number, the common interval of data covered by all data types, the approximate geographic position (latitude and longitude in degrees and minutes), and the elevation above sea level is provided for each climate site.

Table 4.2. Climate variables created for this study cover various months of the year and also include one previous year. Climate variable type, period length and annual occurrence are outlined. Months of the two-year time period covered are represented by only a first letter. Time periods included by each variable are marked in grey, the shortest of which only cover monthly intervals while other variables cover seasonal periods (black vertical lines separate monthly periods while seasonal periods are solid grey with no breaks between months). Variable names are Tmean = average monthly temperature, TRF Deep = thaw/refreeze deep, TRF S = thaw/refreeze surficial, RtFr = root freeze, Tprecp = total monthly precipitation, SD = snow depth, with expanded definitions below.

Table 5.1. Statistics in this Table are calculated between individual tree ring indices produced for each sample site. Sample sites are indicated with the initials of the sites provided in the individual site description section. Each site is represented by a minimum of 24 individual tree cores taken from a minimum of 11 trees but, most sites are represented by 40 tree cores taken from 20 trees. Intra-site/intra-species correlations using Pearson's r-values illustrate the strength of relationships between sampled trees from individual sites. Also presented are average mean sensitivity (AMS) values calculated using all trees at each site. Values for AMS are considered low from 0.1 - 0.19, intermediate from 0.2 - 0.29 and high from $\geq$0.3 (Grissino-Mayer 2001). All two tailed r values significant at ($p<0.0001$).

Table 5.2. The comparative relationships between all ring-width chronologies are illustrated in this intra-species/inter-site correlation matrix with Pearson's r-values for the common period 1850-2006. Pearson's r-values are calculated between standardized tree-ring curves for each site. Cells in this Table are shaded depending on the strength of the r-value indicated; darker shading represents higher r-values while lighter shading indicates lower r-values. Two tailed r-value significance levels indicated by ***** = ($p<0.05$), ****** = ($p<0.01$).

Table 5.3. Pearson's r-values averaged for six **sugar maple** chronologies over 50-year moving intervals lagged by 25-years are presented. This Table was derived from individual inter-site correlation matrices calculated for each 50-year period. All five correlation values are composed of an average r-value computed between all sites in each individual matrix. Two tailed significance levels indicated by ***** = ($p<0.05$), ****** = ($p<0.01$).

Table 5.4. Pearson's r-values averaged for six **yellow birch** chronologies over 50-year moving intervals lagged by 25-years are presented. This Table was derived from individual inter-site correlation matrices calculated for each 50-year period. All five correlation values are composed of an average r-value computed between all sites in each individual matrix. Two tailed significance levels indicated by * = ($p<0.05$), ** = ($p<0.01$).

Table 5.5. Pearson's r-values averaged for six **eastern hemlock** chronologies over 50-year moving intervals lagged by 25-years are presented. This Table was derived from individual inter-site correlation matrices calculated for each 50-year period. All five correlation values are composed of an average r-value computed between all sites in each individual matrix. Two tailed significance levels indicated by * = ($p<0.05$), ** = ($p<0.01$).

Table 5.6. Pearson's r-values averaged for six **red spruce** chronologies over 50-year moving intervals lagged by 25-years are presented. This Table was derived from individual inter-site correlation matrices calculated for each 50-year period. All five correlation values are composed of an average r-value computed between all sites in each individual matrix. Two tailed significance levels indicated by * = ($p<0.05$), ** = ($p<0.01$).

Table 5.7. Pearson's r-values averaged for six **eastern white cedar** chronologies over 50-year moving intervals lagged by 25-years are presented. This Table was derived from individual inter-site correlation matrices calculated for each 50-year period. All five correlation values are composed of an average r-value computed between all sites in each individual matrix. Two tailed significance levels indicated by * = ($p<0.05$), ** = ($p<0.01$).

Table 5.8. Pearson's r-values averaged for six **white pine** chronologies over 50-year moving intervals lagged by 25-years are presented. This Table was derived from individual inter-site correlation matrices calculated for each 50-year period. All five correlation values are composed of an average r-value computed between all sites in each individual matrix. Two tailed significance levels indicated by * = ($p<0.05$), ** = ($p<0.01$).

Table 5.9. The comparative relationships between all ring-width chronologies are illustrated in this inter-species/intra-site correlation matrix with Pearson's r-values for the common period 1850-2006. Pearson's r-values are calculated between standardized tree-ring curves for each site. Cells in this Table are shaded depending on the strength of the r-value indicated; darker shading represents higher r-values while lighter shading indicates lower r-values. Two tailed significance levels indicated by * = ($p<0.05$), ** = ($p<0.01$).

Table 5.10. Pearson's correlation values are illustrated here between site chronologies and the Atlantic Mulitdecadal Oscillation (AMO) at a three year lag. Ten year moving average values follow immediately after the annual resolution data for each site (M-avg). Site names are abbreviated by the retention of the first three consonants in the name. At the bottom of the table the correlation values between regional master curves for each species and the AMO are also presented. Correlation value cells are filled with black for highest postive correlation, 50% grey for zero

correlation, and white for lowest negative correlation. Quantitative text is black for negative and white for positive correlation values. Two tailed significance levels indicated by *=($p<0.01$).

Table 5.11. Pearson's correlation values are illustrated here between site chronologies and the North Atlantic Oscillation (NAO). Ten year moving average values follow immediately after the annual resolution data for each site (M-avg). Site names are abbreviated by the retention of the first three consonants in the name. At the bottom of the table the correlation values between regional master curves for each species and the NAO are also presented. Correlation value cells are filled with black for highest postive correlation, 50% grey for zero correlation, and white for lowest negative correlation. Quantitative text is black for negative and white for positive correlation values. Two tailed significance levels indicated by *=($p<0.01$).

Table 5.12. The least squares stepwise multiple regression model summary information for the AICc selected optimum variable subset is listed here. Model information including the following: site (names abbreviated using first three consonants), tree species (Sp), time period (positive AMO includes only positive multidecadal oscillation periods and negative AMO includes only negative multidecadal oscillation periods), degrees of freedom (DF), elevation lapse rate (ELR) which indicates the elevation level the data was adjusted for, climate station (CS) elevation, number of variables (# Vr) included in the AICc selected model, coefficient of determination (R^2), adjusted coefficient of determination (Adj R^2) which adjusts the R^2 value for the number of explanatory terms in the model and higher values are indicated by a darker cell fill, P-value that indicates the significance of the model through an ANOVA, Durbin-Watson (D-W) statistic which indicates a model has negative autocorrelation of the residuals if >2, positive serial correlation if <2 and serious positive serial correlation problems if <1, variance inflation factor (VIF) which quantifies the level of multicollinearity of a given regression coefficient (a conservative cutoff is considered any value >5 to be correlated with other independent variables in the model, thus increasing substantially the standard error.), finally the last column counts the number of winter variables (WV) included in the model. Winter variables include Root Freeze A or B, TJanA, TFebA, TMarA, TJanB, TFebB, TMarB, SD Index 1 or 2. Only models with a p-value of <0.001 and a durbin-watson value above 1.0 are run on future data and those models are indicated with black text in this table.

Table 5.13. The least squares stepwise multiple regression model summary information for the model run including thaw refreeze independent variables is listed here. The optimum variable subset is again selected by AICc. The table includes all model information listed in Table 5.12, as well as the following additional values: thaw refreeze (TRF) variables included in the AICc selected model are illustrated (TRFD=thaw refreeze deep, TRFS=thaw refreeze surfacial, for both current [A] and prior [B] years). Winter variables include Root Freeze A or B, TJanA, TFebA, TMarA, TJanB, TFebB, TMarB, SD Index 1 or 2, TRF D and TRF S. Only models which experienced a change from those in Table 5.12 are illustrated.

Table 5.14. Independent variables included in each AICc selected multiple regression model are shown here. The 38 independent variables included in the multiple regression analysis are listed in the end columns, with winter variables in white text with grey highlighting. Sites are titled across the

top row and species is specified in row three. Charlo (Ch) model runs from 1940-2005, Edmundston (Ed) models run from 1936-2005, Aroostook (Ar) models run from 1932-2004, Miramichi (Mi), Fredericton (Fr), and Moncton (Mo) models run over the positive AMO periods (indicated by a +), and the negative AMO periods (indicated by a -), which vary between cities due to the length of climate data available. Inclusion of a variable in a model is marked by + or – in a particular cell which signifies the direction of the relationship.

List of Figures

Figure 3.1. Study site map with the approximate geographical positions of the 36 tree-ring sample sites and six climate stations from New Brunswick used in this study. Base map © 2001. Her Majesty the Queen in Right of Canada, Natural Resources Canada.

Figure 4.1. The CGCM3 produces a set of forecast data that is homogenous across a 2.81° X 2.81° grid square, and does so for a global grid. Relevant CGCM3 output grid squares covering the Maritime Provinces are illustrated. Latitudinal and longitudinal boundaries for each grid square are also given. Base map © 2002. Her Majesty the Queen in Right of Canada, Natural Resources Canada.

Figure 5.1. All six **sugar maple** chronologies representing the six sample sites are depicted over the truncated common interval from 1850-2006. All chronologies are standardized using the program ARSTAN and indexed curves are presented. Each curve fluctuates around an average of one represented by the horizontal strike-through lines. Sample depth at each site has a minimum of 30 cores extending back in time 100 years and at least 10 cores extending back 150 years. Site names are presented adjacent to the radial growth curves and order of sites is from north to south with occasional shuffling of sites to preserve nearest neighbour associations.

Figure 5.2. All six **yellow birch** chronologies representing the six sample sites are depicted over the truncated common interval from 1850-2006. All chronologies are standardized using the program ARSTAN and indexed curves are presented. Each curve fluctuates around an average of one represented by the horizontal strike-through lines. Sample depth at each site has a minimum of 10 cores extending back in time 100 years and most have no cores extending back 150 years. Site names are presented adjacent to the radial growth curves and order of sites is from north to south with occasional shuffling of sites to preserve nearest neighbour associations.

Figure 5.3. All six **eastern hemlock** chronologies representing the six sample sites are depicted over the truncated common interval from 1850-2006. All chronologies are standardized using the program ARSTAN and indexed curves are presented. Each curve fluctuates around an average of one represented by the horizontal strike-through lines. Sample depth at each site has a minimum of 11 cores extending back in time 100 years and some have no cores extending back 150 years. Site names are presented adjacent to the radial growth curves and order of sites is from north to south with occasional shuffling of sites to preserve nearest neighbour associations.

Figure 5.4. All six **red spruce** chronologies representing the six sample sites are depicted over the truncated common interval from 1850-2006. All chronologies are standardized using the program ARSTAN and indexed curves are presented. Each curve fluctuates around an average of one represented by the horizontal strike-through lines. Sample depth at each site has a minimum of nine cores extending back in time 100 years and most have no cores extending back 150 years. Site names are presented adjacent to the radial growth curves and order of sites is from north to south with occasional shuffling of sites to preserve nearest neighbour associations.

Figure 5.5. All six **eastern white cedar** chronologies representing the six sample sites are depicted over the truncated common interval from 1850-2006. All chronologies are standardized using the program ARSTAN and indexed curves are presented. Each curve fluctuates around an average of one represented by the horizontal strike-through lines. Sample depth at each site has a minimum of 18 cores extending back in time 100 years and most with no cores extending back 150 years. Site names are presented adjacent to the radial growth curves and order of sites is from north to south with occasional shuffling of sites to preserve nearest neighbour associations.

Figure 5.6. All six **white pine** chronologies representing the six sample sites are depicted over the truncated common interval from 1850-2006. All chronologies are standardized using the program ARSTAN and indexed curves are presented. Each curve fluctuates around an average of one represented by the horizontal strike-through lines. Sample depth at each site has a minimum of 14 cores extending back in time 100 years and most with no cores extending back 150 years. Site names are presented adjacent to the radial growth curves and order of sites is from north to south with occasional shuffling of sites to preserve nearest neighbour associations.

Figure 5.7. The standardized index of the regional master **sugar maple** tree-ring chronology plotted against the AMO at a three year lag. The curves of both the annual variability and smoothed decadal variability (10 year moving average) data are plotted for visual comparison.

Figure 5.8. The standardized index of the regional master **sugar maple** tree-ring chronology plotted against the NAO at a three year lag. The curves of both the annual variability and smoothed decadal variability (10 year moving average) are plotted for visual comparison.

Figure 5.9. The standardized index of the regional master **eastern hemlock** tree-ring chronology plotted against the AMO at a three year lag. The curves of both the annual variability and smoothed decadal variability (10 year moving average) data are plotted for visual comparison.

Figure 5.10. The standardized index of the regional master **eastern hemlock** tree-ring chronology plotted against the NAO at a three year lag. The curves of both the annual variability and smoothed decadal variability (10 year moving average) are plotted for visual comparison.

Figure 5.11. The standardized index of the regional master **red spruce** tree-ring chronology plotted against the AMO at a three year lag. The curves of both the annual variability and smoothed decadal variability (10 year moving average) data are plotted for visual comparison.

Figure 5.12. The standardized index of the regional master **red spruce** tree-ring chronology plotted against the NAO at a three year lag. The curves of both the annual variability and smoothed decadal variability (10 year moving average) are plotted for visual comparison.

Figure 5.13. The standardized index of the regional master **eastern white cedar** tree-ring chronology plotted against the AMO at a three year lag. The curves of both the annual variability and smoothed decadal variability (10 year moving average) data are plotted for visual comparison.

Figure 5.14. The standardized index of the regional master **eastern white cedar** tree-ring chronology plotted against the NAO at a three year lag. The curves of both the annual variability and smoothed decadal variability (10 year moving average) are plotted for visual comparison.

Figure 5.15. The standardized index of the regional master **yellow birch** tree-ring chronology plotted against the AMO at a three year lag. The curves of both the annual variability and smoothed decadal variability (10 year moving average) data are plotted for visual comparison.

Figure 5.16. Significant **sugar maple B1** scenario forecasts are illustrated here. Black lines are actual standardized annual ring-widths, solid white lines are model calibration periods, dotted white lines are modeled future annual ring-widths. Y-axis is standardized ring-width index, while x-axis is the year.

Figure 5.17. Significant **sugar maple A1b** scenario forecasts are illustrated here. Black lines are actual standardized annual ring-widths, solid white lines are model calibration period fits, dotted white lines are modeled future annual ring-widths. Y-axis is standardized ring-width index, while x-axis is the year.

Figure 5.18. Significant **yellow birch B1** scenario forecasts are illustrated here. Black lines are actual standardized annual ring-widths, solid white lines are model calibration period fits, dotted white lines are modeled future annual ring-widths. Y-axis is standardized ring-width index, while x-axis is the year.

Figure 5.19. Significant **yellow birch A1b** scenario forecasts are illustrated here. Black lines are actual standardized annual ring-widths, solid white lines are model calibration period fits, dotted white lines are modeled future annual ring-widths. Y-axis is standardized ring-width index, while x-axis is the year.

Figure 5.20. Significant **eastern hemlock B1** scenario forecasts are illustrated here. Black lines are actual standardized annual ring-widths, solid white lines are model calibration period fits, dotted white lines are modeled future annual ring-widths. Y-axis is standardized ring-width index, while x-axis is the year.

Figure 5.21. Significant **eastern hemlock A1b** scenario forecasts are illustrated here. Black lines are actual standardized annual ring-widths, solid white lines are model calibration period fits, dotted white lines are modeled future annual ring-widths. Y-axis is standardized ring-width index, while x-axis is the year.

Figure 5.22. Significant **red spruce B1** scenario forecasts are illustrated here. Black lines are actual standardized annual ring-widths, solid white lines are model calibration period fits, dotted white lines are modeled future annual ring-widths. Y-axis is standardized ring-width index, while x-axis is the year.

Figure 5.23. Significant **red spruce A1b** scenario forecasts are illustrated here. Black lines are actual standardized annual ring-widths, solid white lines are model calibration period fits, dotted white lines

are modeled future annual ring-widths. Y-axis is standardized ring-width index, while x-axis is the year.

Figure 5.24. Significant **eastern white cedar B1** scenario forecasts are illustrated here. Black lines are actual standardized annual ring-widths, solid white lines are model calibration period fits, dotted white lines are modeled future annual ring-widths. Y-axis is standardized ring-width index, while x-axis is the year.

Figure 5.25. Significant **eastern white cedar A1b** scenario forecasts are illustrated here. Black lines are actual standardized annual ring-widths, solid white lines are model calibration period fits, dotted white lines are modeled future annual ring-widths. Y-axis is standardized ring-width index, while x-axis is the year.

Figure 5.26. Significant **white pine B1** scenario forecasts are illustrated here. Black lines are actual standardized annual ring-widths, solid white lines are model calibration period fits, dotted white lines are modeled future annual ring-widths. Y-axis is standardized ring-width index, while x-axis is the year.

Figure 5.27. Significant **white pine A1b** scenario forecasts are illustrated here. Black lines are actual standardized annual ring-widths, solid white lines are model calibration period fits, dotted white lines are modeled future annual ring-widths. Y-axis is standardized ring-width index, while x-axis is the year.

Abstract

The radial growth of New Brunswick tree species have been affected by both short and long-term suppression periods in the past (Phillips and Laroque 2007, 2008, 2009a, 2009b). This study examines the tree-rings of six tree species [sugar maple (*Acer saccharum* Marsh), yellow birch (*Betula alleghaniensis* Britt.), eastern hemlock (*Tusga canadensis* (L.) Carriere), red spruce (*Picea rubens* Sarg.), eastern white cedar (*Thuja occidentalis* L.) and white pine (*Pinus strobus* L.)], sampled near six New Brunswick climate stations through a dendroclimatological analysis. The objectives of the analysis are to: a) evaluate past radial growth relationships among species and sample sites, b) investigate long-term radial growth relationships with Global Coupled Ocean-atmosphere Interactions, and c) use multiple linear regression methods in a model building exercise to forecast future potential radial growth based on historic climate data and future Coupled Global Climate Model data covering the period 2010-2100.

By sampling and constructing tree-ring chronologies near long-term climate stations in New Brunswick, more accurate analysis between climate and tree growth is possible. Following the approach of the 2009 dendroclimatological study of sugar maple, this investigation was to use similar methodology to uncover related and unrelated radial growth trends among important tree species, across geographic variations and climatic gradients (Phillips and Laroque 2009b). Sugar maple displayed long-term relationships to North Atlantic Ocean conditions and generally negative future radial growth forecasts were the result that 2009 study. Based on those results, it became important to consider other species' relationships to ocean influence and determine if forecasting their radial growth over the rest of the century could be confidently completed.

The results of 56 radial growth models illustrate inconsistency and relatively low explained variance values. This suggests non-linear relationships exist between radial tree growth and climate.

Pertinent to the inconsistency of the models were the radial growth relationships to North Atlantic Ocean conditions. The shade tolerant tree species, sugar maple, eastern hemlock, red spruce and eastern white cedar, displayed long-term positive correlation with the Atlantic Multidecadal Oscillation and negative correlation with the North Atlantic Oscillation. A moderately shade tolerant species, yellow birch, exhibited long-term negative correlation with the Atlantic Multidecadal Oscillation, while white pine illustrated no correlations with ocean conditions.

It is therefore reasonable to suggest that the internal climate variability produced in the oceans has a broad impact on New Brunswick forests. Periods of cool North Atlantic sea surface temperatures have, in the past, slowed the radial growth rates of shade tolerant tree species and will likely again. Furthermore, periods of positive phase sea surface pressure in the North Atlantic have also occurred along side radial growth suppression periods. These types of internal climate variability are currently very difficult to predict, however probability suggests the Atlantic Multidecadal Oscillation will return to a cool negative phase somewhere around 2020 or shortly thereafter. The effects of which could manifest themselves in reduced radial growth and potential stress in the shade tolerant forest community.

Acknowledgements

It is admirable that the Fundy Model Forest has placed importance on the future of New Brunswick forests. Their vision and awareness will result in a better future for our forest communities. They deserve recognition for their ongoing financial support of this research. Also the financial support of the Natural Sciences and Engineering Research Council (NSERC) funding to Dr. Colin Laroque has, in part, made this research possible.

Members of the MAD lab deserve acknowledgment for their help in the field. Thanks to Sarah Quann, Chris Kennedy, and especially Amanda Young. For their help in the field and the donation of their time, I would also like to thank Chris Phillips, Dan Phillips and Greg Jonah.

Chapter 1

1.0 Establishing the Framework

1.1 Introduction

Compositional shifts to maintain climatic associations are expected in forests around the world as they respond to unprecedented climatic conditions (IUFRO 2009). Tree species migration is often modeled when the long-term effects of climate change are contemplated (McKenney et al. 2007, Iverson et al. 2008), while the response of currently rooted trees to various forms of unusual disturbances and the new climate regimes is less quantifiable (IUFRO 2009). Even though external, anthropogenically forced climate change is likely to eventually produce new climate envelops over many areas; internal, unforced climate variation will temporarily swing climatic influence to greater extremes (Murphy et al. 2009). The vulnerability of stressed forest ecosystems to anomalous climate regimes remains highly uncertain, and that uncertainty extends to the tree species of New Brunswick's Acadian Forest (Vasseur and Catto 2008).

Sugar maple (*Acer saccharum* Marsh) is of particular concern in the Acadian Forest Region and its climatic associations were examined in 2009 by Phillips and Laroque. It has experienced periods of growth stress throughout its range, mainly in the latter half of the 20th century, which have been associated with freezing and drought related causes (Bauce and Allen 1991, Robitaille et al. 1995, Auclair et al. 1996, Payette et al. 1996, Auclair 2005). Other events such as nutrient limitation, insect outbreaks and pollution have also been implicated as sugar maple stressors (Pitelka and Raynal 1989, Hartmann and Messier 2008, St. Clair et al. 2008). Some combination of climatic triggering events (Bauce and Allen 1991, Payette et al. 1996), further exacerbated by local site factors (St.Clair et al. 2008) seem to have been the cause of sugar maple crown dieback and radial growth reductions in the past. Moreover, Auclair has linked ocean-atmosphere interactions, northern

hemisphere temperatures and general climate change to the occurrence of climatic triggering events (Auclair et al. 1996, Auclair 2005). In 2009, for the central region of the Maritime sugar maple range, Phillips and Laroque established moderate to strong relationships between North Atlantic Ocean conditions and sugar maple radial growth suggesting periods of suppressed ring-width production and potential dieback are associated with negative phases of the Atlantic Multidecadal Oscillation (AMO) and positive phases of the North Atlantic Oscillation (NAO). If ocean conditions can exhibit similar, long-term, multidecadal patterns to that of sugar maple radial growth fluctuations, the question of whether or not the ring-width production of other important New Brunswick tree species can be linked to oscillating ocean conditions becomes crucial? Other tree species such as yellow birch (*Betula alleghaniensis* Britt.) have suffered from periods of dieback in New Brunswick in the past (Bourque et al. 2005) which suggests the answer to the question may be yes.

A mix of continental and maritime air masses influence the climate over the Acadian Forest Region resulting in less drought (Phillips 1990, Payette et al. 1996) but more thaw/refreeze events then in other portions of the northeastern temperate forest range due to the closer proximity of oceanic influences (Phillips 1990). This difference in climate from other areas of the northeastern North American hardwood biome may predispose trees in the Acadian Forest Region to more frequent freezing stressors. Analysis of the historic growth response of trees to these types of stressors throughout northeastern temperate forests has been performed routinely through tree-ring investigations in more continental regions (Bauce and Allen 1991, Lane et al. 1993, Yin and Arp 1994, Payette et al. 1996, Tardiff et al. 2001, Goldblum and Rigg 2005), but has only been attempted in a more maritime environment with sugar maple (Phillips and Laroque 2009b).

Dendroclimatological analysis is well suited to assess the past extent of tree stress and evaluate the potential future success of tree species. Long time periods can be examined for radial

growth suppression through this technique, while models of future radial growth rates can be produced. Typically, monthly resolution climate data is regressed onto annual tree-ring measurement indices to estimate the extent and timing of climatic influence on radial growth (Payette el al. 1996, Tardiff et al. 2001, Goldblum and Rigg 2005, Phillips and Laroque 2008,). However, the ability of monthly climatic data to capture daily or weekly extreme events has been questioned by both Graumlich (1993) and Payette et al. (1996). It is therefore the objective of this study, like the 2009 sugar maple analysis (Phillips and Laroque 2009b), to use a reconstruction of potential stress events from the instrumental daily climate record together with the more traditional monthly format data for model development. Although the 2009 attempt by Phillips and Laroque to model sugar maple ring-width production was only partially successful, this type of model building exercise applied to other important Acadian Forest tree species is important for evaluation of the methodology and the understanding of tree response to climate in New Brunswick.

1.2 Objectives

In the 2009 dendroclimatic analysis of sugar maple, modeled future radial growth was impeded by the shifting climatic influences of ocean conditions (Phillips and Laroque 2009b). Cross-site comparison of model results enabled the interpretation of general climatic influence even though weak ring-width production models were created. Despite the challenges of radial growth forecasting for various tree species under such a potentially complex series of influences, this study will investigate yellow birch, eastern hemlock (*Tusga canadensis* (L.) Carriere), red spruce (*Picea rubens* Sarg.), eastern white cedar (*Thuja occidentalis* L.) and white pine (*Pinus strobus* L.) using a similar methodology as Phillips and Laroque 2009. Six sample sites from New Brunswick are to be used in this investigation and sugar maple samples previously collected from these sites will be reexamined for direct comparison to the five new tree species studied. To be completed are; an

analysis of past radial growth relationships, an analysis of radial growth to ocean conditions of the newly sampled tree species, and an attempt to model future radial growth using multiple linear regression and Coupled Global Climate Model data.

Chapter 2

2.0 Climatically Forced Suppression and Dieback

2.1 Crown Dieback Defined

Crown dieback in trees is a type of branch-related mortality that first occurs at the terminal end of the branch and advances toward the bole. This phenomenon must appear in the upper crown of the tree to be considered dieback and have no obvious physical injury signs; in other words, inward to outward affliction (Auclair 2005). An obvious characteristic symptom of dieback is reduced radial growth due to the inability of the tree to fix enough carbon to form normal annual growth rings (Auclair 1993a).

Crown dieback was studied by many researchers throughout the 20th century. Early research centered on climatic causes then transitioned to atmospheric pollution theories of causation (Walker et al. 1990, Millers et al. 1989). More recently causation theories have moved forward to attribute thaw-freeze and drought as the major underlying problem (Bauce and Allen 1991, Auclair et al. 1993b, Auclair et al. 1996, Robitaille et al. 1995, Payette et al. 1996, Auclair 2005, Beier et al. 2008).

2.2 Dieback Research

In 2009 researchers from the west coast of North America released a report illustrating increasing mortality rates in forests from that area. They contributed evidence that this mortality occurring among young and old trees was connected to a changing climate in which water deficits are more frequent (van Mantgem et al. 2009). A year earlier in 2008, researchers in southeastern Alaska produced evidence supporting theories that warming winters were causing late winter severe thaw-freeze events manifesting in the decline and mortality of yellow cedar (*Chamaecyparis nootkatensis* (D. Don) Spach) (Beier et al. 2008). Most recently on the east coast, Auclair (2005) has shown a 22 year cycle of dieback affecting sugar maple, multiple ash species, multiple birch species, and red spruce . Another study from the same year assessed the spatial extent of past winter thaw-freeze events in relation to birch declines across eastern North America (Bourque et al. 2005). Previous to these more recent projects, Auclair completed extensive work in dieback associated with winter thaw-freeze in northern hardwoods of North America, western white pine (*Pinus monticola* D.Don) from the Pacific Northwest, and Norway spruce (*Picea abies* (L.) H. Karst) and silver fir (*Abies alba* Mill.) in Europe (Auclair et al. 1990, Auclair 1993, Auclair et al. 1996). This research along with many prior studies, consistently relate climatic events to externally expressed symptoms on various tree species covering many disjunct regions.

Payette et al. (1996) completed an extensive dendrochronological investigation on the probable causes of sugar maple crown dieback during the 1980s in Quebec. They concluded that winter thaw-freezes and summer droughts often coincided with periods of radial tree growth suppression. The conclusions of past field research was important evidence in the formulation of this study, and the results of experimental research were also essential.

2.3 Experimental Research

Over the past two decades, experimental work regarding thaw-freeze has been done with many researchers attempting to get at the root of the problem. Many studies on various tree species have illustrated that freezing and thawing of stem, branch, twig, and root portions of trees causes air bubbles to form in the xylem vessels of the wood (Sperry et al. 1988, Hacke and Sauter 1996, Zhu et al. 2002, Cox and Zhu 2003). These breaks in the fluid tension are more commonly referred to as xylem cavitations or xylem embolisms and can also be caused by water stress or drought conditions (Hacke and Sperry 2001). Different tree species have dissimilar xylem morphology, which triggers variance in response to climatic events amongst species (Hacke and Sperry 2001). The result of a high percentage of xylem cavitations is reduced water flow to the canopy and decreased canopy productivity, which can be extensive enough to cause the individual organism to suffer decreased vigor for several years or even cause death (Bergeron and Sedio 1999). Xylem cavitation is a regular part of seasonal change in many temperate tree species, but when severe winter temperature events happen, the root systems can be damaged in several potential poorly understood ways or depleted of the necessary energy to fully restore xylem conductivity (Robitaille et al. 1995, Hacke and Sauter 1996). These results can then be seen in crown dieback, potential mortality, and reduced radial growth or temporary growth suppression (Beier et al. 2008). Despite the research cited here, there is still a need to develop a more specific understanding of winter ecological processes. The lack of winter study regarding Acadian Forest tree species' climate response will continue to affect the comprehension of potential effects of weather events during that time of year, ultimately resulting in continuing predictive uncertainty (Campbell et al. 2005).

2.4 Potential Connections to Ocean Conditions

Trees growing on most continents have shown strong connections to multidecadal oscillating ocean conditions (Gray et al. 2008, Cook and D'Arrigo 2002). Auclair et al. (1996) found a strong relationship among global climate phenomena and episodes of dieback in the northern temperate forests of eastern North America. More specifically, links were made between the Southern Oscillation Index (SOI) and Northern Hemisphere temperatures. While the influence of the SOI on northeastern areas of the North American continent is relatively weak (Auclair et al. 1996), Northern Hemisphere temperatures are also known to be modified by conditions in the North Atlantic Ocean (Sutton and Hodson 2005). This suggests North Atlantic Ocean conditions such as the North Atlantic Oscillation and the Atlantic Multidecadal Oscillation may play a role in the climatic drivers associated with tree growth and dieback episodes as they were linked in the 2009 study by Phillips and Laroque with sugar maple. In this regard, a winter-spring connection that may link these phenomena to thaw-refreeze events could also be underlying parts of the dieback processes. Direct assessments of these potential oceanic influences have yet to address other Acadian Forest tree species and they may provide important insights into tree responses in the Maritime Provinces.

Chapter 3

3.0 Study Area

3.1 Study Sites

Six sampling sites were selected in New Brunswick for this study and were mainly chosen near Adjusted Historic Canadian Climate Data (AHCCD) centres. Five locations near AHCCD centres were selected while one other site was chosen that did not have an AHCCD centre nearby.

The study site area is bordered by Maine, U.S.A. at 67˚ 47' W on the western side and by the Gaspe Peninsula, Quebec to the north at approximately 48˚ N. To the east the Gulf of St. Lawrence, and more specifically Chaleur Bay and Northumberland Straight, create a marine boundary at approximately 64˚ 30' W. Finally to the south, New Brunswick is bordered by another marine body in the Bay of Fundy which crosses the 45˚ latitude on a 45˚ angle above which all sites are located (Fig. 3.1).

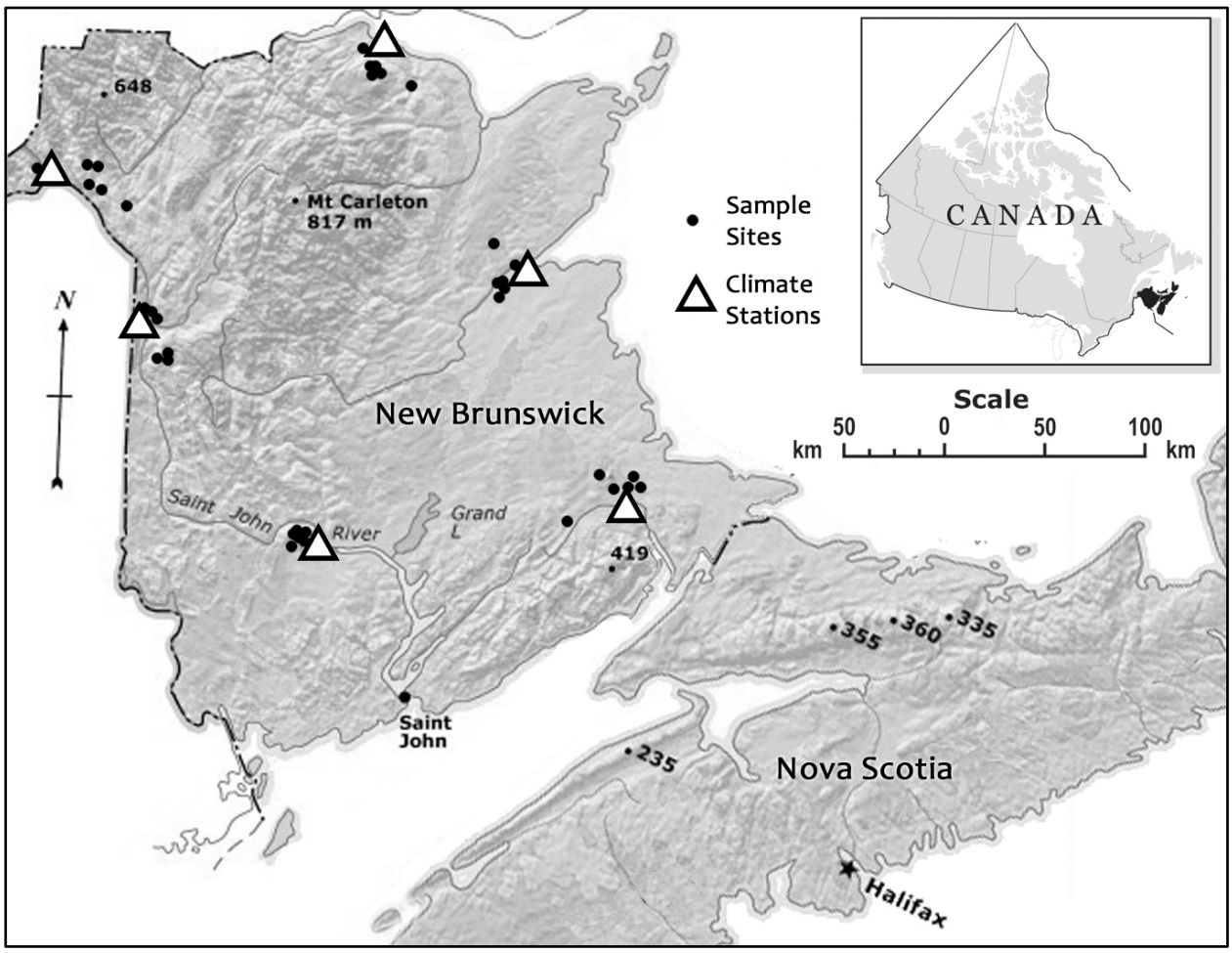

Figure 3.1. Study site map with the approximate geographical positions of the 36 tree-ring sample sites and six climate stations from New Brunswick used in this study. Base map © 2001. Her Majesty the Queen in Right of Canada, Natural Resources Canada.

3.2 Climate

In the study site region, predominant winds flow from the west bringing with them a strong continental influence which subdues much of the marine effect produced by the various water bodies (Phillips, 1990). Coastal regions are still dominated by the marine influence and incursions of marine air masses into central areas do occur. The Gulf of St. Lawrence waters consistently freezes near land in winter and the surface warms substantially in summer months to a high of 18˚C due to its shallow depths (Phillips, 1990). In the south, the Bay of Fundy produces the highest tides in the world and its constantly-overturning deep waters produce surface temperatures ranging from a low

of 0-4˚C in winter to 8-12˚C in summer, which results in foggy, cool air masses adjacent to the land (Phillips, 1990). Along New Brunswick's southern coast, fog normally occurs on a third of the days in July (Phillips, 1990). Finally the Atlantic Ocean carries the Gulf Stream off the southern coast of Nova Scotia, with mean 16˚C waters mediating the temperature extremes in the southwest (Phillips, 1990).

Elevation in the region rises from sea level to a pinnacle of 820 m above sea level (asl), although most sample sites are found between 20m and 400m asl (Table 3.1). A quantitative description of each site can be found in Table 3.1. Due to a predominate westerly flow of air masses, combined with substantial continental effects to the north and west, and the many marine influences to the east and south, a complex set of localized climate conditions are created. July mean temperatures range through 16.5˚C to 19.5˚C and January mean temperatures range from -12.2˚C to -6˚C (Phillips, 1990, Clayden, 2000). Growing degree days above 5˚C, range from slightly below 1300 to over 1800 across the region (Clayden, 2000). Precipitation normally ranges from 1000 mm to 1200 mm depending upon the marine proximity and elevation (Phillips, 1990). Snowfall amounts typically accumulate from 300 to 400 cm in northwest New Brunswick accounting for 33% of annual precipitation (Phillips, 1990). In southern areas of New Brunswick, less than 20% of precipitation falls as snow totaling from 200 to 300 cm (Phillips, 1990). These mean temperatures and precipitation types can be substantially influenced in the winter months by the variation in air masses, from cold arctic, to warm maritime (Phillips, 1990).

Table 3.1. Tree-ring sample sites including the species, site elevation (m), geographic position (latitude and longitude in degrees and minutes), distance from the nearest climate station (km), and the elevation difference (m), abbreviated as Elv., between the site and climate station for each of the 36 sample sites.

Site Name	Species	Geographic	Site	Distance	Elv.
Benjamin River	SM, YB, RS, EC	47°54' N, 66°15' W	267	11	227
Jacket River	WP	47°50'N, 66°03' W	103	27	99
Blackland	EH	47°57'N, 66°14' W	119	8.5	79
Hunter Brook	RS	47°24' N, 68° W	235	25	80
Quisibis Mountain	SM	47°26'N, 68°01' W	343	25	188
Davis Mill	WP	47°21'N, 68°07'W	246	17	91
Rivere Verte	EC	47°22'N, 68°10' W	230	12	75
Michaud Mountain	YB	47°22'N, 68°21' W	340	1.5	185
Harrison Ridge	EH	47°16'N, 67°52' W	265	37	110
Kintore Ridge	SM, YB, RS	46°42'N, 67°38' W	414	12	305
Aroostook River	EC, EH	46°49'N, 67°45' W	90	3	-1
Aroostook Bluff	WP	46°49'N, 67°43' W	130	2	39
Horseshoe Ridge	SM	47°14' N, 65°43' W	168	31	135
Stewart Brook	YB, EH, RS, EC	46°57' N, 65°39' W	10	16	-23
Beaubear Island	WP	46°59'N, 65°34' W	9	9	-24
Odell Park	SM, YB, EH, RS, EC,	45°57' N, 66°40' W	70	5	50
Indian Mountain	SM	46° 10' N, 64°55' W	157	19	85
Irishtown Reservoir	EH, RS, WP	46°09' N, 64° 44' W	52	7.5	-20
McLaughlin Reservoir	YB	46°09' N, 64° 50' W	62	7	-10
Intervale Pasturelands	EC	45°57' N, 65°14' W	42	45	-30

3.3 Biota

The Acadian Forest Region covers all of the Maritime Provinces except New Brunswick's central highlands. The Acadian Forest Region is distinguished as a mixed wood transition zone between the more northerly coniferous dominated forest and the more southerly deciduous dominated forests (Loo and Ives, 2003). Tree species such as yellow birch, sugar maple, American beech, eastern hemlock, white pine, and balsam fir (*Abies balsamea* (L.) Mill.) are typical of the

Acadian Forest Region. Red spruce is the most distinguishing feature of the Acadian Forest Region, occurring in most forest types (Mosseler et al., 2003). It should be noted that 300 to 400 years of land clearing and harvesting have substantially shifted forest composition and age distribution of the Acadian Forest Region to that of younger forests with less hardwood dominance (Loo and Ives, 2003, Mosseler et al., 2003). These anthropogenically manipulated forest characteristics affect this study by changing the abundance and age classes of targeted species, making it more difficult to find mature or old growth stands.

3.4 Individual Site Ecodistrict Descriptions

The following individual site descriptions detail the characteristics of the immediate area at each site and give a summary of the local ecodistrict based on the Ecological Land Classification for New Brunswick. A general explanation of the major climatic features of the greater ecoregion is presented, followed by a more specific description of the climate and biota found within the smaller ecodistrict subsection. Tree species sampled at each site are listed.

Benjamin River (BR) – Tjigog Ecodistrict

This site is located on an inland plateau near the Bay of Chaleur at 267 m elevation (Fig. 3.1). This mixed stand of unevenly aged forest contained co-dominant mature sugar maple, yellow birch, red spruce, eastern white cedar, and balsam fir. There were minor components of red maple and white birch (*Betula papyrifera* Marsh.) in the area with a patchy, yet dense, American beech understory. The site is fairly flat and exhibited sporadic wet spots. Sugar maple, yellow birch, red spruce and eastern white cedar were sampled here.

The Northern Uplands Ecoregion in which this ecodistrict is located is slightly cooler than other upland areas as most slopes face north (Zelazny et al. 2003). Although this region has a lower

elevation then the adjacent highlands, winter temperatures are known to be extreme in areas far enough away from the Bay of Chaleur (Zelazny et al. 2003). The local climate of the ecodistrict is moderated by the Bay of Chaleur and it lies in the rain shadow of the highlands to the west and the Gaspe Peninsula to the north. These influences cause this site to receive a low to medium amount of precipitation in the growing season relative to other sites and make fires more frequent here than most other parts of the study area (Zelazny et al. 2003). The moderation of temperatures by the Bay of Chaleur extend the growing season length within the ecodistrict, allowing species with more southern affinities to persist (Zelazny et al. 2003).

Jacket River (JR) - Tjigog Ecodistrict

This site occurs on a talus south facing slope overlooking the Jacket River. It is just outside the current boundary of the Jacket River protected area. The base of the slope begins at approximately 50m and climbs to an elevation of roughly 150m. The most conspicuous organisms at this site are the dominant white and red pines (*Pinus resinosa* Aiton). These pines are fire scared on the upslope or northern side but are otherwise healthy. Ages of the pines range from 80 to over 250 years old while many younger trees grow in the understory. A majority of Acadian Forest tree species exist in the understory including multiple species of maple (*Acer*), birch (*Betula*), aspen (*Populus*), and spruce (*Picea*) as well as beech (*Fagus grandifolia* Ehrh), eastern white cedar, balsam fir and possibly others. Many species of shrubs and other understory plants are also present including pine drops (*Pterospora andromedea* Nutt.). Where the talus is exposed to the atmosphere, thick beds of lichens proliferate. White Pine was the only species sampled here.

For a description of the local climate in the Tjigog Ecodistrict review the information provided in the preceding "Benjamin River (BR) – Tjigog Ecodistrict" section.

Blackland (BL) - Nicolas Denys Ecodistrict

This site is sandwiched between the Route 11 highway to the north and transmission lines to the south. The slightly sloping topography seemed well drained and sat at approximately 80 metres elevation. At this site an uneven aged stand of dominant eastern hemlock grows, sheltering sapling hemlocks below. Other species such as red maple (*Acer rubrum* L.), striped maple (*Acer pensylvanicum* L.), yellow birch, beech, fir, spruce and cedar grow mainly as understory trees. Many of the mature hemlock trees reach over 200 years old and some of these trees are over 300 years old. Eastern hemlock was the only species sampled here.

The presence of this site within the boundaries of the Nicolas Denys Ecodistrict means it is closer to the Bay of Chaleur and thus more related climatically to the conditions of the Charlo climate station than the Tjigog Ecodistrict or other ecodistricts in the Northern Uplands Ecoregion. Although its somewhat closer proximity to a large water body may further limit temperature extremes, it still shares a very similar climate of comparably dry and cool conditions. Eastern Hemlock is very rare in this region of the province, so it is likely its northern presence here is facilitated by the moderating influences of the bay.

Quisibis Mountian (QM) – Madawaska Ecodistrict

This site is located in a hilly upland area at 343 m elevation near the base of the highest peak in the area, Quisibis Mountain. The site has the remnants of an old sugar shack and is dominated by uneven-aged sugar maple with minor components of mature yellow birch and American beech. The canopy was very tight and the slightly sloping site was well drained and facing southeast. Sugar maple was the only species sampled here.

Unlike the Northern Uplands Ecoregion, the Central Uplands Ecoregion, in which this site is located, slopes face predominantly south and west. The aspect of the slopes combined with the daytime cool air drainage into the numerous valley landforms results in warmer upland forests. This

area is on the windward side of the highlands region where the effects of orthographic lifting bring higher precipitation and less frequent forest fires. The Madawaska Ecodistrict's high elevations produce a cool, damp climate which supports many hilltop tolerant hardwood stands (Zelazny et al. 2003).

Hunter Brook (HB) – Madawaska Ecodistrict

Down stream from Quisibis Mountain along the flat bottom lands of Hunter Brook are stands of pure spruce. At 235 metres elevation, on mossy ground with regenerating balsam fir, the competitive spruces reach for sunlight. Although the sampled stand was identified as red spruce, some hybridization with black spruce had likely occurred based on the characteristics of the cones, bark, twigs and general tree morphology. The likely hybridized red spruces were the only species sampled here.

A description of the cool, moist Madwaska Ecodistrict of the Central Uplands Ecoregion can be found in the preceding "Quisibis Mountain (QM) – Madawaska Ecodistrict" section.

Davis Mill (DM) - Madawaska Ecodistrict

Following the Hunter Brook drainage south, we arrive on the border of the Madawaska Ecodistrict, near the Davis Mill area. At 246 metres on a well drained rolling landscape, scattered throughout an area of obvious human disturbance in the forest, are large dominant white pines that have been allowed to grow. The trees are uneven aged to an extent, and the older specimens have ladder structures and platforms constructed far up the tree trunks. Remnants of an abandoned rail bed are visible while much of the surrounding forest was recently removed. The surviving forest is composed of intolerant species and is dwarfed by the mega-floral pines. White pine was the only species sampled here.

Again, a description of the cool, moist Madwaska Ecodistrict of the Central Uplands Ecoregion can be found in the preceding "Quisibis Mountain (QM) – Madawaska Ecodistrict" section.

Rivere Verte (RV) – Madawaska Ecodistrict

Not far from Davis Mill, across the Rivere Verte, a stand of dominant cedar grows on a concave slope. This site occurs at 230 metres elevation and appeared to maintain relatively moist soils. The stand was comparatively even aged and many of the trees exhibited butt-rot in the stems. Other understory species included striped maple and balsam fir. Eastern white cedar was the only species sampled here.

Additionally, a description of the cool, moist Madwaska Ecodistrict of the Central Uplands Ecoregion can be found in the preceding "Quisibis Mountain (QM) – Madawaska Ecodistrict" section.

Michaud Mountain (MM) – Madawaska Ecodistrict

Over looking the city of Edmundston and the climate station's central position at 340 metres elevation is a tolerant hardwood slope. This well drained east facing slope, composed of mainly sugar maple, contained scattered yellow birches and a thick carpeting layer of Canadian yew (*Taxus canadensis* Marshall). The closed canopy forest was relatively even aged and exhibited healthy, vigorous trees. Yellow birch was the only species sampled here.

Once again, a description of the cool, moist Madwaska Ecodistrict of the Central Uplands Ecoregion can be found in the preceding "Quisibis Mountain (QM) – Madawaska Ecodistrict" section.

Harrison Saddle (HS) – Sisson Ecodistrict

This site supports a very rare and small hemlock stand at 265 metres elevation. A muted ridge runs north south with a depression in the middle. This "saddle" shaped depression is where

the uneven aged hemlocks are found mixed with cedar, other softwoods and some hardwood. The hemlocks occur on the south facing side of the saddle toward the bottom of the slope where moisture gathers into a small stream. Eastern hemlock was the only species sampled here.

The Sisson Ecodistrict, like the Madawaska, is located within the Central Uplands Ecoregion. See the preceding "Quisibis Mountain (QM) – Madawaska Ecodistrict" section for a description of the climate.

Kintore Ridge (KR) – Brighton Ecodistrict

This is the highest site located at 414 m elevation on an unlogged portion of crown land. It is dominated by sugar maple mixed with mature beech, yellow birch, red spruce and balsam fir. Most of the site has vigorous beech undergrowth. The site is located on a well drained slope with a western aspect. Sugar maple, yellow birch and red spruce were sampled here.

The Brighton Ecodistrict is another in the Central Uplands Ecoregion but with a much more southern geographic position. The elevation here results in higher precipitation amounts and cooler temperatures than other parts of the study area, however the location within the ecodistrict exposes the area to more moderate temperatures acquired from further down the slopes in the Saint John and Tobique river valleys. Tolerant hardwood stands are plentiful in this ecodistrict (Zelazny et al. 2003).

Aroostook River (AR) – Blue Bell Ecodistrict

Along the southern (north facing) bank of the Aroostook River, approximately four kilometres from the river's confluence with the Saint John River, the shore is populated with a forest dominated by cedar and hemlock with some aspen mixed in. Growing above the river's high water mark but at the bottom of a long slope; the forest benefits from a seeping water table. The 90

metre high rocky site is bordered by an old rail bed up slope, which has allowed easy access to the site and resulted in the dumping of refuse into the forest. The remnants of very large old hemlocks scatter the forest floor and mechanically cut stumps are absent, indicating the uneven aged forest has not been harvested in any significant way. Both eastern white cedar and eastern hemlock were sampled here.

As part of the Valley Lowlands Ecoregion, the Blue Bell Ecodistrict is located far inland, away from immediate marine influences. Although its proximity to the Central Uplands Ecoregion is relatively close, the reduced elevation here produces less orthographic lifting and results in a much dryer climate (Zelazny et al. 2003). The summers are warmer but night time cold air drainage into the valleys causes intermittent frost in the shoulder seasons (Zelazny et al. 2003).

Aroostook Bluff (AB) – Blue Bell Ecodistrict

Overlooking the confluence of the Aroostook and Saint John Rivers, this site is 130 metres in elevation on a rocky outcrop facing southwest. The edge of the outcrop is dominated by white pines that are relatively even aged. White pine was the only species sampled here.

A description of the relatively warm dry climate of the Blue Bell Ecodistrict can be found in the preceding "Aroostook River (AR) – Blue Bell Ecodistrict" section.

Horseshoe Ridge (HR) – Tabusintac Ecodistrict

This site is located at 168 m elevation and supports an even-age stand of sugar maple mixed with a minor portion of American beech and yellow birch. Vigorous American beech regeneration is common throughout the site. The landscape is generally flat yet the area appeared well drained. Sugar maple was the only species sampled here.

Horseshoe Ridge is one of two sites sampled in the largest ecoregion of the Eastern Lowlands. The ecoregion lies in the rain shadow of the highland and upland regions and is therefore dry and prone to more frequent forest fires. The most noted example of this is the massive 1825 Miramichi fire which consumed the forests over much of the region (Zelazny et al. 2003). The Tabusintac Ecodistrict is cooled in summer by the waters of the Gulf of St. Lawrence. Tolerant hardwood stands where sugar maple is normally found occur infrequently in this ecoregion (Zelazny et al. 2003).

Stewart Brook (SB) – Red Bank Ecodistrict

At 10 metres elevation, this site is at the confluence of Stewart Brook and the northern branch of the Miramichi River. The property is and has been owned by the Miramichi Salmon Conservation Centre since 1873. According to their records no timber removal has been carried out during their tenure. The 1825 Great Miramichi Fire likely removed much of the forest cover at that time but nearly two centuries have passed since then. Today mixed forests dominated by cedar, hemlock and white pine with smaller amounts of red spruce and birch line the brook banks. Although the forest cover is uneven aged, no individual trees are older than 185 years. The forest is rooted well above the high water line of the river and the sometimes steeply sloping river bank is well drained. Eastern hemlock, eastern white cedar, red spruce, and yellow birch were all sampled here.

The Red Bank Ecodistrict belongs in the Eastern Lowlands Ecoregion. This ecoregion lies in the rain shadow of the western highland and southern upland regions and is therefore dry and prone to more frequent forest fires (Zelazny et al. 2003). The nearby waters in the Northumberland Straight warm substantially in the summer offering little moderating effects to warm westerly land

based air flows (Zelazny et al. 2003). The proximity to the waters of the straight does provide moderation of cold weather in early winter before the straight freezes over.

Beaubear's Island (BI) – Red Bank Ecodistrict

Beaubear's Island lies at the confluence of the Northwest Miramichi and Southwest Miramichi Rivers. Its elevation peaks at nine meters and the island is dominated by large white pines. The island has a storied history as it was a deadly refuge for fleeing Acadians during the deportation of 1755 and it was later the site of ship building for over a century. As most of the area was burned by the Great Miramichi fire of 1825, it is likely any remaining unharvested forest cover may have been burned. The existing white pines on the island are over 150 years old so reforestation of parts of the island must have begun by 1850. The potential human influence on this regrowth is unknown however. White pine was the only species sampled here.

Climatic description can be found in the preceding "Stewart Brook (SB) – Red Bank Ecodistrict" section.

Odell Park (OP) – Aukpaque Ecodistrict

This site is found at 70 m elevation within the boundaries of a city park that is said to have never been logged. Much of the park is dominated by large old-growth eastern hemlock and white pine with subordinate red spruce, cedar and many other species. The central lower reaches are dominated by uneven-aged sugar maple with lesser amounts of beech, white ash (*Fraxinus americana* L.), yellow birch and basswood (*Tilia americana* L.). The site features much exposed bedrock, is well drained and the aspect of the slope faces northeast. The park was established in 1954 and is criss-crossed by a number of hard packed trails. Sugar maple, yellow birch, eastern hemlock, red spruce, eastern white cedar and white pine were all sampled here.

Odell Park is on the edge of the warmest ecoregion of New Brunswick called the Grand Lake Lowlands. Due to the lag in heat transfer between the atmosphere and Grand Lake, the length of the growing season is extended and the frost free period is longer than any other area in New Brunswick (Zelazny et al. 2003). This results in warmer falls and an early finish of the winter season. The Aukpaque ecodistrict itself is located over the majority of the lower Saint John River Valley area. The sample site is located up river from Grand Lake but is still moderated by the large volume of water in the river (Zelazny et al. 2003). Although this ecodistrict supports many species with more southern affinities, the dominant stands are composed of red spruce, balsam fir, sugar maple, beech, white pine and hemlock. It should be noted that Odell Park borders on the Valley Lowlands Ecoregion and the Grand Lake Lowlands characteristics could be near their limits here (Zelazny et al. 2003).

Indian Mountain (IM) – Petitcodiac Ecodistrict

This site is on private land at 157 m elevation on the Indian Mountain plateau where the North River originates and later becomes the Petitcodiac River. Historically this stand of tolerant hardwoods, composed of uneven-aged sugar maple, yellow birch, beech, white ash and ironwood (*Ostrya virginiana* (Mill.) K. Koch), was used for maple syrup production. The site is relatively flat and incised with drainage channels making the slightly south facing slope well drained. A number of old wood roads traverse the stand although they are little used today. Minor amounts of logging have been carried out by the land owners but more value was placed in the stand for maple sugar production thus allowing many of the trees to achieve old ages. Sugar maple was the only species sampled here.

The large Eastern Lowlands Ecoregion covers this site and is influenced by the higher elevation areas to the northwest and southwest. These taller landforms cast a rain shadow over the

lowlands as well as protecting it from onshore breezes off the Bay of Fundy. The result is a relatively dry climate with warm summers comparable to the Valley Lowlands Ecoregion and winter temperatures moderated by the Northumberland Straight (Zelazny et al. 2003). The particular ecodistrict which the Indian Mountain sugar maple stand is best characterized by is somewhat ambiguous. Indian Mountain, Steeves Mountain and Lutes Mountain form an area of higher elevation at the intersection of the low-elevation Castaway, Kouchibouguac and Petitcodiac ecodistricts. The Petitcodiac ecodistrict most likely lends the best climatic description as a transition zone between the warm, dry lowlands and the cool, wet Fundy Coastal Ecoregion (Zelazny et al. 2003). The elevation here would be expected to both increase precipitation amounts and result in cooler temperatures than the lowlands. Also the tolerant hardwood growing on the higher elevation areas here are somewhat of a departure from the typical lower elevation species comprised of intolerant hardwood and coniferous stands.

Irishtown Reservoir (IR) - Petitcodiac Ecodistrict

This retired reservoir is now a city park and is mainly reforested with intolerant trees species after likely intensive harvesting over the past 150 years. Scattered white pine tower above the rest of the forest and the east side of the reservoir harbours a stand of red spruce and hemlock around which recent harvesting is evident. The flat landscape sits at an elevation of 52 meters and white pine, red spruce and eastern hemlock were sampled here.

Descriptions of the Eastern lowlands Ecoregion, within which the Petitcodiac Ecodistrict is located, can be found in the preceding "Indian Mountain (IM) – Petitcodiac Ecodistrict" section.

McLaughlin Reservoir (MR) - Petitcodiac Ecodistrict

This active back-up reservoir is only five kilometres from the Irishtown reservoir and it is very similar in characteristics. On the western side of the reservoir a hill raises up to 62 metres in elevation where a tolerant hardwood stand grows. Recently this forest has been strip cut and balsam fir is regenerating between the remaining dominant yellow birch and sugar maples. Moderate drainage is likely as the slope is not steep.

Again descriptions of the Eastern lowlands Ecoregion, within which the Petitcodiac Ecodistrict is located, can be found in the preceding "Indian Mountain (IM) – Petitcodiac Ecodistrict" section.

Intervale Pasturelands (IP) - Petitcodiac Ecodistrict

This site is situated in the headwater region of the Petitcodiac River at 42 metres elevation. Here a cedar swamp occurs in a forested area among many farms. It is a low lying flat landscape where the uneven aged cedar trees grow. The drainage is poor and the soils are deep and dark. Eastern white cedar was the only species sampled here.

Although this site is located on the opposite side of the Petitcodiac Ecodistrict from the Irishtown and McLaughlin Reservoirs, it has similar climatic influences except less influence by the Northumberland Straight. For a more thorough description of the Eastern lowlands Ecoregion, within which the Petitcodiac Ecodistrict is located, note the preceding "Indian Mountain (IM) – Petitcodiac Ecodistrict" section.

Chapter 4

4.0 Data Composition and Analysis Procedures

4.1 Instrumental Climate Data

Climate data used in this analysis was obtained through four sources. The most heavily relied upon data set was daily instrumental data from the Adjusted Historical Canadian Climate Data (AHCCD) set available through Environment Canada (Vincent and Gullet 1999, 2002). The second data source was daily snow depth reconstruction data accessed through the Canadian Daily Snow Depth Database Main Documentation (Brown and Braaten 1998). These two data sets were supplemented with the raw, unadjusted Canadian Daily Climate Data (CDCD), available through Environment Canada, and the U.S. Historical Climatology Network (USHCN) data (Williams et al. 2006). Several reasons arose for the need of supplemental data; the first, not all desired locations had AHCCD data available, and second, many days, weeks, and sometimes months worth of data were missing in the adjusted and reconstructed data. To fill these gaps, nearby climate data collection stations were used to provide the missing data at the station in question.

Nearby climate data sets were extracted from the CDCD data and sometimes used to extend the AHCCD data further back in time. By using data from other climate stations to infill missing data, a level of error was introduced into the chosen climate station series. Data from several stations, covering various periods of time, located at numerous elevations, and at assorted places within their communities had to be pieced together. Every effort was made to avoid using climate data of debatable quality, and instead to substitute missing values with data from the nearest, and most similar neighbour station. However, this was not always possible and the original adjusted and

homogenized data obtained from the AHCCD data set were altered in the end. The outcome of this compilation was that 10 complete data sets covering the time periods and areas outlined in Table 4.1. were constructed. From these data sets, both daily and monthly values were made available for the production of the climate variables needed in the analysis. It should also be noted that during the climate data set construction, lapse rates were applied to temperature and snow depth measurements in an attempt to account for the relatively large differences in elevation between climate stations and sample sites.

Table 4.1. Environment Canada climate station information for the main station used for each sample site. Climate station identification including, the station ID number, the common interval of data covered by all data types, the approximate geographic position (latitude and longitude in degrees and minutes), and the elevation above sea level is provided for each climate site.

Main Station	Station ID	Common	Geographic Position	Elevation asl
Charlo, N.B.	8100885	1940-2005	47° 59' N, 66° 20' W	40 m
Edmundston, N.B.	810AL00	1936-2003	47° 21' N, 68° 11' W	155 m
Aroostook, N.B.	8100300	1932-2004	46° 48' N, 67° 43' W	91 m
Miramichi, N.B.	8101000	1876-2004	47° 01' N, 65° 28' W	33 m
Fredericton, N.B.	8101500	1878-2005	45° 52' N, 66° 32' W	20 m
Moncton, N.B.	8103200	1901-2005	46° 06' N, 64° 41' W	72 m

4.2 Coupled Global Climate Model Data

Third Generation Coupled Global Climate Model (CGCM3), produced by the Canadian Centre for Climate Modeling and Analysis, was used to predict the future climate data applied in the tree growth forecasts. Monthly and daily data were calculated for the grid squares within the latitudes from 43°15' N to 48°50' N and longitudes from 61°52' W to 70°19' W (Fig. 4.1).

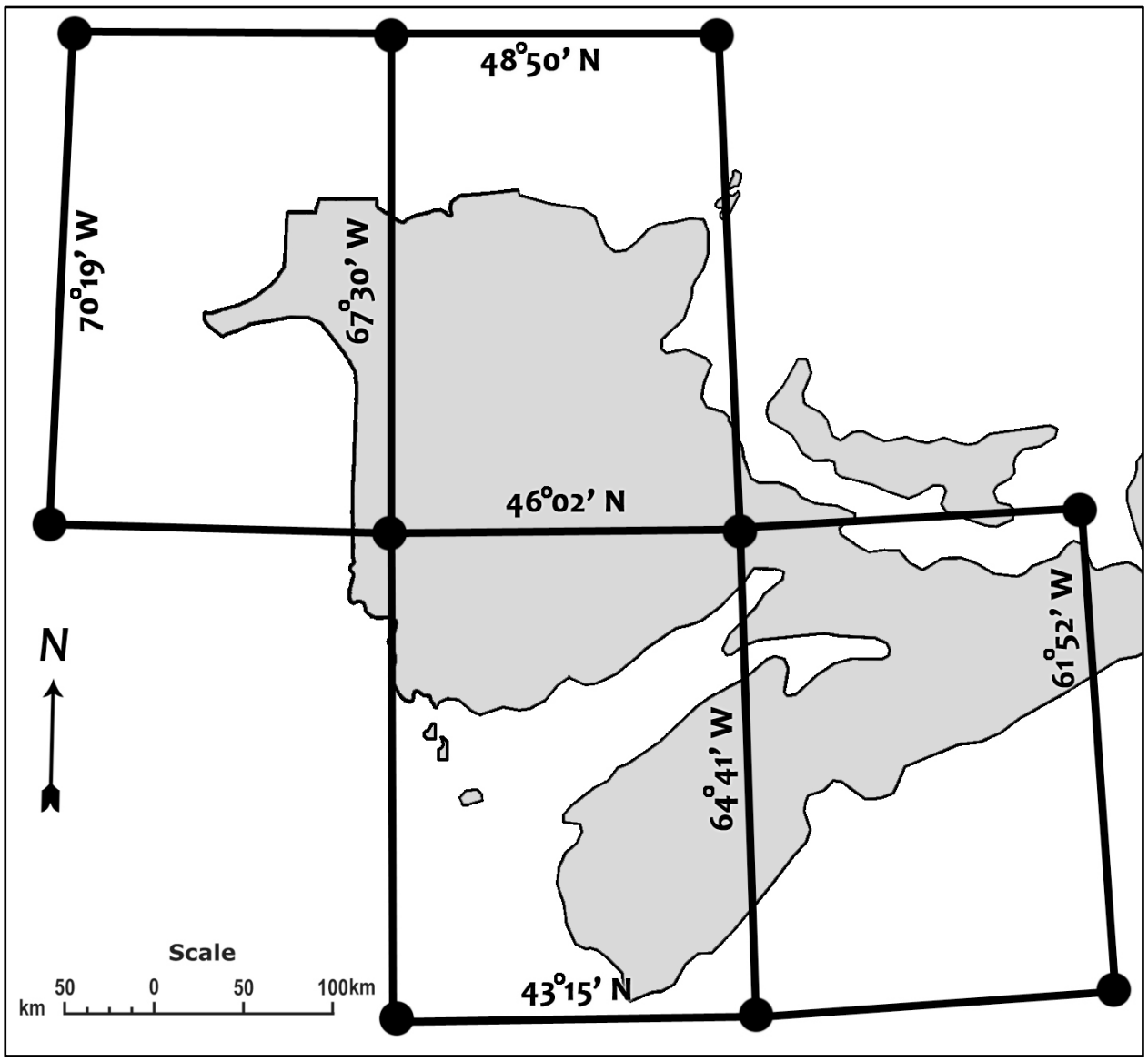

Figure 4.1. The CGCM3 produces a set of forecast data that is homogenous across a 2.81˚ X 2.81˚ grid square, and does so for a global grid. Relevant CGCM3 output grid squares covering the Maritime Provinces are illustrated. Latitudinal and longitudinal boundaries for each grid square are also given. Base map © 2002. Her Majesty the Queen in Right of Canada, Natural Resources Canada.

4.3 Climate Change Scenarios

This study takes a conservative approach to future climate model data. Data used are based on two scenarios from the Special Report on Emissions Standard (SRES) published by the IPCC (2007). The CGCM3 data used are based on the SRES B1 and SRES A1B scenarios. The B1 scenario is a

low estimate and assumes a 550 parts per million (ppm) leveling of CO_2 emissions by the year 2100. The A1B scenario is an intermediate estimate and assumes a 720 ppm leveling of CO_2 emissions by the year 2100. These two scenarios were chosen from a range of scenarios which place atmospheric CO_2 concentrations between 550 ppm and 1000 ppm by the end of this century. As will be explained later, more extreme climate change scenarios were not deemed appropriate for this study.

4.4 Coupled Global Climate Model Calibration

The CGCM3 grid squares superimposed over the study area covered more than five degrees of latitude and over eight degrees of longitude, including several distinct water bodies. These grid squares overlap a zone much larger than the study area, and data represent an average homogenous result of temperature and precipitation over the entire heterogeneous region of each grid square. Because of this generalized upscaling, a "change factor" conversion was needed, at least on the basic monthly temporal scale. This was deemed possible, as a baseline climatological record from each climate station was available, and the calculations were relatively simple compared to a "statistical downscaling" approach (Diaz-Nieto and Wilby 2005).

For each month of every year, the CGCM3 data were subtracted from the point source data at each station for the longest period possible. The resulting calculations were then averaged for each month over the same period creating mean monthly divergence values. The divergence values were then added back onto the CGCM3 uniform data set to shift the magnitude of the values to that of the point source climate station values, and in doing so, they did not alter the variation of the data. The same operation was repeated for the daily data from each climate station. The output divergence values were then applied to the future CGCM3 data adapting it to be representative for the future local climate at each site. A possible drawback to this process, is that the Coupled Global Climate Model (CGCM) data are not altered to reflect the local climate but only shifted to a similar

magnitude as the local climate. Although not ideal, this was the most appropriate conversion possible given the relative large amount of data and the available time.

4.5 Climate Variables

The abiotic influence of climate on tree growth is complex. The combination of long- and short-term weather events that coalesce over time to form the climate can echo through the environment for days, years, decades and sometimes centuries after they occur. Although instrumentation to quantify this multidimensional continuous chain of weather events has evolved tremendously over the past century, we must still rely on the climatic description provided by those first meteorological instruments if we wish to peer relatively far back in time. Not only are we limited by the types of data collected by these early instruments, but we are also limited by the geographic extent within which measurements were taken.

In the Maritimes we are lucky to have a comparatively long climate record, reaching back over 130 years in some locations. The large majority of climate stations that extend back in time long enough to be of use to this study, are positioned within populated areas, often at low elevations. These older data records are subject to errors in documentation and collection as well as lack of uniform procedures and a lack of quality control (Vincent and Gullet 2002).

Many variables were constructed from the climate records made available through the sources listed above. The temporal periods of these variables are summarized in Table 4.2 and each variable definition is given below. Three variable sets were assembled; the first composed of traditional mean monthly temperature (MMT) variables, the second constructed of total monthly precipitation (TMP) variables and the third set consisted of several winter indexes from daily compiled temperature (DCT) values. Components of both temperature variable sets were combined and paired with the precipitation set to produce a hybrid assemblage of 38 variables for the analysis.

Due to anticipated high levels of autocorrelation normally associated with most temperate tree species (Fritts, 1976), variables were produced for current year, plus one lagged year. This strategy is undertaken to account for energy reserves produced in previous growing seasons and carried forward to the current year of growth.

Table 4.2. Climate variables created for this study cover various months of the year and also include one previous year. Climate variable type, period length and annual occurrence are outlined. Months of the two-year time period covered are represented by only a first letter. Time periods included by each variable are marked in grey, the shortest of which only cover monthly intervals while other variables cover seasonal periods (black vertical lines separate monthly periods while seasonal periods are solid grey with no breaks between months). Variable names are Tmean = average monthly temperature, TRF Deep = thaw/refreeze deep, TRF S = thaw/refreeze surficial, RtFr = root freeze, Tprecp = total monthly precipitation, SD = snow depth, with expanded definitions below.

Vari-able	1st Year Lag												Current Year											
Month	J	F	M	A	M	J	J	A	S	O	N	D	J	F	M	A	M	J	J	A	S	O	N	D
Tmean																								
TRF D																								
TRF S																								
RtFr																								
Tprecp																								
SD																								

Monthly Mean Temperature (MMT) Variable Set

Tmean – This variable set included mean monthly temperatures for each month over the three year period minus November and December of the current year. Also several months were aggregated into seasonal values to decrease the total number of variables in this set (Table 4.2).

Total Monthly Precipitation (TMP) Variable Set

Tprecp – This variable set included total monthly precipitation amounts from April to September in the current and first lagged years, and in the second lagged year, total seasonal precipitation amounts for spring and summer were provided (Table 4.2).

SD – This variable averaged monthly snow depth from December to March of each year and summed them in a snow depth index (Table 4.2). The purpose of this variable was to combine several variables to shrink the overall variable count, while providing a more representative perspective on the ecological effects of winter precipitation.

Daily Compiled Temperature (DCT) Variable Set

TRF D – The 'thaw/refreeze deep' variable summed the freezing degree days (FDD) following a thaw, defined as a period accumulating 15 growing degree days in March, April or May (Table 4.2). Auclair et al. (1996), Payette et al. (1996), Bourque et al. (2005) and Brier et al. (2008) all defined a similar winter thaw-freeze variable.

TRF S – The 'thaw/refreeze surficial' variable represented the lowest negative temperature value (<-4˚C) following a period accumulating 15 growing degree days in March, April or May when no FDD (number of accumulated negative daily mean temperatures) were experienced but a nighttime freeze occurred (Table 4.2). Because many thaws represented the final thaw of the winter season, yet were not followed by an accumulation of FDD, it was felt a surficial freeze variable was necessary to describe significant, but short-term (one night freezing) events (<-4˚C) more commonly known as frost.

RtFr – This root freeze variable summed FDD for each winter month depending on the depth of snow present. The following accumulation of FDD was employed; FDD (base 0˚C) were calculate when snow depth equaled zero to ten centimeters, FDD (base -5˚C) were calculated when snow depth equaled 10 to 20 cm, FDD (base -10˚C) were calculated when snow depth equaled 20 to 30 cm, FDD (base -15˚C) were calculated when snow depth equaled 30 to 40 cm, no FDD were calculated when snow depth was greater than 40 cm. The FDD accumulation was determined for the months from December to March. FDD were calculated for each day in this time period using these constraints

then summed for each month and the month in each year with the greatest absolute number of FDD represented that year (Table 4.2). Through experimental work, Robitaille et al. (1995) found freezes over bare ground caused reduced radial growth in sugar maple for several years following the event.

4.6 Global Coupled Ocean-Atmosphere Interactions

Climate data representing global coupled ocean-atmosphere interactions (GCOAI) which vary at low frequencies relative to the annual scale of tree-rings were also used in the analysis of sugar maple response to climate. The Atlantic Multidecadal Oscillation (AMO), the North Atlantic Oscillation (NAO), the Southern Oscillation Index (SOI) and the Pacific Decadal Oscillation (PDO), were all assessed for relationships to sugar maple radial growth. The AMO is expressed by sea surface temperature (SST) anomalies between 0˚ - 70˚ N latitude in the Atlantic Ocean (Enfield et al. 2001). The NAO is identified through a principal component analysis of winter sea level pressure (SLP) anomalies measured between 20˚ N -70˚ N latitude and 90˚ W - 40˚ E longitude in the Atlantic Ocean (Hurrell et al. 2003). The Southern Oscillation Index (SOI) is the measured SST anomalies between 5˚ N - 5˚ S latitude and 170˚ W - 120˚ W longitude in the Pacific Ocean (Kaplan et al. 1998). The PDO is again identified through principal component analysis of SST above 20˚ N latitude in the Pacific Ocean (Mantua et al. 1997).

The AMO unsmoothed monthly index data (1856 -2008) were accessed through the Physical Sciences Division (PSD) of the Earth Systems Research Laboratory (ESRL) of the National Ocean and Atmospheric Administration (NOAA). Data for the winter (Dec-Mar) station based NAO index (1864 - 2008) and the SOI signal monthly index data (1866 -2008) were both accessed through the Climate Analysis Section (CAS) of the Climate and Global Dynamics (CGD) division of the National Centre for Atmospheric Research (NCAR). The PDO standardized monthly index (1900 – 2008) was accessed through the Joint Institute for the Study of the Atmosphere and Ocean (JISAO).

4.7 Tree-Ring Data

At each sampling site at least 40 core samples were taken from 20 trees using a 5.1mm increment boring tool, except in cases where less than 20 trees existed. Sampling only occurred on sites where trees were 100+ years old. Sites were also selected, based on their proximity to a nearby climate station. Due to the difficulties in finding suitable sampling sites 100+ years old near urban based climate stations, other selection criteria such as slope, aspect, elevation, and substrate were often ignored. The resulting tree-ring data were therefore a consequence of a somewhat opportunistic sampling strategy. Although micro-site characteristics were largely disregarded, the large majority of sampled stands occurred in typical habitat for the particular species under investigation.

Increment cores were prepared using standard dendrochronological procedures (Stokes and Smiley 1968). Following preparation, all cores were visually cross-dated and then ring-widths were measured to 0.001 mm using a VELMEX measuring system or to 0.01 mm using a WINDENDRO™ scanning system. Statistical cross-dating of the measured ring width patterns was carried out using the program COFECHA (Holmes 1992, Grissino-Mayer 2001). A small number of problematic cores with poor correlation values identified through this procedure were eliminated. The remaining cores for each site were standardized to remove non-climatic, low frequency growth signals, such as age-related trends and competition-induced growth suppression. Using the interactive version of the program ARSTAN (Cook 1985), ring-width series were single detrended, using one of a variety of detrending curves which were fit visually to each individual ring-width curve. These detrending curves were fit with the intention of removing biotic growth trends while not influence long-term multi-decadal growth trends associated with climate. Following the detrending procedure ARSTAN indexed the ring-width values for each chronology and created master site chronologies. Following

detrending procedures, the individual site chronologies were entered into correlation matrices to determine the strength of inter-site and inter-species relationships.

4.8 Tree-ring Chronology Analysis

Each of the 36 standardized tree-ring chronologies developed for this study were analyzed for intra-species/intra-site relationships, between trees, to produce averaged individual site Pearson product-moment correlation coefficients (r-values based on overlapping 50-year segments) and an average mean sensitivity was calculated. Pearson's r-value describes the strength of linear dependence between each tree core's growth curve and an overall master chronology, while the average mean sensitivity (AMS) calculation measures the high-frequency variation between annual rings by calculating average deviation (Fritts 1976, Grissino-Mayer 2001). Values of the AMS between 0.1 and 0.19 are considered low, values between 0.2 and 0.29 are considered moderate while any value over 0.3 is considered high and these values are recognized to be a good measure of a tree's sensitivity to climate (Grissino-Mayer 2001).

The relationship between the 36 standardized chronologies from the six tree species, collected across the six climate sites, were assessed using Pearson's r over the common interval of tree-ring data in four ways. First, the intra-species/inter-site relationships are evaluated. For example, sugar maple master chronologies from all sites would be analyzed against each other. Analysis across the range of sample sites is intended to reveal geographic patterns resulting from an uneven landscape and regional climatic variation. Second, the intra-site/inter-species relationships are calculated. For example, all chronologies from one site would be analyzed against each other. Analysis across the range of tree species within each site is intended to reveal the amount of shared radial growth response among the various species sample groups. Third, the intra-species/inter-site relationships are assessed over shorter time periods of 50 years overlapped by 25 years which

progress across the 1850-1999 time span, producing a series of five 50 year outputs for each species. Analysis across the range of sample sites using shorter time periods is intended to reveal temporal patterns resulting from climatic fluctuations or modifications of the radial growth response to climate over time. Finally, the standardized chronologies for each site were assessed for relationships with the GCOAI data to search for influence of these larger climatic fluctuations on the ring-width patterns of the six tree species. Due to the low frequency multidecadal nature of the GCOAI phases, correlation analysis was performed on smoothed curves (10 year moving averages) and curves of annual variability of both the GCOAI and standardized tree ring curves. Correlations were calculated for the entire period of available instrumental data for each GCOAI.

4.9 Radial Growth-climate Analysis

A least squares stepwise linear regression technique was used to establish and forecast the growth-climate relationship as it has in previous research using an "F to enter" of 0.20 and an "F to remove" of 0.25 (*c.f.,* Laroque and Smith 2003, Goldblum and Rigg 2005, Phillips and Laroque 2007, 2008, 2009a, 2009b, Girardin et al. 2008). The stepwise regression process outputs a range of models consisting of increasing quantities of explanatory variables until the "F to enter" and "F to remove" values constrain the process and all potential variables are included. To select the best subset model from the range of models created, Akaike's Information Criteria corrected (AICc) for models with high variable to observation value ratios was used (Burnham 2002). This approach estimates Kullback-Leibler (K-L) information and the best model minimizes the K-L information or distance between reality and the model (Burnham 2002). The main drawback to this approach concerns models that are not in the set under consideration. Akaike's Information Theory will select the best model from the available set, but if all the models in the set under consideration are poor, then the selected best model from this set will still remain poor. To assess the goodness-of-fit of the

AICc-selected best model an adjusted coefficient of determination (adj R^2) was used. This gives a measure of how well the model, may predict future situations. The adjusted R^2 corrects the coefficient of determination for increasing degrees of freedom in the model (Burnham and Anderson 1998). It only raises the adjusted R^2 value if an additional variable explains more variability than would be expected to occur by chance. The significance of the models is indicated with a P-value, calculated through an ANOVA. The Durbin-Watson (D-W) statistic is used to expose autocorrelation in the residuals of the regression analysis. The D-W statistic indicates a model has negative autocorrelation of the residuals if >2, positive autocorrelation if <2 and serious positive autocorrelation problems if <1. The variance inflation factor (VIF) is used to quantify the level of multicollinearity of a given regression coefficient in a model. A conservative cutoff for the VIF is considered any value >5 to be correlated with other independent variables in the model, thus increasing substantially the standard error of the particular model.

Chapter 5

5.0 Results and Discussion

5.1 Tree-ring Chronologies

The initial length of the tree-ring chronologies generated from the sampled trees in this study varied substantially, depending on the site. Although some trees were sampled with enough solid wood to measure over 200 years of radial growth, each site chronology was truncated at 1850 and all chronology analysis was performed on the shared 157 year common interval from 1850-2006. Several chronologies were truncated at 1875 and still others were truncated at 1890 and in one instance a chronology was truncated at 1900 due to a shallow sample depth in the period before these dates. Inter-series r-values produced for each chronology through the mean series correlation statistic exemplify the common environmental response among trees at individual sample sites. Table 5.1 illustrates the mean site r-values ranging from 0.469 to 0.606 with a mean of 0.551 for sugar maple, 0.446 to 0.556 with a mean of 0.491 for yellow birch, 0.561 to 0.643 with a mean of 0.607 for eastern hemlock, 0.527 to 0.597 with a mean of 0.556 for red spruce, 0.524 to 0.586 with a mean of 0.556 for eastern white cedar and 0.481 to 0.611 with a mean of 0.544 for white pine, which signifies that the majority of the trees in this study are all displaying a strong common signal. Average mean sensitivity values also calculated for each chronology range from 0.256 to 0.324 with a mean of 0.293 for sugar maple, 0.273 to 0.328 with a mean of 0.298 for yellow birch, 0.237 to 0.295 with a mean of 0.267 for eastern hemlock, 0.228 to 0.249 with a mean of 0.241 for red spruce, 0.183 to 0.207 with a mean of 0.195 for eastern white cedar and 0.185 to 0.237 with a mean of 0.206 for white pine (Table 5.1). These sensitivity values illustrate a medium to high sensitivity for sugar maple and yellow birch chronologies, a medium sensitivity for eastern hemlock and red spruce, and a low to medium

sensitivity for eastern white cedar and white pine. Six southern located sugar maple and yellow birch sites exceeded 0.300 which indicates they are very sensitive to climate (Grissino-Mayer 2001). The r-values within the intra-species/inter-site correlation matrix illustrate a large amount of variability in their relationships between site master chronologies (1850-2006), ranging from 0.177 to 0.639 with a mean of approximately 0.37 for sugar maple, 0.178 to 0.699 with a mean of approximately 0.5 for yellow birch, -0.012 to 0.540 with a mean of approximately 0.32 for eastern hemlock, 0.138 to 0.809 with a mean of approximately 0.38 for red spruce, 0.086 to 0.770 with a mean of approximately 0.35 for eastern white cedar and 0.114 to 0.521 with a mean of approximately 0.28 for white pine (Table 5.2). These inter-site correlation values not only vary significantly between sites revealing inconsistent geographic patterns but those relationships change considerably through time. Table 5.3 illustrates the average r-values among all sites for five 50-year moving intervals, lagged 25 years, calculated over the 1850-2000 common period. The correlation values range from 0.121 to 0.420 for sugar maple (Table 5.3), 0.159 to 0.611 for yellow birch (Table 5.4), 0.210 to 0.420 for eastern hemlock (Table 5.5), 0.084 to 0.527 for red spruce (Table 5.6), 0.229 to 0.462 for eastern white cedar (Table 5.7), and 0.196 to 0.385 for white pine (Table 5.8) representing periods of relative agreement and disagreement between ring-width curves. Visual representations of standardized ring-width curves for all sites are found in Figures 5.1 to 5.6. The inter-species/intra-site correlation matrix illustrates weak negative to medium-strong positive relations ranging from -0.236 to 0.311 for Charlo, -0.112 to 0.501 for Edmundston, 0.016 to 0.592 for Aroostook, -0.299 to 0.543 for Miramichi, -0.021 to 0.498 for Fredericton, and 0.065 to 0.664 for Moncton (Table 5.9).

Table 5.1. Statistics in this Table are calculated between individual tree ring indices produced for each sample site. Sample sites are indicated with the initials of the sites provided in the individual site description section. Each site is represented by a minimum of 24 individual tree cores taken from a minimum of 11 trees but, most sites are represented by 40 tree cores taken from 20 trees. Intra-site/intra-species correlations using Pearson's r-values illustrate the strength of relationships between sampled trees from individual sites. Also presented are average mean sensitivity (AMS) values calculated using all trees at each site. Values for AMS are considered low from 0.1 - 0.19, intermediate from 0.2 - 0.29 and high from $\geq$0.3 (Grissino-Mayer 2001). All two tailed r values significant at ($p<0.0001$).

Climate Station	Charlo	Edmundston	Aroostook	Miramichi	Fredericton	Moncton
Sugar Maple	BR	QM	KR	HR	OP	IM
r	0.581	0.578	0.554	0.606	0.517	0.469
AMS	0.256	0.296	0.298	0.307	0.301	0.3
Yellow Birch	BR	MM	KR	SB	OP	MR
r	0.473	0.497	0.446	0.466	0.509	0.556
AMS	0.273	0.278	0.311	0.293	0.303	0.328
Eastern Hemlock	BL	HS	AR	SB	OP	IR
r	0.643	0.569	0.599	0.638	0.629	0.561
AMS	0.295	0.284	0.285	0.237	0.257	0.245
Red Spruce	BR	HB	KR	SB	OP	IR
r	0.555	0.543	0.572	0.597	0.541	0.527
AMS	0.248	0.228	0.238	0.237	0.249	0.246
Eastern Cedar	BR	RV	AR	SB	OP	IP
r	0.532	0.58	0.524	0.547	0.564	0.586
AMS	0.204	0.207	0.198	0.183	0.195	0.185
White Pine	JR	DM	AB	BI	OP	IR
r	0.599	0.486	0.481	0.611	0.568	0.518
AMS	0.193	0.237	0.185	0.204	0.209	0.206

Table 5.2. The comparative relationships between all ring-width chronologies are illustrated in this intra-species/inter-site correlation matrix with Pearson's r-values for the common period 1850-2006. Pearson's r-values are calculated between standardized tree-ring curves for each site. Cells in this Table are shaded depending on the strength of the r-value indicated; darker shading represents higher r-values while lighter shading indicates lower r-values. Two tailed r-value significance levels indicated by * = ($p<0.05$), ** = ($p<0.01$).

Sugar Maple	Charlo	Edmundston	Aroostook	Miramichi	Fredericton
Edmundston	0.409**				
Aroostook	0.443**	0.639**			
Miramichi	0.215**	0.453**	0.391**		
Fredericton	0.158	0.530**	0.366**	0.604**	
Moncton	0.177*	0.352**	0.262**	0.141	0.383**
Yellow Birch	Charlo	Edmundston	Aroostook	Miramichi	Fredericton
Edmundston	0.488**				
Aroostook	0.210*	0.558**			
Miramichi	0.681**	0.619**	0.441**		
Fredericton	0.178	0.615**	0.433**	0.332**	
Moncton	0.562**	0.575**	0.581**	0.699**	0.559**
Eastern Hemlock	Charlo	Edmundston	Aroostook	Miramichi	Fredericton
Edmundston	0.350**				
Aroostook	0.294**	0.429**			
Miramichi	0.368**	0.329**	0.382**		
Fredericton	0.349**	0.372**	0.540**	0.341**	
Moncton	-0.011	0.257**	0.449**	-0.012	0.335**
Red Spruce	Charlo	Edmundston	Aroostook	Miramichi	Fredericton
Edmundston	0.809**				
Aroostook	0.471**	0.564**			
Miramichi	0.188*	0.138	0.017		
Fredericton	0.492**	0.478**	0.440**	0.345**	
Moncton	0.227*	0.242**	0.565**	0.163	0.551**
Eastern White Cedar	Charlo	Edmundston	Aroostook	Miramichi	Fredericton
Edmundston	0.403**				
Aroostook	0.213*	0.654**			
Miramichi	0.373**	0.391**	0.286**		
Fredericton	0.155	0.503**	0.770**	0.387**	
Moncton	0.086	0.354**	0.101	0.368**	0.202*
White Pine	Charlo	Edmundston	Aroostook	Miramichi	Fredericton
Edmundston	0.387**				
Aroostook	0.335**	0.481**			
Miramichi	0.134	0.141	0.196*		
Fredericton	0.241**	0.234**	0.255**	0.295**	
Moncton	0.114	0.203*	0.521**	0.282**	0.418**

Table 5.3. Pearson's r-values averaged for six **sugar maple** chronologies over 50-year moving intervals lagged by 25-years are presented. This Table was derived from individual inter-site correlation matrices calculated for each 50-year period. All five correlation values are composed of an average r-value computed between all sites in each individual matrix. Two tailed significance levels indicated by * = ($p<0.05$), ** = ($p<0.01$).

Time Period	1850-1899	1875-1924	1900-1949	1925-1975	1950-1999
Mean r-value	0.121	0.154	0.394**	0.236	0.420**

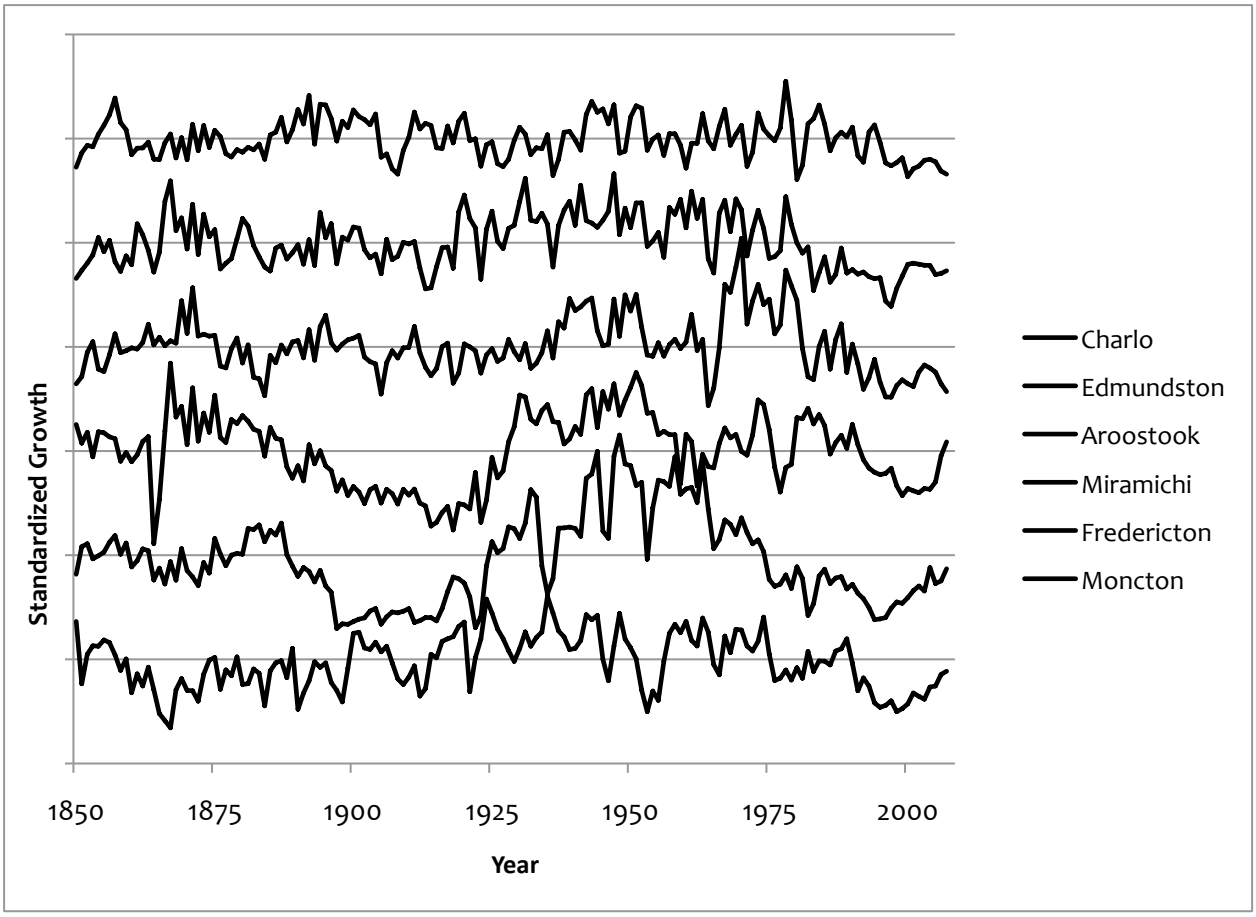

Figure 5.1. All six **sugar maple** chronologies representing the six sample sites are depicted over the truncated common interval from 1850-2006. All chronologies are standardized using the program ARSTAN and indexed curves are presented. Each curve fluctuates around an average of one represented by the horizontal strike-through lines. Sample depth at each site has a minimum of 30 cores extending back in time 100 years and at least 10 cores extending back 150 years. Site names are presented adjacent to the radial growth curves and order of sites is from north to south with occasional shuffling of sites to preserve nearest neighbour associations.

Table 5.4. Pearson's r-values averaged for six **yellow birch** chronologies over 50-year moving intervals lagged by 25-years are presented. This Table was derived from individual inter-site correlation matrices calculated for each 50-year period. All five correlation values are composed of an average r-value computed between all sites in each individual matrix. Two tailed significance levels indicated by * = ($p<0.05$), ** = ($p<0.01$).

Time Period	1850-1899	1875-1924	1900-1949	1925-1975	1950-1999
Mean r-value	0.159	0.256	0.593**	0.611**	0.385**

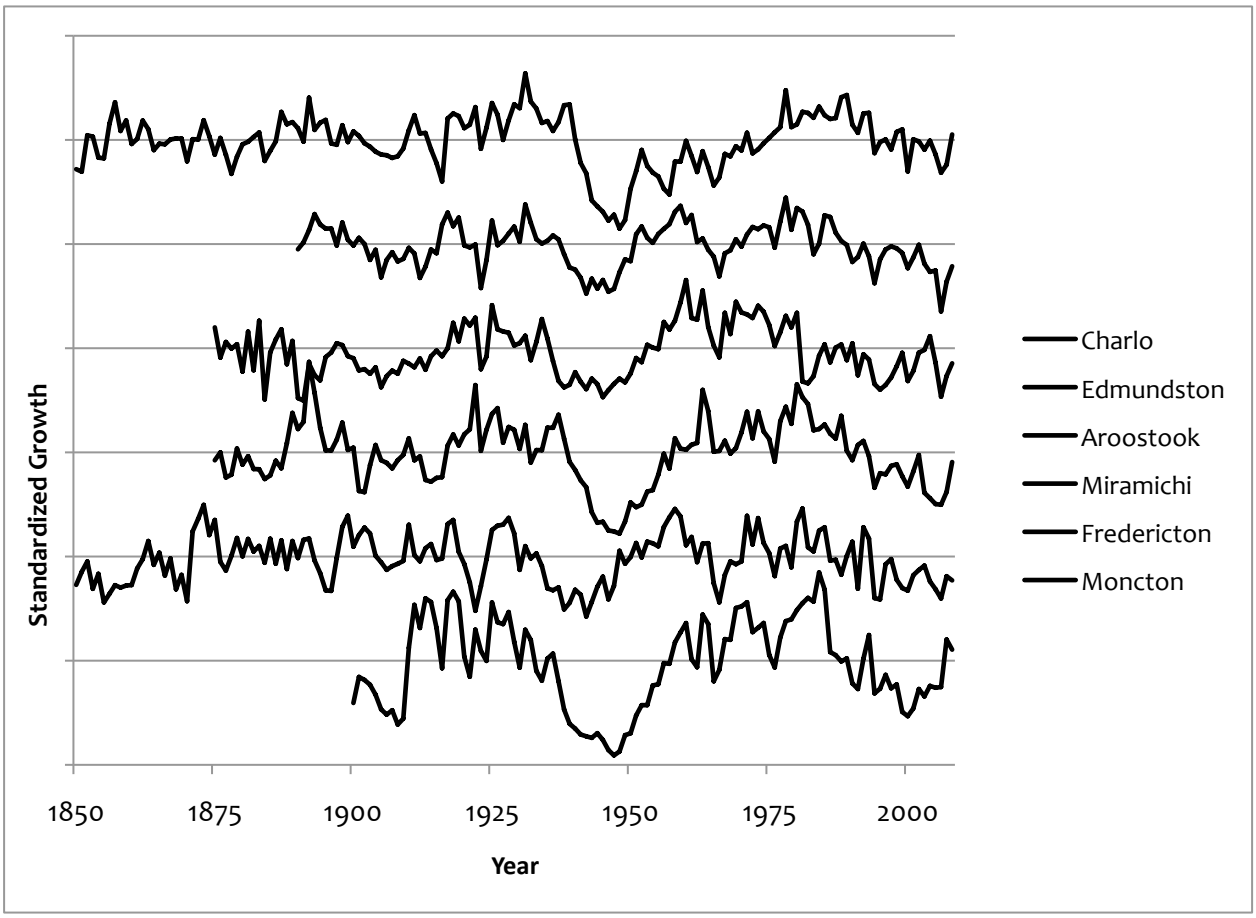

Figure 5.2. All six **yellow birch** chronologies representing the six sample sites are depicted over the truncated common interval from 1850-2006. All chronologies are standardized using the program ARSTAN and indexed curves are presented. Each curve fluctuates around an average of one represented by the horizontal strike-through lines. Sample depth at each site has a minimum of 10 cores extending back in time 100 years and most have no cores extending back 150 years. Site names are presented adjacent to the radial growth curves and order of sites is from north to south with occasional shuffling of sites to preserve nearest neighbour associations.

Table 5.5. Pearson's r-values averaged for six **eastern hemlock** chronologies over 50-year moving intervals lagged by 25-years are presented. This Table was derived from individual inter-site correlation matrices calculated for each 50-year period. All five correlation values are composed of an average r-value computed between all sites in each individual matrix. Two tailed significance levels indicated by * = ($p<0.05$), ** = ($p<0.01$).

Time Period	1850-1899	1875-1924	1900-1949	1925-1975	1950-1999
Mean r-value	0.355*	0.376**	0.420**	0.210	0.258

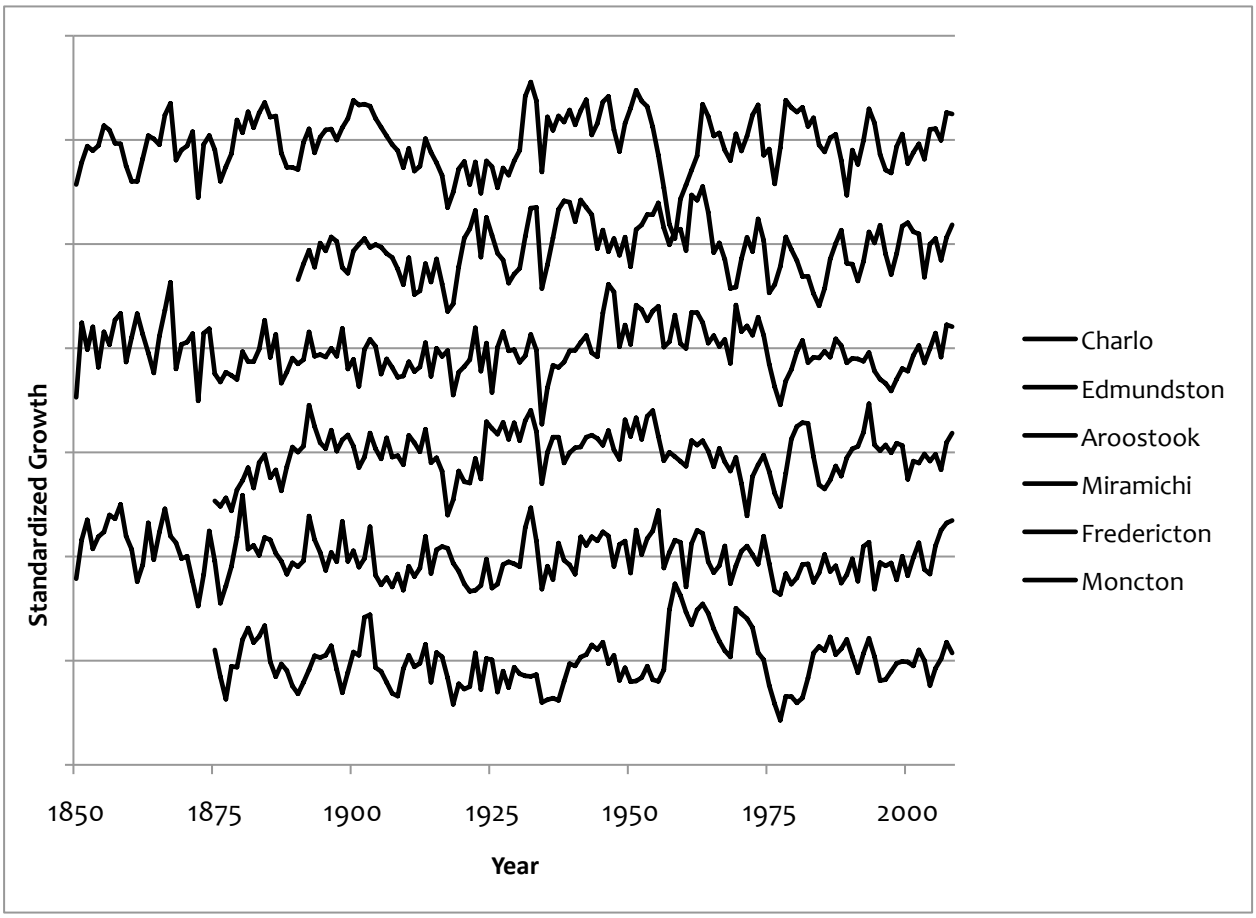

Figure 5.3. All six **eastern hemlock** chronologies representing the six sample sites are depicted over the truncated common interval from 1850-2006. All chronologies are standardized using the program ARSTAN and indexed curves are presented. Each curve fluctuates around an average of one represented by the horizontal strike-through lines. Sample depth at each site has a minimum of 11 cores extending back in time 100 years and some have no cores extending back 150 years. Site names are presented adjacent to the radial growth curves and order of sites is from north to south with occasional shuffling of sites to preserve nearest neighbour associations.

Table 5.6. Pearson's r-values averaged for six **red spruce** chronologies over 50-year moving intervals lagged by 25-years are presented. This Table was derived from individual inter-site correlation matrices calculated for each 50-year period. All five correlation values are composed of an average r-value computed between all sites in each individual matrix. Two tailed significance levels indicated by * = (p<0.05), ** = (p<0.01).

Time Period	1850-1899	1875-1924	1900-1949	1925-1975	1950-1999
Mean r-value	0.084	0.507**	0.527**	0.187	0.293*

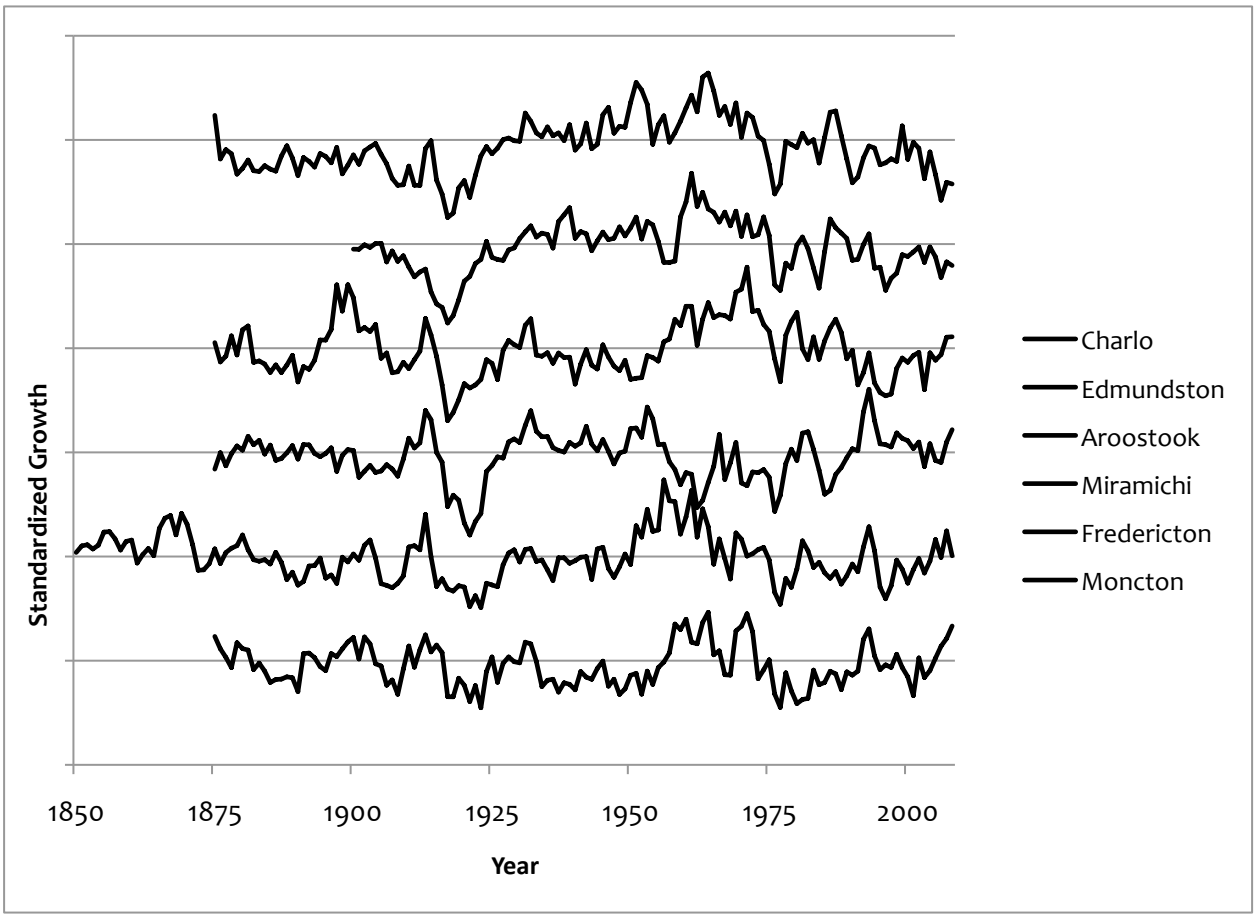

Figure 5.4. All six **red spruce** chronologies representing the six sample sites are depicted over the truncated common interval from 1850-2006. All chronologies are standardized using the program ARSTAN and indexed curves are presented. Each curve fluctuates around an average of one represented by the horizontal strike-through lines. Sample depth at each site has a minimum of nine cores extending back in time 100 years and most have no cores extending back 150 years. Site names are presented adjacent to the radial growth curves and order of sites is from north to south with occasional shuffling of sites to preserve nearest neighbour associations.

Table 5.7. Pearson's r-values averaged for six **eastern white cedar** chronologies over 50-year moving intervals lagged by 25-years are presented. This Table was derived from individual inter-site correlation matrices calculated for each 50-year period. All five correlation values are composed of an average r-value computed between all sites in each individual matrix. Two tailed significance levels indicated by * = ($p<0.05$), ** = ($p<0.01$).

Time Period	1850-1899	1875-1924	1900-1949	1925-1975	1950-1999
Mean r-value	0.341*	0.380**	0.338*	0.229	0.462**

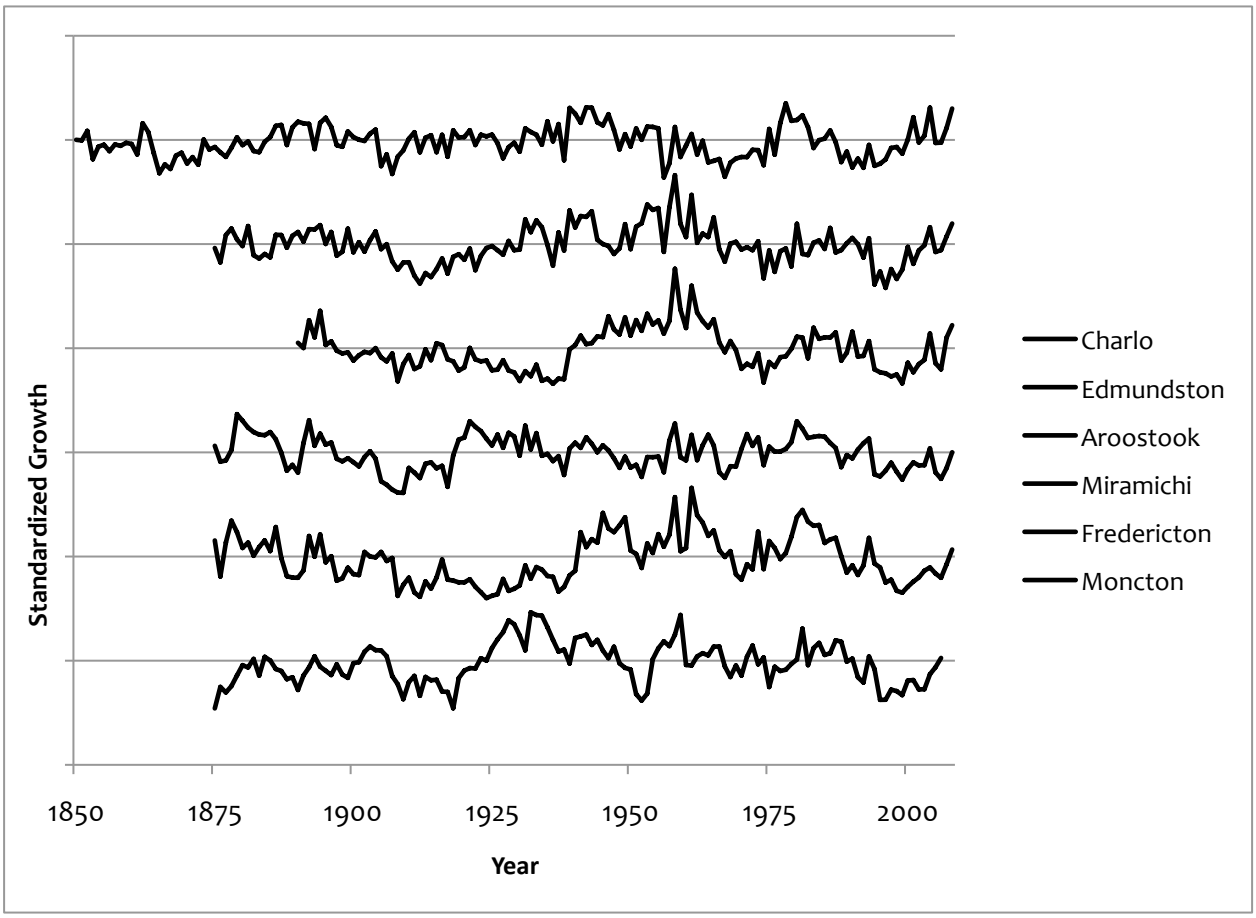

Figure 5.5. All six **eastern white cedar** chronologies representing the six sample sites are depicted over the truncated common interval from 1850-2006. All chronologies are standardized using the program ARSTAN and indexed curves are presented. Each curve fluctuates around an average of one represented by the horizontal strike-through lines. Sample depth at each site has a minimum of 18 cores extending back in time 100 years and most with no cores extending back 150 years. Site names are presented adjacent to the radial growth curves and order of sites is from north to south with occasional shuffling of sites to preserve nearest neighbour associations.

Table 5.8. Pearson's r-values averaged for six **white pine** chronologies over 50-year moving intervals lagged by 25-years are presented. This Table was derived from individual inter-site correlation matrices calculated for each 50-year period. All five correlation values are composed of an average r-value computed between all sites in each individual matrix. Two tailed significance levels indicated by * = ($p<0.05$), ** = ($p<0.01$).

Time Period	1850-1899	1875-1924	1900-1949	1925-1975	1950-1999
Mean r-value	0.385**	0.219	0.196	0.200	0.350*

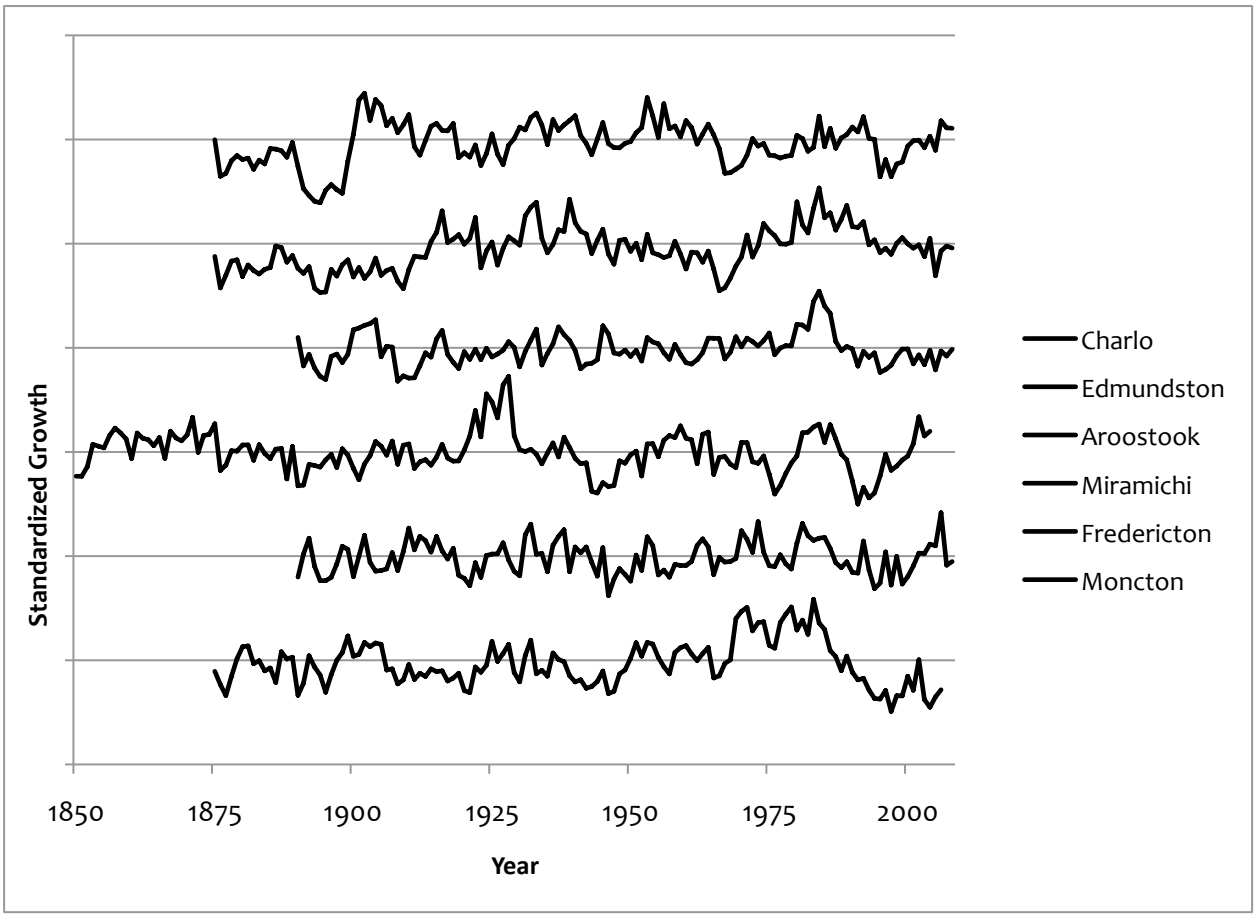

Figure 5.6. All six **white pine** chronologies representing the six sample sites are depicted over the truncated common interval from 1850-2006. All chronologies are standardized using the program ARSTAN and indexed curves are presented. Each curve fluctuates around an average of one represented by the horizontal strike-through lines. Sample depth at each site has a minimum of 14 cores extending back in time 100 years and most with no cores extending back 150 years. Site names are presented adjacent to the radial growth curves and order of sites is from north to south with occasional shuffling of sites to preserve nearest neighbour associations.

Table 5.9. The comparative relationships between all ring-width chronologies are illustrated in this inter-species/intra-site correlation matrix with Pearson's r-values for the common period 1850-2006. Pearson's r-values are calculated between standardized tree-ring curves for each site. Cells in this Table are shaded depending on the strength of the r-value indicated; darker shading represents higher r-values while lighter shading indicates lower r-values. Two tailed significance levels indicated by * = (p<0.05), ** = (p<0.01).

Charlo	SM	YB	EH	RS	EC
YB	0.091				
EH	0.211**	-0.035			
RS	0.145	-0.236	0.311**		
EC	0.202*	0.069	0.311**	-0.027	
WP	-0.158	-0.089	0.126	0.162	-0.004
Edmundston	SM	YB	EH	RS	EC
YB	0.220*				
EH	0.340**	-0.112			
RS	0.440**	0.043	0.501**		
EC	0.399**	0.149	0.428**	0.488**	
WP	-0.004	0.154	0.034	-0.066	0.090
Aroostook	SM	YB	EH	RS	EC
YB	0.300**				
EH	0.226**	0.048			
RS	0.310**	0.387**	0.299**		
EC	0.146	0.080	0.592**	0.206*	
WP	0.053	0.016	0.177	0.284**	0.112
Miramichi	SM	YB	EH	RS	EC
YB	-0.132				
EH	0.153	-0.022			
RS	0.327**	-0.299	0.543**		
EC	0.293**	0.377**	0.034	-0.093	
WP	-0.010	0.326**	0.025	-0.185	0.236**
Fredericton	SM	YB	EH	RS	EC
YB	0.055				
EH	0.315**	-0.011			
RS	0.426**	0.171*	0.498**		
EC	0.433**	0.179*	0.275**	0.415**	
WP	-0.021	0.303**	0.234**	0.211*	0.019
Moncton	SM	YB	EH	RS	EC
YB	0.154				
EH	0.179*	0.106			
RS	0.065	0.244**	0.664**		

EC	0.500**	0.066	0.183*	0.050	
WP	0.257**	0.514**	0.139	0.112	0.253**

5.2 Tree-ring Chronology Observations

The individual tree-ring chronologies for each species display highly significant within-site correlation values and the average inter-series r-value for all chronologies is approximately 0.55. Although the majority of chronologies generate an inter-series r-value relatively close to the mean, eastern hemlock consistently illustrates above average values and yellow birch generally presents below average values. These deviations are likely a result of the dispersion characteristics of these two species in the forest. While eastern hemlock is normally found in aggregate situations of pure stands with the old trees influencing the young, yellow birch is most often found scattered among tolerant hardwoods and shade tolerant softwood, with dissimilar species influencing the pre-canopy yellow birch growth. This situation would, therefore, be expected to increase the common signal in eastern hemlock while reducing the common signal in yellow birch. Another possible contributor to a weaker signal among yellow birch was noticed in the cross-dating process. Despite the vast majority of increment cores pairs from the same tree displaying nearly identical radial growth patterns, the cores from yellow birch trees had a much greater incidence of divergent radial growth patterns from one side of the tree to the other.

The variability in AMS among this sample group indicates that the most shade tolerant species generally have the highest sensitivity to climate (Table 5.1). Yellow birch is anomalous in this relationship as it is only moderately shade tolerant yet it displays the highest sensitivity. White pine also appears overly sensitive considering it is the least shade tolerant of the species examined. Further to these irregularities, a few other interesting sensitivity patterns should be noted. Yellow birch had its least sensitive sites in the northern portion of the study area, eastern hemlock had its

most sensitive sites in the north and eastern white cedar was marginally more sensitive in the north then it was in the south.

Across the sample area, the intra-species/inter-site chronologies varied substantially (Table 5.2) with an approximate correlation mean of 0.37 between all species. Three outliers from this average r-value exist. Yellow birch exhibits an approximate average 0.5 correlation value for all inter-site relationships of the species, exemplifying the comparatively strong common signal between yellow birch sites. The 50 year moving interval correlation values in Table 5.4 and the graphic representations of all the yellow birch ring-width curves in Figure 5.2, reveal a period covering much of the 20th century over which this strong common signal is established through longer-term large magnitude radial growth fluctuation. Eastern hemlock illustrates an approximate average 0.32 correlation value, indicating the relatively weak common signal between sites of that species. The 50 year moving interval correlation values in Table 5.5 and the graphic representations of all eastern hemlock ring-width curves in Figure 5.3 display a period of comparatively weak common signal between sites over the last half of the 20th century based on short-term radial growth deviations between sites. White pine reveals an approximate average 0.28 correlation value, demonstrating the weak common signal among white pine sites. The 50 year moving interval correlation values in Table 5.8 and the graphic representations of all white pine ring-width curves in Figure 5.6 specify a long period from the late 19th century into the latter half of the 20th century where white pine chronologies present a weak common signal. This weak signal is predicated upon relatively small magnitude, frequent short-term divergence from any shared radial growth response. Beyond these three outlier examples, the trend across all ring-width chronologies in relation to the 50 year moving interval correlation values and the graphic representations of all chronologies is the reoccurrence of radial growth suppression periods. These serve as a synchronization trigger across large geographic space, helping to establish the common radial growth signal.

5.3 Relationship to Ocean-Atmosphere Interactions

Correlations between ring-width chronologies and GCOAIs were completed using annual data and were also plotted using ten year moving averages (10-mavg). Regional master chronologies were also plotted against GCOAI's. Values included in this report for relationships with the AMO are calculated based on a three year lag of the index, as the AMO condition three years prior to current tree growth had the highest correlation values. The AMO illustrated many significant positive correlations across sugar maple, eastern hemlock, red spruce and eastern white cedar (Table 5.10). Correlations were often significant with these species in both annual and moving average data sets. Yellow birch and AMO illustrated significant negative correlations with both annual and moving average data sets, while white pine only produced minor significance values to the AMO (Table 5.10). Medium to strong correlation values were produced in the moving average regional master chronologies of sugar maple ($r = 0.405$), yellow birch ($r = -0.593$), eastern hemlock ($r = 0.745$), red spruce ($r = 0.578$) and cedar ($r = 0.380$) (Table 5.10). Visual displays of these ring-width curves versus the AMO index can be found in Figures 5.7, 5.9, 5.11, 5.13 and 5.15.

The winter season measurements of the NAO index produced the highest correlation values to the ring-width chronologies at no lag in the NAO data. Significant negative correlations with a large majority of tree-ring chronologies in this study were produced (Table 5.11). Sugar maple, eastern hemlock, red spruce and eastern white cedar all produced significant negative correlations to the NAO. Yellow birch and white pine, other than one significant positive correlation each, illustrate no significant correlation to the NAO. Moderately strong correlation values between the regional master ring-width chronologies and the NAO were produced in sugar maple ($r = -0.556$), eastern hemlock ($r = -0.456$), red spruce ($r = -0.555$), and eastern white cedar ($r = -0.409$) (Table 5.11).

Visual displays of these ring-width curves versus the NAO index can be found in Figures 5.8, 5.10, 5.12 and 5.14.

Results of analysis between ENSO, SOI, PDO and the ring-width chronologies did not produce as clear and obvious results as the analysis between AMO, NAO and the ring-width chronologies. Although significant and moderate correlation values were produced in the analysis between ENSO and the tree-ring chronologies, the results were inconsistent and weaker than prior analyses. The SOI displayed a further drop in significance and strength of correlation values against the ring-width chronologies. The PDO illustrated comparatively highly significant and stronger correlation values than ENSO or SOI, however they matched the pattern found in the NAO correlation results. The PDO and the NAO display very similar multidecadal trends, explaining the matching patterns produced by the two analyses. Given the strength of the results produced from the analysis with the AMO and NAO, the proximity of those two macro-climatic patterns to the study area and the absence of documented influence over the New Brunswick climate by the Pacific ocean-atmosphere interactions, it is likely any significant correlations found in the ENSO, SOI and PDO analyses, are largely coincidental which warranted the omission of their confusing results.

Table 5.10. Pearson's correlation values are illustrated here between site chronologies and the Atlantic Mulitdecadal Oscillation (AMO) at a three year lag. Ten year moving average values follow immediately after the annual resolution data for each site (M-avg). Site names are abbreviated by the retention of the first three consonants in the name. At the bottom of the table the correlation values between regional master curves for each species and the AMO are also presented. Correlation value cells are filled with black for highest postive correlation, 50% grey for zero correlation, and white for lowest negative correlation. Quantitative text is black for negative and white for positive correlation values. Two tailed significance levels indicated by *=($p<0.01$).

	Sugar Maple		**Yellow Birch**		**Eastern Hemock**		**Red Spruce**		**Eastern Cedar**		**White Pine**	
	AMO	M-avg	AMO	M-avg	AMO	M-avg	AMO	M-avg	AMO	M-avg	AMO	M-avg
Chr	**-0.053**		**-0.297***		**0.214***		**0.222**		**0.188**		**0.188**	
M-avg		**-0.076**		**-0.553***		**0.355***		**0.508***		**0.145**		**0.102**
Edm	**0.148**		**-**		**0.352***		**0.331***		**0.460***		**-0.147**	
M-avg		**0.338***		**-0.397***		**0.838***		**0.634***		**0.725***		**-0.235***
Ars	**-0.066**		**-0.174**		**0.243***		**0.097**		**0.326***		**-0.061**	
M-avg		**0.053**		**-0.278***		**0.472***		**0.052**		**0.444***		**-0.184**
Mrm	**0.323***		**-0.313***		**0.151**		**0.283***		**0.064**		**-0.054**	
M-avg		**0.545***		**-0.567***		**0.364***		**0.530***		**-0.066**		**-0.129**
Frd	**0.387***		**-0.127**		**0.327***		**0.428***		**0.257***		**-0.011**	
M-avg		**0.616***		**-0.358***		**0.782***		**0.595***		**0.358***		**-0.303***
Mnc	**-0.032**		**-**		**0.267***		**0.225***		**0.177**		**-0.215**	
M-avg		**-0.062**		**-0.720***		**0.357***		**0.224**		**0.283***		**-0.352***
MSTR	**0.206**		**-0.331***		**0.352***		**0.354***		**0.318***		**-0.034**	
M-avg		**0.405***		**-0.593***		**0.745***		**0.578***		**0.380***		**-0.216**

Table 5.11. Pearson's correlation values are illustrated here between site chronologies and the North Atlantic Oscillation (NAO). Ten year moving average values follow immediately after the annual resolution data for each site (M-avg). Site names are abbreviated by the retention of the first three consonants in the name. At the bottom of the table the correlation values between regional master curves for each species and the NAO are also presented. Correlation value cells are filled with black for highest postive correlation, 50% grey for zero correlation, and white for lowest negative correlation. Quantitative text is black for negative and white for positive correlation values. Two tailed significance levels indicated by *=(p<0.01).

	Sugar Maple		Yellow Birch		Eastern		Red Spruce		Eastern Cedar		White Pine	
	NAO	M-	NAO	M-avg	NAO	M-avg	NAO	M-	NAO	M-avg	NAO	M-avg
Chr	-0.050		0.099		-0.031		-0.201		-0.061		0.041	
M-avg		-0.208		0.365*		-0.054		-0.517*		-0.049		0.183
Edm	-0.175		-0.159		-0.062		-0.107		-0.087		0.185	
M-avg		-0.622*		-0.179		-0.482*		-0.587*		-0.549*		0.394*
Ars	-0.196		-0.223*		-0.135		-0.115		-0.107		0.041	
M-avg		-0.443*		-		-0.490*		-		-0.425*		0.033
Mrm	-0.024		-0.084		0.104		0.107		-0.036		-0.046	
M-avg		-0.263*		-0.076		0.100		0.179		-0.199		-0.094
Frd	-0.242*		-0.030		-0.047		-0.079		-0.065		-0.134	
M-avg		-0.592*		-0.048		-0.531*		-		-0.349*		-0.181
Mnc	-0.084		-0.066		-0.110		-0.150		-0.023		-0.091	
M-avg		-0.297*		-0.037		-0.467*		-		-0.209		-0.198
MSTR	-0.193		-0.091		-0.066		-0.132		-0.052		-0.018	
M-avg		-0.556*		-0.073		-0.456*		-0.555*		-		0.070

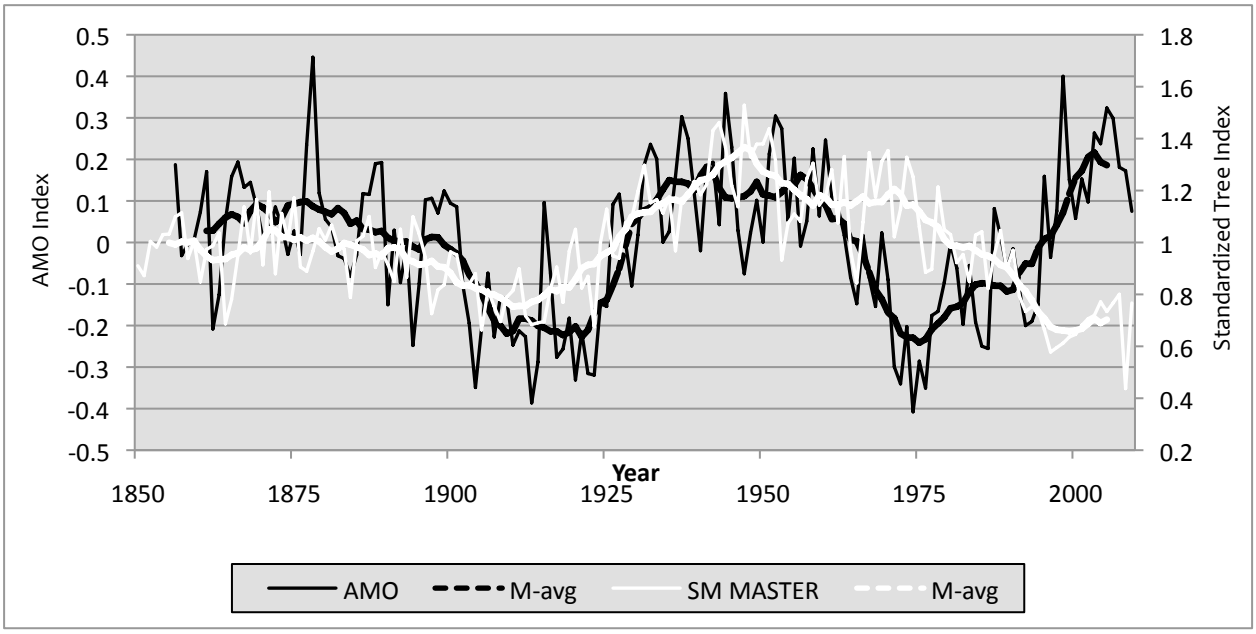

Figure 5.7. The standardized index of the regional master **sugar maple** tree-ring chronology plotted against the AMO at a three year lag. The curves of both the annual variability and smoothed decadal variability (10 year moving average) data are plotted for visual comparison.

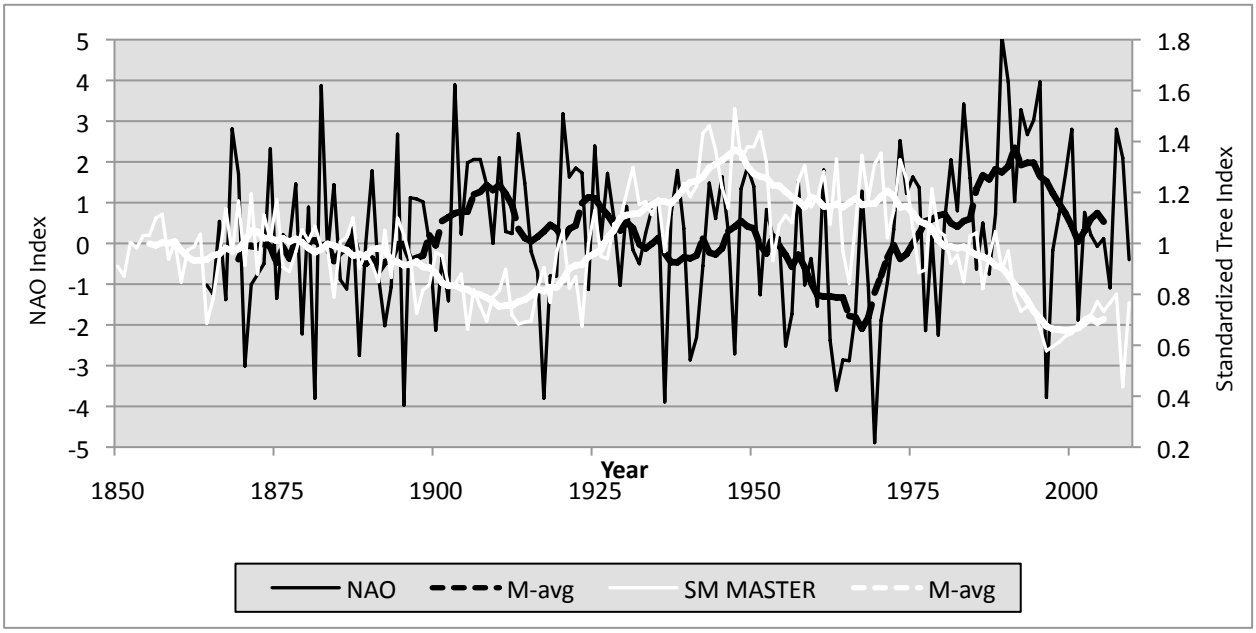

Figure 5.8. The standardized index of the regional master **sugar maple** tree-ring chronology plotted against the NAO at a three year lag. The curves of both the annual variability and smoothed decadal variability (10 year moving average) are plotted for visual comparison.

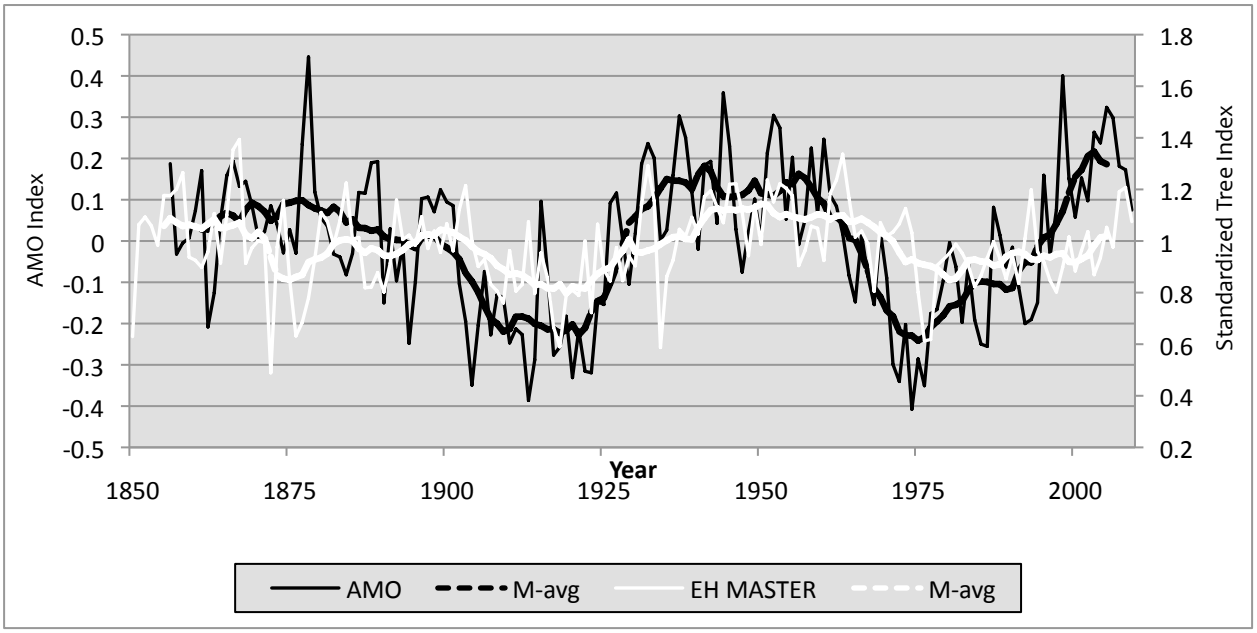

Figure 5.9. The standardized index of the regional master **eastern hemlock** tree-ring chronology plotted against the AMO at a three year lag. The curves of both the annual variability and smoothed decadal variability (10 year moving average) data are plotted for visual comparison.

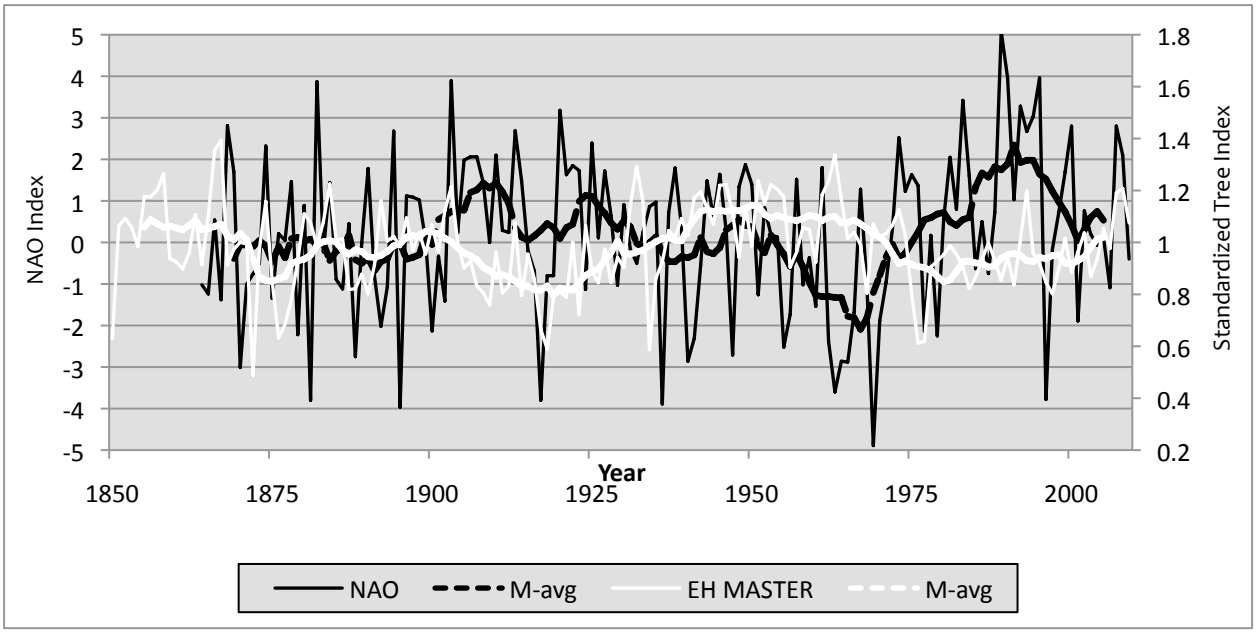

Figure 5.10. The standardized index of the regional master **eastern hemlock** tree-ring chronology plotted against the NAO at a three year lag. The curves of both the annual variability and smoothed decadal variability (10 year moving average) are plotted for visual comparison.

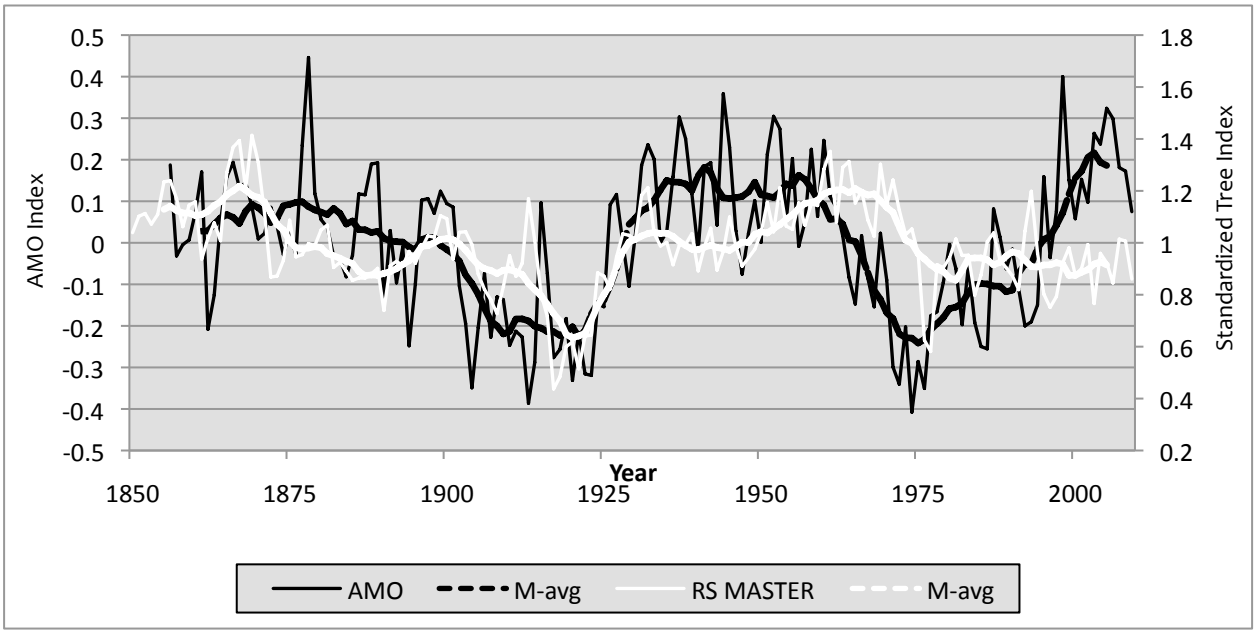

Figure 5.11. The standardized index of the regional master **red spruce** tree-ring chronology plotted against the AMO at a three year lag. The curves of both the annual variability and smoothed decadal variability (10 year moving average) data are plotted for visual comparison.

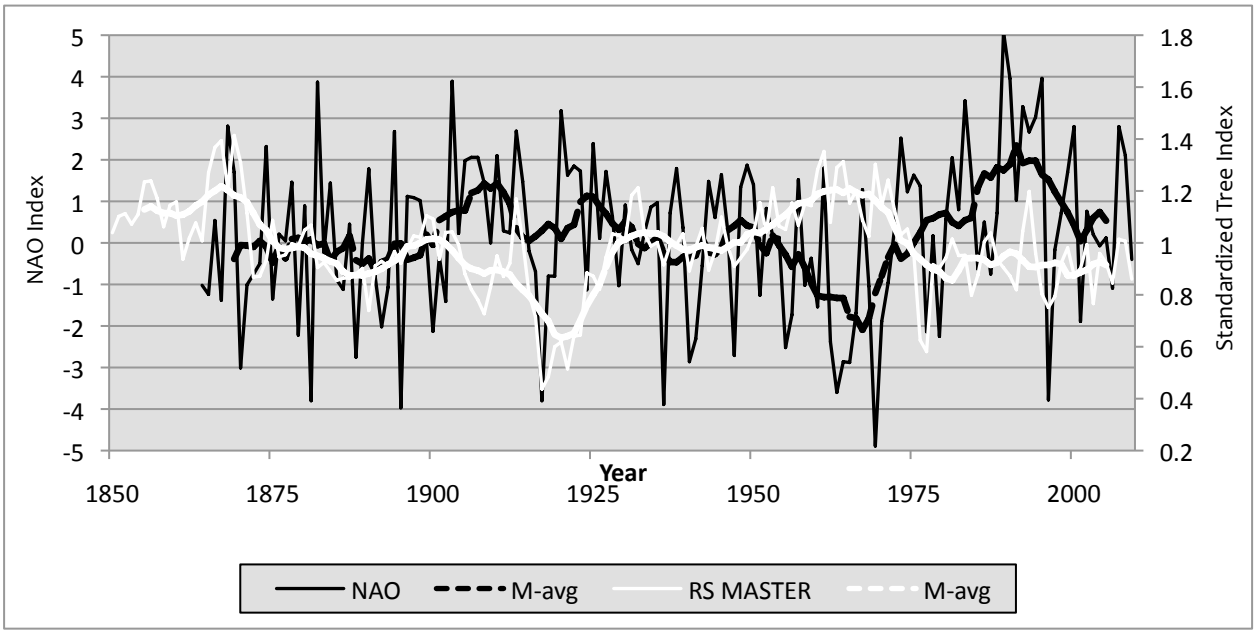

Figure 5.12. The standardized index of the regional master **red spruce** tree-ring chronology plotted against the NAO at a three year lag. The curves of both the annual variability and smoothed decadal variability (10 year moving average) are plotted for visual comparison.

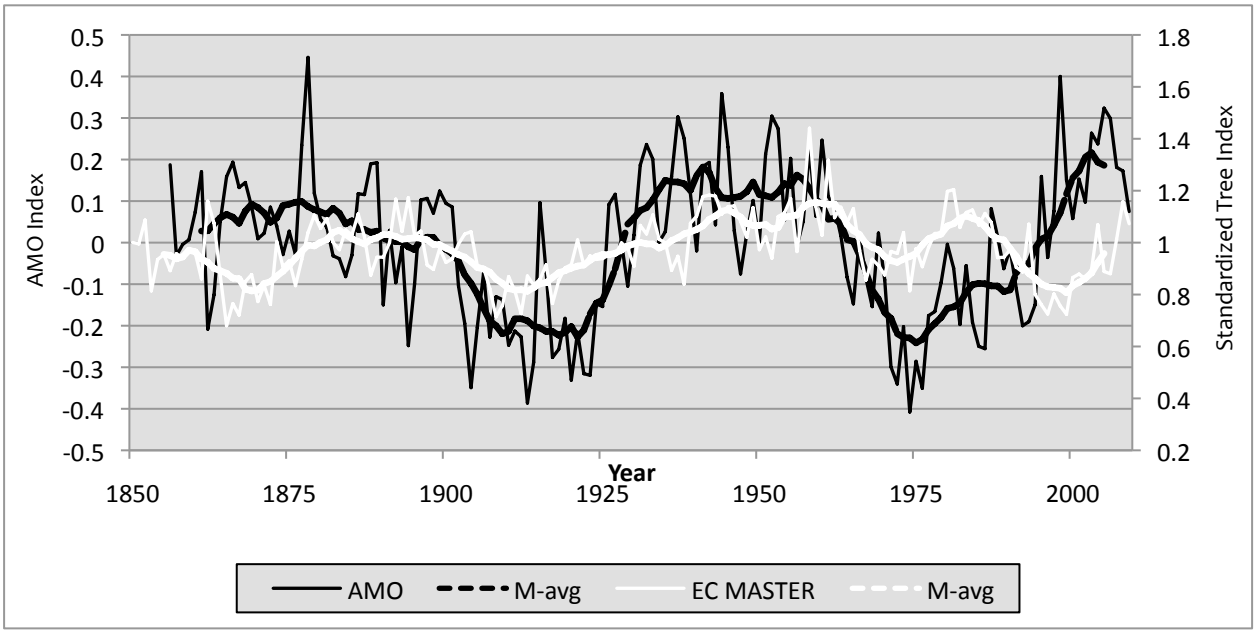

Figure 5.13. The standardized index of the regional master **eastern white cedar** tree-ring chronology plotted against the AMO at a three year lag. The curves of both the annual variability and smoothed decadal variability (10 year moving average) data are plotted for visual comparison.

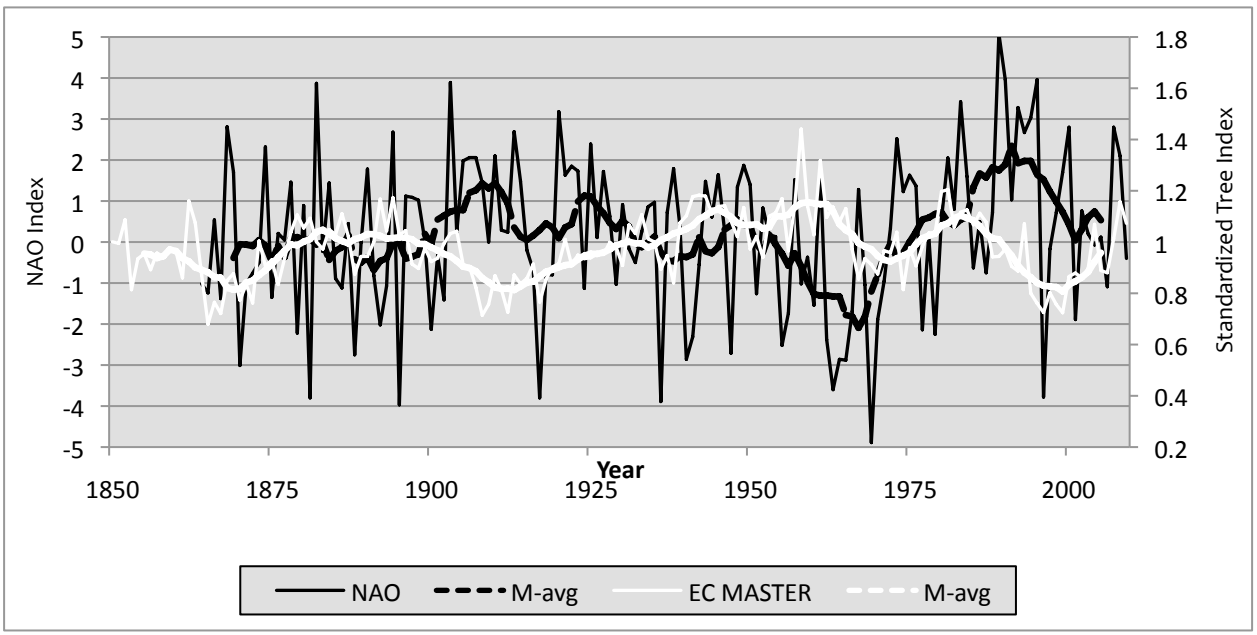

Figure 5.14. The standardized index of the regional master **eastern white cedar** tree-ring chronology plotted against the NAO at a three year lag. The curves of both the annual variability and smoothed decadal variability (10 year moving average) are plotted for visual comparison.

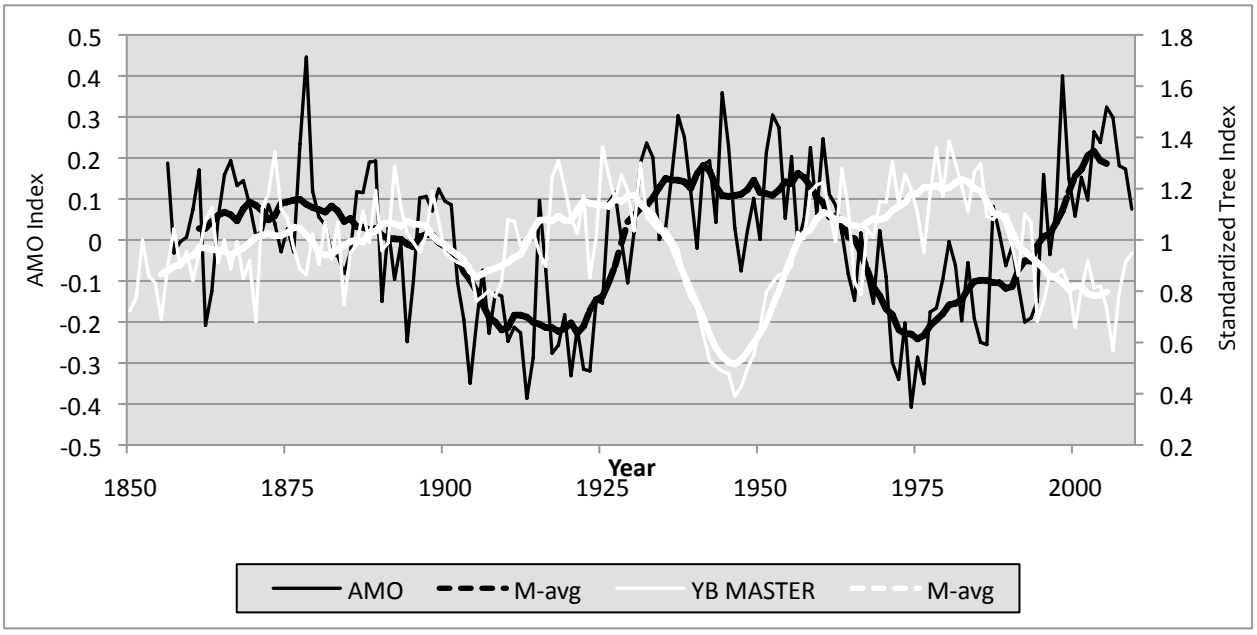

Figure 5.15. The standardized index of the regional master **yellow birch** tree-ring chronology plotted against the AMO at a three year lag. The curves of both the annual variability and smoothed decadal variability (10 year moving average) data are plotted for visual comparison.

5.4 Modulation of Radial Tree Growth through GCOAIs

The precedent setting element of this report is clearly the relationships of some of New Brunswick's most important tree species to the climatic effects of the North Atlantic Ocean. The analysis employed is relatively simple and cannot imply causation however; the long-term trends in the radial growth of the majority of the tree species studied illustrate moderate to strong relationships to the oscillations in long-term ocean conditions of sea surface temperature and sea level pressure.

The ten year moving average correlation analysis using the tree-ring chronologies from the 36 sample sites and the instrumental measurements of the AMO and NAO produced variable, yet primarily highly significant results (Tables 5.10 and 5.11). The patterns across the sample area indicate the effects of long-term ocean-atmosphere fluctuation reach far inland, against the westerly air flow of the Maritime latitude. Generally speaking, the shade tolerant tree species displayed positive

reaction to positive phases of the AMO and a negative reaction to positive phases of the NAO. Depending on species, the effects were geographically uneven. Sugar maple exhibited a positive response to AMO at mid-latitudes of the study area and a negative response to NAO that was continentally stronger. Yellow birch demonstrated a negative response to AMO that was stronger in coastal areas but, the species showed random and insignificant response to the NAO. Eastern hemlock illustrated a positive response to AMO and a negative response to NAO that were both stronger continentally. Red spruce revealed a nearly geographically balanced positive response to AMO and negative response to NAO; both were somewhat spotty across the study area. Eastern white cedar presented a positive response to AMO and a negative response to NAO that were both stronger continentally. White pine established generally insignificant results with both the AMO and NAO but exhibited an interesting weak positive response to NAO in the most northern portion of the study area and a weak negative response to NAO in the most southern reaches.

These results suggest the AMO and NAO effect shade tolerant tree species to a greater degree in more continental positions. Yellow birch, a moderately shade tolerant species, displays the opposite response to the AMO and does so more strongly in coastally proximate areas. Besides the insignificant results of the white pine, the effects of these two ocean-atmosphere oscillating conditions do not seem to have any effects across the latitudinal gradient of the study area. Beyond the pattern of influence, it appears the two most widespread and destructive outbreaks of spruce budworm (*Choristoneura fumiferana*) in the 20th century both occurred during negative phases of the AMO; suggesting that periods of unfavorable climate may reduce the ability of spruce to defend against insect attack or negative phases of the AMO provide favorable climatic conditions for spruce budworm. This multi-species, multi-site analysis, in which a great majority of sample sites exhibit significant results illustrating distinctive geographical patterns, contributes a new perspective on the modulating role the ocean may play in influencing the growth and health of New Brunswick forests.

5.5 Regional Climatic Links to GCOAIs

Through various climatic pathways the ocean-atmosphere conditions of the North Atlantic Ocean are able to influence the radial growth of New Brunswick trees. Identification of these pathways would aid in understanding the mechanics of this relationship. General observations suggest positive phases of the AMO are associated with increased summer temperatures in North America (Murphy et al. 2009). Although the NAO index used in this study is measured over the winter months, its influence can affect the evolution of the climate system over the rest of the year (Hurrell et al. 2003). Positive phases of the NAO are associated with colder air masses being drawn southward over New Brunswick and lowering land temperatures in the winter season (Hurrell et al. 2003). A northeastward shift in storm tracks are also associated with positive phases of the NAO which could result in less storms across southern portions of the study area (Hurrell et al. 2003).

After a multiple regression analysis using the AMO and NAO indexes as dependent variables, and the independent climate variables representing the six sample sites from the radial tree growth analysis (data not shown), several patterns of climatic association were evident. These models did exhibit similar problems, likely related to non-linear relationships, as the radial tree growth models which will be discussed later. The results of this analysis demonstrated higher winter temperatures, precipitation anomalies in late spring and early summer, and higher late summer temperatures in positive phases of the AMO. Increased spring precipitation and spring temperatures were connected to positive phases of the NAO, as well as decreased late summer precipitation in northern areas of New Brunswick. These connections to the New Brunswick climate were present across the majority of regression models, however, it is likely more relationships are unidentified.

5.6 Radial Growth Future Forecasts

This section illustrates the results of the multiple stepwise regression models based on the hybrid independent variable set (section 4.5 Climate Variables). This variable set included 38 independent variables consisting of Tmean, Tprecip, SD and RtFr, with the notable exclusion of the TRF D and TRF S thaw/refreeze variables (Table 4.2). Table 5.12 contains descriptive statistics for the models representing the 36 tree-ring chronologies. For the north western sites (Charlo, Edmundston, and Aroostook), all available years during the common interval were used to calibrate the regression models. For the south eastern sites (Miramichi, Fredericton and Moncton), longer common intervals were available and the years were broken into two evaluation periods, corresponding with the positive and negative periods of the AMO, over which two model calibrations were conducted. This produced nine models over the six sites.

The percentage of variance explained by these models is inconsistent across species and sites. Using the adjusted R^2 value to calculate explained variance; the best model explains 74% of actual ring-width variability, the worst model explains only 8% of actual ring-width variability, while the mean explained variance for all models is 35%. Even though all model calibration statistics are illustrated in Table 5.12, only significant models with a P-value less than 0.001 are graphed and applied to Coupled Global Climate Model data for the purpose of forecasting future ring-widths. Further to this constraint on model application, any model with a Durbin-Watson value less than 1.0 was also not utilized for ring-width forecasting. Variance Inflation Factor was one other criterion used to evaluate the strength of the models, however, there were no instances where any model variable exceeded the threshold of greater than 5.0. All significant individual tree-ring master chronologies, model calibration, and future model forecasts are illustrated in Figures 5.16 to 5.27.

The independent variables included in each model are listed in Table 5.14 as a + sign or a – sign, signifying the direction of relationship of each variable to the overall model.

The primary run of models did not include the TRF D and TRF S thaw/refreeze variables as the CGCM3 model did not recreate a usable data set for forecasting this variable (Phillips and Laroque 2009b). A secondary run of models was conducted using 42 independent variables, consisting of the original 38 variables used in the primary run plus the four thaw/refreeze variables. These models are not applied to the future climate data for forecasting purposes, however they are useful to gage the potential importance of thaw/refreeze cycles in the modeling of past radial tree growth in New Brunswick. Of the 54 models produced in the primary run, 28 of these models completed the secondary run with distinctive results. These 28 models included one or all thaw/refreeze variables in the best optimum subset model, most often improving the explained variance of the model. The results of the models that changed in the secondary run are listed in Table 5.13. The changes in explained variance were most pronounced across species rather than across sites. Yellow birch and eastern hemlock models underwent an approximate 12% average increase in explained variance, red spruce and white pine models experienced a 7% average increase in explained variance, while sugar maple models only improved by an average of 4% and eastern white cedar models were nearly unchanged with an average 1.5% improvement in explained variance. Across the sample sites, Charlo models were unchanged after the secondary model run, Edmundston models improved by an average of 7%, Aroostook models improved by an average of 9%, Miramichi models improved by an average of 11%, Fredericton models improved by an average of 5% and Moncton models improved by an average of 6%.

Table 5.12. The least squares stepwise multiple regression model summary information for the AICc selected optimum variable subset is listed here. Model information including the following: site (names abbreviated using first three consonants), tree species (Sp), time period (positive AMO includes only positive multidecadal oscillation periods and negative AMO includes only negative multidecadal oscillation periods), degrees of freedom (DF), elevation lapse rate (ELR) which indicates the elevation level the data was adjusted for, climate station (CS) elevation, number of variables (# Vr) included in the AICc selected model, coefficient of determination (R^2), adjusted coefficient of determination (Adj R^2) which adjusts the R^2 value for the number of explanatory terms in the model and higher values are indicated by a darker cell fill, P-value that indicates the significance of the model through an ANOVA, Durbin-Watson (D-W) statistic which indicates a model has negative autocorrelation of the residuals if >2, positive serial correlation if <2 and serious positive serial correlation problems if <1, variance inflation factor (VIF) which quantifies the level of multicollinearity of a given regression coefficient (a conservative cutoff is considered any value >5 to be correlated with other independent variables in the model, thus increasing substantially the standard error.), finally the last column counts the number of winter variables (WV) included in the model. Winter variables include Root Freeze A or B, TJanA, TFebA, TMarA, TJanB, TFebB, TMarB, SD Index 1 or 2. Only models with a p-value of <0.001 and a durbin-watson value above 1.0 are run on future data and those models are indicated with black text in this table.

Site	Sp	Time Period	DF	ELR	CS	# Vr	R^2	Adj R^2	P-value	D-W	VIF	WV
Chr	SM	1940-2005	58	267m	40m	7	0.399	**0.326**	<0.0001	1.5	<1.3	1
	YB	1940-2005	58	267m	40m	7	0.411	**0.340**	<0.0001	1.0	<1.2	3
	EH	1940-2005	58	115m	40m	7	0.398	**0.326**	<0.0001	1.4	<1.3	1
	RS	1940-2005	58	267m	40m	5	0.313	**0.254**	<0.001	1.3	<1.2	2
	EC	1940-2005	53	267m	40m	12	0.673	**0.599**	<0.0000001	1.5	<1.5	5
	WP	1940-2005	61	115m	40m	4	0.187	**0.134**	0.012	0.7	<1.1	2
Edm	SM	1936-2005	59	343m	155m	10	0.616	**0.551**	<0.0000001	1.2	<1.8	2
	YB	1936-2005	59	343m	155m	10	0.476	**0.387**	<0.0001	1.1	<1.6	5
	EH	1936-2005	63	250m	155m	6	0.371	**0.311**	<0.0001	1.1	<1.4	2
	RS	1936-2005	57	250m	155m	8	0.455	**0.379**	<0.0001	1.1	<1.2	2
	EC	1936-2005	59	250m	155m	10	0.531	**0.451**	0.000001	1.4	<1.3	3
	WP	1936-2005	55	250m	155m	14	0.601	**0.500**	<0.000001	1.4	<1.5	2
Ars	SM	1932-2004	64	414m	91m	8	0.367	**0.288**	<0.001	0.8	<1.5	—
	YB	1932-2004	68	414m	91m	4	0.205	**0.158**	<0.01	0.7	<1.1	2
	EH	1932-2004	63	91m	91m	9	0.557	**0.494**	<0.0000001	1.1	<1.7	5

	RS	1932-2004	67	414m	91m	4	0.201	0.153	<0.01	0.8	<1.1	1
	EC	1932-2004	64	91m	91m	8	0.441	0.372	<0.00001	1.0	<1.4	4
	WP	1932-2004	65	91m	91m	7	0.412	0.349	<0.00001	1.2	<1.2	3
Mrm	SM	Positive AMO	63	168m	33m	6	0.360	0.299	<0.0001	0.8	<1.3	3
	SM	Negative AMO	53	168m	33m	5	0.572	0.532	<0.0000001	1.3	<1.1	3
	YB	Positive AMO	65	33m	33m	4	0.266	0.221	<0.001	0.5	<1.1	1
	YB	Negative AMO	53	33m	33m	5	0.292	0.226	<0.01	1.2	<1.2	3
	EH	Positive AMO	59	33m	33m	10	0.575	0.503	<0.0000001	1.4	<1.4	3
	EH	Negative AMO	49	33m	33m	9	0.439	0.336	<0.001	0.9	<1.4	2
	RS	Positive AMO	61	33m	33m	6	0.344	0.280	<0.001	1.1	<1.1	1
	RS	Negative AMO	35	33m	33m	12	0.691	0.585	<0.00001	1.7	<2	4
	EC	Positive AMO	62	33m	33m	7	0.462	0.401	0.000001	1.5	<1.2	2
	EC	Negative AMO	55	33m	33m	3	0.177	0.132	0.013	0.8	<1.1	2
	WP	Positive AMO	66	33m	33m	3	0.119	0.079	0.038	1.0	<1.1	1
	WP	Negative AMO	54	33m	33m	4	0.264	0.210	<0.01	0.9	<1.1	—
Frd	SM	Positive AMO	63	70m	20m	5	0.292	0.236	<0.001	0.7	<1.1	1
	SM	Negative AMO	51	70m	20m	7	0.471	0.398	<0.0001	0.9	<1.3	2
	YB	Positive AMO	61	70m	20m	7	0.318	0.240	0.001	1.1	<1.3	—
	YB	Negative AMO	53	70m	20m	5	0.419	0.364	<0.0001	1.4	<1.2	1
	EH	Positive AMO	56	70m	20m	12	0.495	0.387	<0.0001	2.0	<1.5	5
	EH	Negative AMO	51	70m	20m	7	0.394	0.311	<0.001	1.4	<1.4	1
	RS	Positive AMO	58	70m	20m	10	0.446	0.351	<0.001	1.1	<1.5	4
	RS	Negative AMO	44	70m	20m	9	0.498	0.395	<0.001	1.4	<1.3	3
	EC	Positive AMO	60	70m	20m	8	0.345	0.258	<0.001	1.1	<1.3	3
	EC	Negative AMO	47	70m	20m	11	0.628	0.541	<0.000001	1.4	<1.4	2
	WP	Positive AMO	49	70m	20m	7	0.314	0.216	<0.01	1.4	<1.2	1
	WP	Negative AMO	53	70m	20m	5	0.559	0.518	<0.0000001	1.4	<1.3	—
Mnc	SM	Positive AMO	34	157m	72m	13	0.814	0.743	<0.0000001	1.8	<1.6	3
	SM	Negative AMO	49	157m	72m	7	0.348	0.255	<0.01	1.0	<1.4	—
	YB	Positive AMO	43	72m	72m	4	0.325	0.262	<0.01	0.5	<1.2	—
	YB	Negative AMO	48	72m	72m	8	0.559	0.486	<0.00001	1.2	<1.5	1
	EH	Positive AMO	45	72m	72m	2	0.136	0.098	0.037	0.7	<1.1	—
	EH	Negative AMO	52	72m	72m	4	0.320	0.268	<0.001	0.9	<1.2	1
	RS	Positive AMO	43	72m	72m	4	0.282	0.216	<0.01	0.7	<1.1	—
	RS	Negative AMO	44	72m	72m	4	0.273	0.207	<0.01	0.9	<1.2	1
	EC	Positive AMO	37	72m	72m	10	0.718	0.642	<0.000001	1.5	<1.5	2
	EC	Negative AMO	50	72m	72m	6	0.353	0.276	0.001	1.0	<1.2	2
	WP	Positive AMO	31	72m	72m	16	0.786	0.675	<0.00001	1.6	<3.9	6
	WP	Negative AMO	46	72m	72m	10	0.518	0.413	<0.0001	1.5	<1.4	4

Table 5.13. The least squares stepwise multiple regression model summary information for the model run including thaw refreeze independent variables is listed here. The optimum variable subset is again selected by AICc. The table includes all model information listed in Table 5.12, as well as the following additional values: thaw refreeze (TRF) variables included in the AICc selected model are illustrated (TRFD=thaw refreeze deep, TRFS=thaw refreeze surfacial, for both current [A] and prior [B] years). Winter variables include Root Freeze A or B, TJanA, TFebA, TMarA, TJanB, TFebB, TMarB, SD Index 1 or 2, TRF D and TRF S. Only models which experienced a change from those in Table 5.12 are illustrated.

Site	Sp	Time Period	DF	ELR	CS	#Vr	R^2	AdjR^2	P-value	DW	VIF	TRFD	TRFS	WV
Edm	SM	1936-2005	58	343m	155m	11	0.650	0.584	<0.000000001	1.2	<1.8	—	A	3
	EH	1936-2005	59	250m	155m	10	0.470	0.381	<0.0001	1.2	<1.6	—	A, B	4
	RS	1936-2005	51	250m	155m	14	0.598	0.487	<0.00001	1.3	<2.2	A	A,B	5
	EC	1936-2005	56	250m	155m	13	0.602	0.510	<0.000001	1.6	<1.3	A	B	4
Ars	YB	1932-2004	66	414m	91m	6	0.270	0.203	<0.01	1.1	<1.3	A,B	—	3
	EH	1932-2004	60	91m	91m	12	0.638	0.565	<0.0000001	1.4	<1.7	—	A	5
	WP	1932-2004	60	91m	91m	12	0.580	0.496	<0.000001	1.5	<1.3	B	A	5
Mrm	SM	Negative	52	168m	33m	6	0.593	0.546	0.00000001	1.3	<1.1	A	—	4
	YB	Positive	61	33m	33m	8	0.438	0.364	<0.0001	0.7	<1.2	—	A,B	4
	YB	Negative	50	33m	33m	10	0.465	0.379	<0.0001	1.3	<2.2	A	A	5
	EH	Positive	59	33m	33m	10	0.571	0.498	0.0000001	1.4	<1.4	B	—	4
	EH	Negative	42	33m	33m	16	0.697	0.581	<0.00001	1.4	<1.8	A	B	4
	RS	Positive	57	33m	33m	12	0.570	0.480	<0.000001	1.3	<1.6	—	A	3
	RS	Negative	31	33m	33m	15	0.789	0.687	<0.000001	2.3	<1.6	A, B	—	5
	WP	Positive	65	33m	33m	4	0.174	0.124	0.013	1.1	<1.2	B	—	2
Frd	SM	Positive	61	70m	20m	7	0.380	0.309	<0.0001	0.8	<1.2	B	—	2
	YB	Negative	50	70m	20m	8	0.588	0.522	<0.000001	1.8	<1.5	B	A	2
	EH	Positive	56	70m	20m	12	0.503	0.396	<0.0001	1.9	<1.5	B	—	6
	EH	Negative	50	70m	20m	8	0.516	0.439	<0.00001	1.5	<1.4	B	A	4
	RS	Positive	60	70m	20m	8	0.389	0.307	<0.001	1.0	<1.4	—	B	4
	EC	Negative	46	70m	20m	12	0.661	0.572	<0.000001	1.3	<1.4	A	—	3
	WP	Positive	50	70m	20m	6	0.287	0.201	<0.01	1.3	<1.1	B	—	1
	WP	Negative	50	70m	20m	8	0.658	0.603	<0.0000001	1.9	<1.3	A, B	—	2
Mnc	SM	Negative	50	157m	72m	6	0.370	0.294	0.001	1.0	<1.4	A	—	1
	EH	Negative	37	72m	72m	12	0.674	0.568	<0.00001	1.4	<2.1	B	A,B	6
	RS	Negative	45	72m	72m	4	0.256	0.190	<0.01	1.0	<1.1	B	—	2
	EC	Positive	40	72m	72m	7	0.647	0.585	<0.000001	1.5	<1.5	—	B	2
	EC	Negative	49	72m	72m	7	0.392	0.306	0.001	0.8	<1.2	A	—	3

	Ch	Ed	Ar	Mi	Mi	Fr	Fr	Mo	Mo	Ch	Ed	Ar	Mi	Mi	Fr	Fr	Mo	Mo	Ch	Ed	Ar	Mi	Mi	Fr	Fr	Mo	Mo	Ch	Ed	Ar	Mi	Mi	Fr	Fr	Mo	Mo	Ch	Ed	Ar	Mi	Mi	Fr	Fr	Mo	Mo	
				+	-	+	-	+	-				+	-	+	-	+	-				+	-	+	-	+	-				+	-	+	-	+	-				+	-	+	-		
	SM	SM	SM	SM	SM	SM	SM	SM	SM	YB	YB	YB	YB	YB	YB	YB	YB	YB	EH	EH	EH	EH	EH	EH	EH	EH	EH	RS	RS	RS	RS	RS	RS	RS	RS	RS	EC	EC	EC	EC	EC	EC	EC	EC	EC	WP	WP	WP	WP	WP	WP	WP	WP	WP	
SDIndex2		-		-										+							-	-								-	-								-	-						+		SDIndex2
PAprB	-							-															+												-			+						-		PAprB
PMayB									-								-																										+	-				PMayB
PJunB	+		+	+											-	+			+				-	+						+	-							+	+								PJunB
PJulB		-			-										+	+	+	+						+	+														-	+					+	+	PJulB
PAugB								+					+													+							+					-			+					PAugB
PSepB															-		-	-		+							-															+		-	-	PSepB
POctB			-		-		-	-							+			+	+																		+	+						-	-	POctB
PNovB	+	+							+													-	+					+	+		-			+	+	-			+	-		+	+	-			PNovB
Root FrB		-			+	+	+			+	+	+							-	-				-		+							-	-								-	+	Root FrB
TJan B										-															-			+															+			TJan B
TFebB								-			+													-	+														+	+	+			+			TFebB
TMarB				-																	+																		-			+			+		TMarB
TAprB			-				-	-		+																														-				+			TAprB
TMayB								+	-									+																+									+			TMayB
TJunB				-		-	+	-												-																				+	-			-			TJunB
TJulB	-							-										+		-		+							+		+															TJulB
TAugB													-		-						+																		-				+				TAugB
TSepB	-										-					+							+	-															+					-	-		TSepB
TO-N-DB																					+	+																					+				TO-N-DB
SDIndex1				-												+				-	-	-	-	-									-		-												SDIndex1
PAprA		+								+	+				+				+				-									-	+					+					-			PAprA
PMayA		-							-										+	-		+												+									+				PMayA
PJunA			+	+		+		+									+		+				-									-					+						+	+		PJunA
PJulA												+				+	+	+	+					+	+	+																	+	+	+		PJulA
PAugA											+		+		+									+									+									+	+	+		+	PAugA
PSepA		+	+									+			-		-				+							+	+	+													-	-			PSepA
Root FrA	-				+		+	-			+	+		+														-				+	+				-					-	+		Root FrA
TJanA																		-									+											-		+			+			TJanA
TFebA					+			-			+		-				+				+	-					+							+	+	-	+	+		+			+		TFebA
TMarA														+							+								-					+		+						-				TMarA
TAprA	-	-					-		-													+																	+	+							TAprA
TMayA								+	-	+					-						-																		+				+	+			TMayA
TJunA						-								+										-															-	-	-			-			TJunA
TJulA		+	+																			+	-	-														-	-							TJulA
TAugA							+	-	+													-					-														+			-			TAugA
TSepA			-											-												-														-					-		TSepA
TOctA		+	+			+				-	-														+															+	+				-	-	TOctA

Table 5.14. Independent variables included in each AICc selected multiple regression model are shown here. The 38 independent variables included in the multiple regression analysis are listed in the end columns, with winter variables in white text with grey highlighting. Sites are titled across the top row and species is specified in row three. Charlo (Ch) model runs from 1940-2005, Edmundston (Ed) models run from 1936-2005, Aroostook (Ar) models run from 1932-2004, Miramichi (Mi), Fredericton (Fr), and Moncton (Mo) models run over the positive AMO periods (indicated by a +), and the negative AMO periods (indicated by a -), which vary between cities due to the length of climate data available. Inclusion of a variable in a model is marked by + or – in a particular cell which signifies the direction of the relationship.

5.7 Sugar Maple Model Interpretation for SRES B1 Scenario

The performance of the sugar maple regression models resulted in four of nine models passing the acceptability criteria (Table 5.12). The application of the four approved models to the CGCM3 future climate data scenario SRES B1 predicted future radial growth divergence of approximately 45% declines in Charlo, 10% increases Edmundston, 45% increases in Miramichi with the negative AMO model and 100% declines in Moncton with the positive AMO model (Figure 5.16). These four models produced a relatively high average explained variance of 54%.

Due to poor geographic coverage, it is difficult to assess potential change in sugar maple growth despite several strong models. Across all sugar maple models, several patterns in variable selection were apparent, despite important variables likely being absent from these models. Table 5.14 displays the importance of high June precipitation, especially during positive phases of the AMO. A negative response to warm April temperatures is a commonly selected variable, as is a negative response to warm June temperatures in the previous growing season. Other then these general patterns the selection of variables among the sugar maple models is somewhat random. It would be expected that geographically distant sites would produce models with inconsistent variable selection, especially considering the poor correlations between several of the sugar maple chronologies.

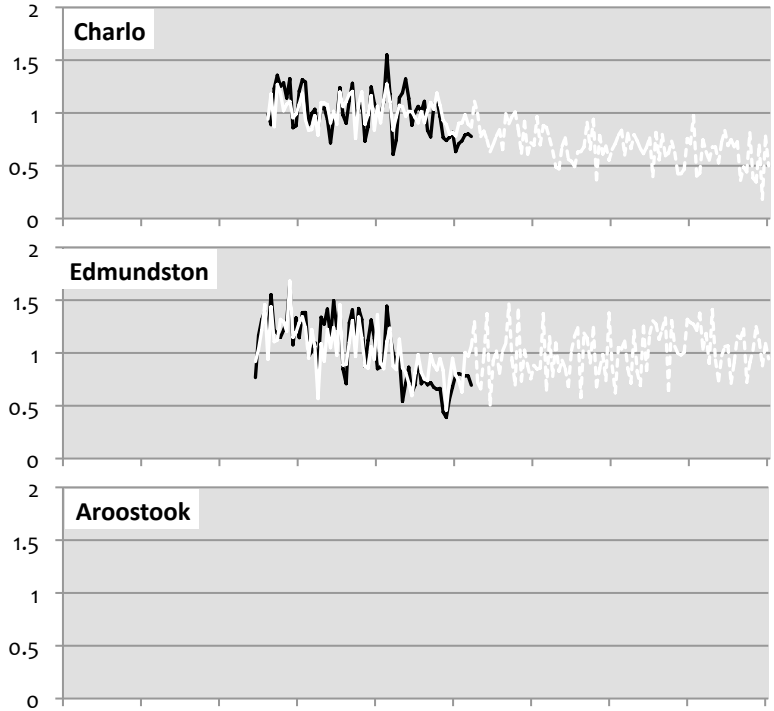
Charlo
Edmundston
Aroostook
2
1.5
1
0.5
0


Miramichi +AMO
Miramichi -AMO
Fredericton +AMO
Fredericton -AMO
2
1.5
1
0.5
0
1875
1900
1925
1950
1975
2000
2025
2050
2075
2100

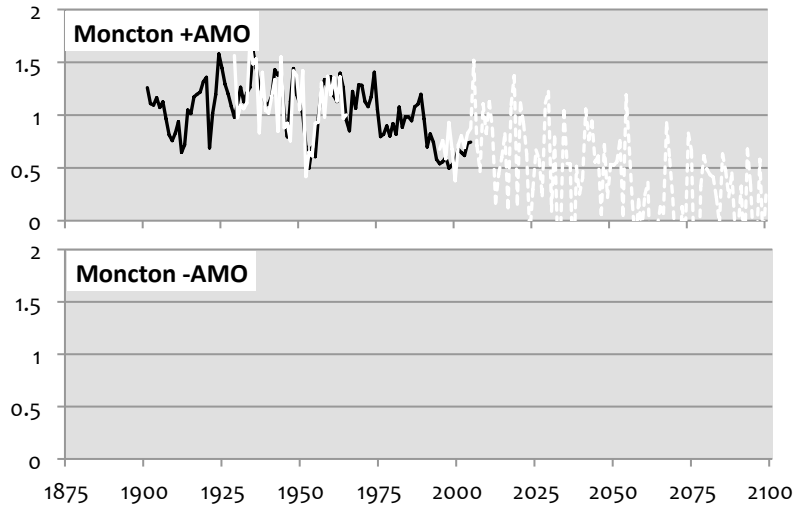

Figure 5.16. Significant **sugar maple B1** scenario forecasts are illustrated here. Black lines are actual standardized annual ring-widths, solid white lines are model calibration periods, dotted white lines are modeled future annual ring-widths. Y-axis is standardized ring-width index, while x-axis is the year.

5.8 Sugar Maple Model Interpretation for SRES A1b Scenario

The performance of the sugar maple regression models resulted in four of nine models passing the acceptability criteria (Table 5.12). The application of the four approved models to the CGCM3 future climate data scenario SRES A1b predicted future radial growth divergence of approximately 65% declines in Charlo, 20% increases Edmundston, 40% increases in Miramichi with the negative AMO model and 100% declines in Moncton with the positive AMO model (Figure 5.17). The A1b model outputs make it equally difficult to assess potential future growth patterns of sugar maple due to poor geographic coverage.

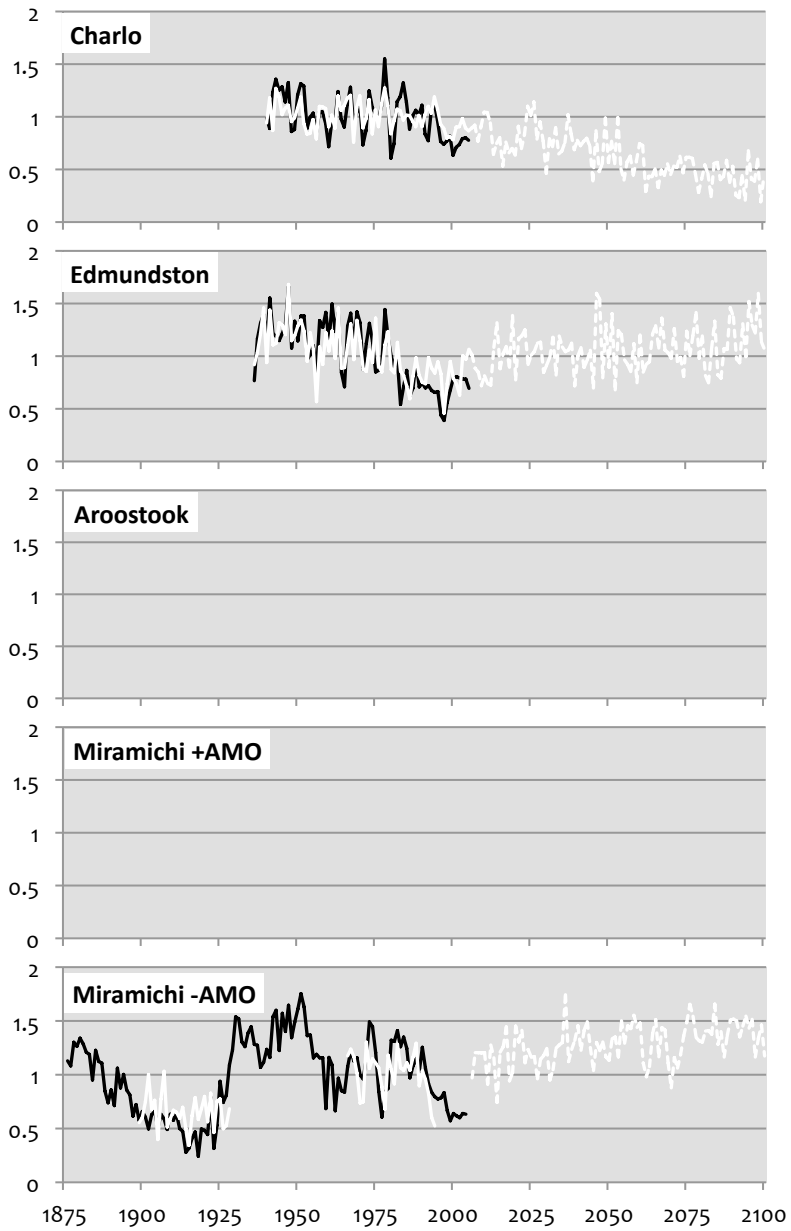

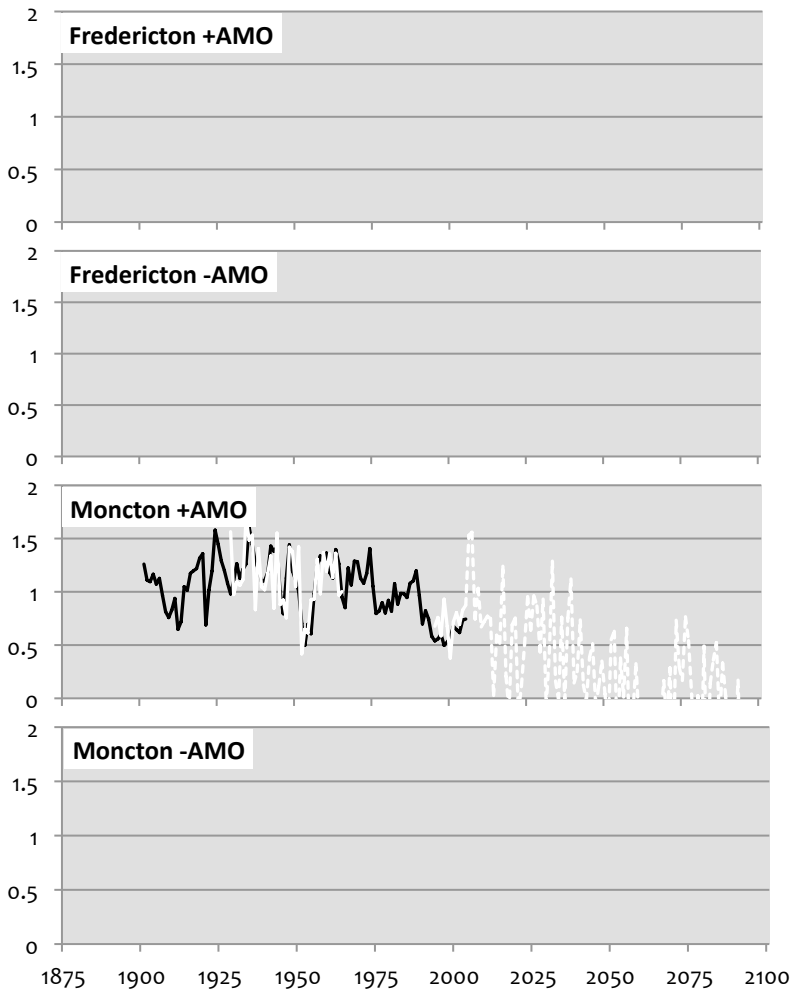

Figure 5.17. Significant **sugar maple A1b** scenario forecasts are illustrated here. Black lines are actual standardized annual ring-widths, solid white lines are model calibration period fits, dotted white lines are modeled future annual ring-widths. Y-axis is standardized ring-width index, while x-axis is the year.

5.9 Yellow Birch Model Interpretation for SRES B1 Scenario

The performance of the yellow birch regression models resulted in five of nine models passing the acceptability criteria (Table 5.12). The application of the five approved models to the CGCM3 future climate data scenario SRES B1 predicted future radial growth divergence of approximately 25% declines in Charlo, 20% increases Edmundston, 40% decreases in Fredericton with the positive AMO model, 20% increases with the negative AMO model, and 65% increases in Moncton with the negative AMO model (Figure 5.18). These five models result in an average 34% explained variance.

Poor geographic coverage, constrains the potential to interpret the future trends of yellow birch radial growth and the low explained variance is a limiting factor when interpreting the patterns in the selected variables of the models. Although important variables have likely been left out of these models there is still an evident pattern of positive response in yellow birch to high precipitation in July and August (Table 5.14). This species, therefore, appears to be most limited by summer drought. Northern sites, oddly, display a positive reaction to high levels of the root freeze index. Beyond those alignments among the variables, the remaining predictors exhibit a more random distribution.

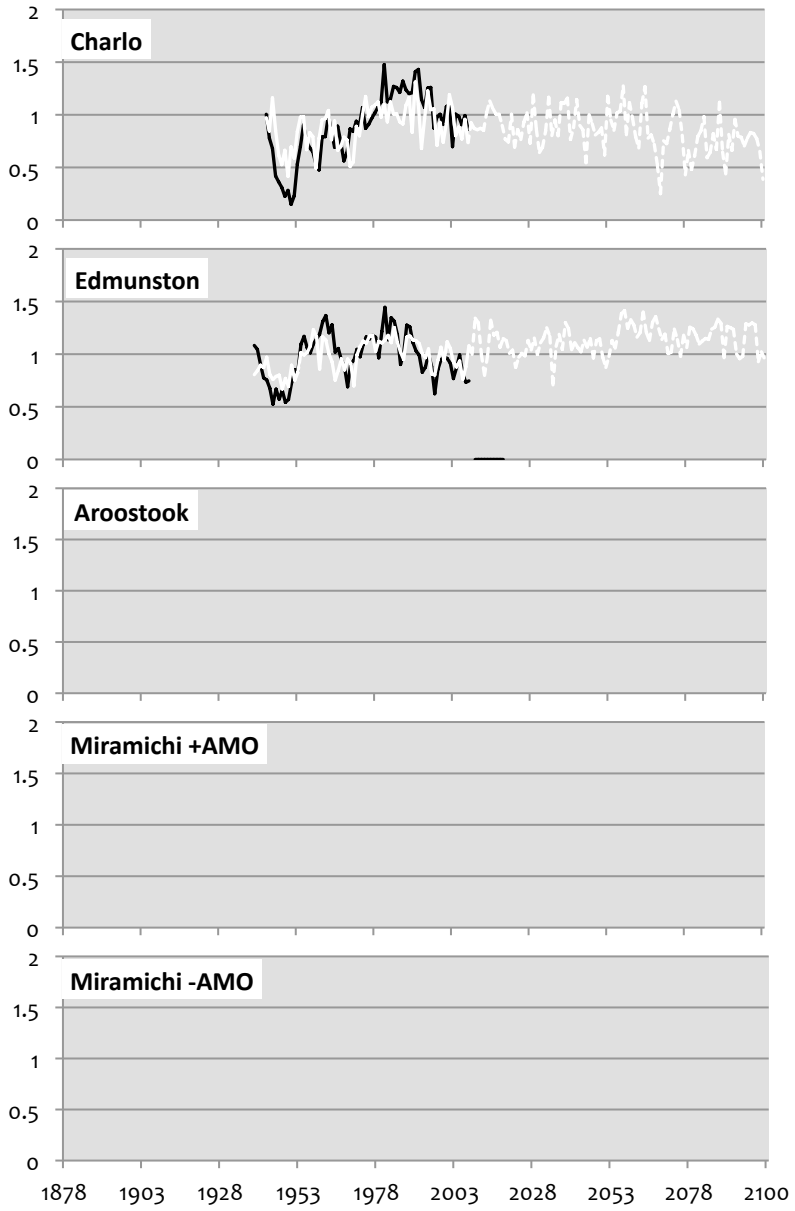

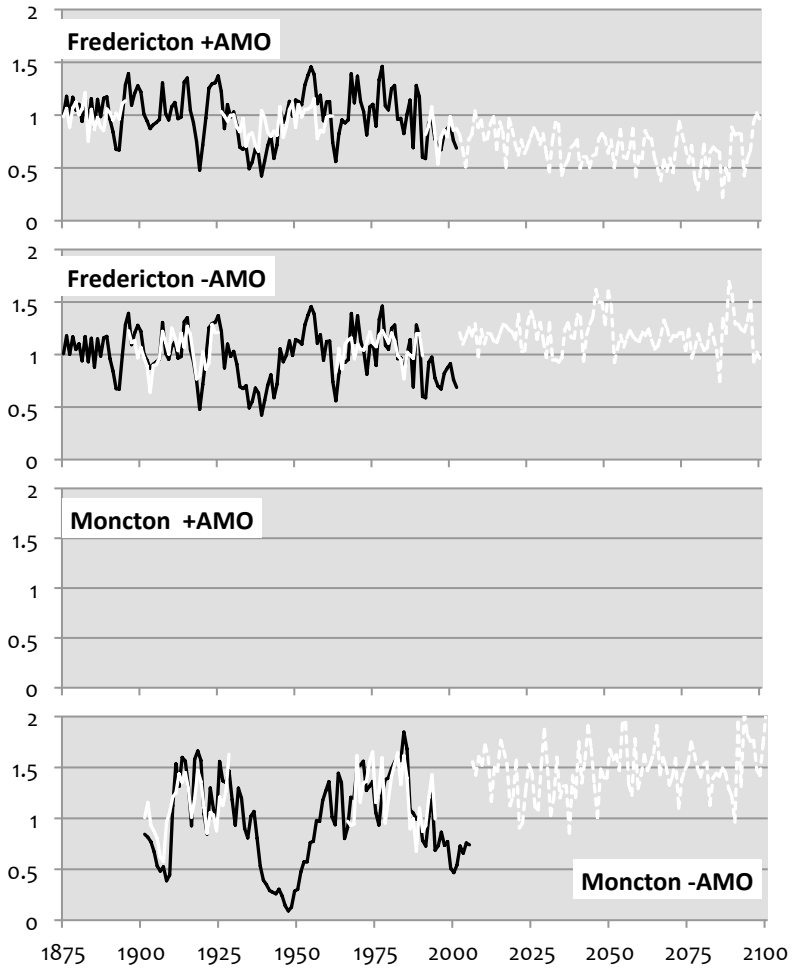

Figure 5.18. Significant **yellow birch B1** scenario forecasts are illustrated here. Black lines are actual standardized annual ring-widths, solid white lines are model calibration period fits, dotted white lines are modeled future annual ring-widths. Y-axis is standardized ring-width index, while x-axis is the year.

5.10 Yellow Birch Model Interpretation for SRES A1b Scenario

The performance of the yellow birch regression models resulted in five of nine models passing the acceptability criteria (Table 5.12). The application of the five approved models to the CGCM3 future climate data scenario SRES A1b predicted future radial growth divergence of approximately 30% declines in Charlo, 30% increases Edmundston, 50% decreases in Fredericton with the positive AMO model, 30% increases with the negative AMO model, and 80% increases in Moncton with the negative AMO model (Figure 5.19). The SRES A1b climate change scenario resulted in the radial growth models moving to more extreme changes, although there was no clear direction to those changes.

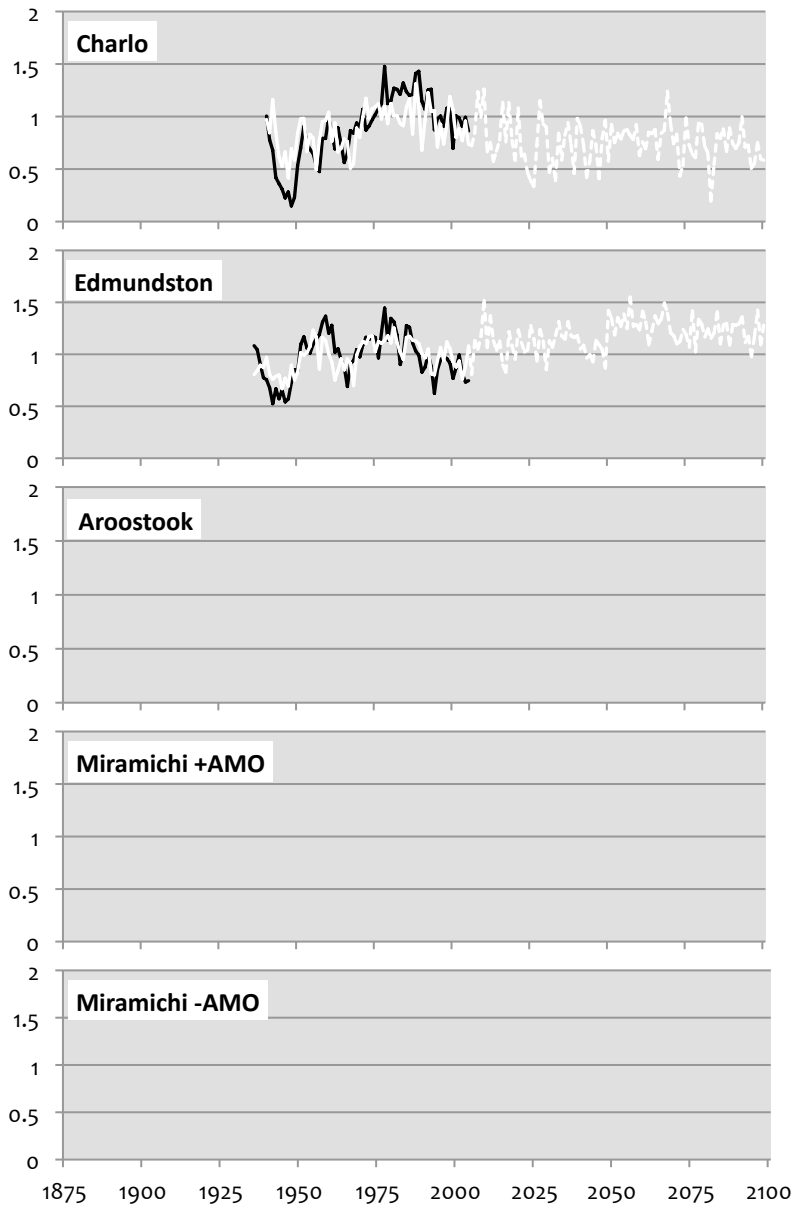

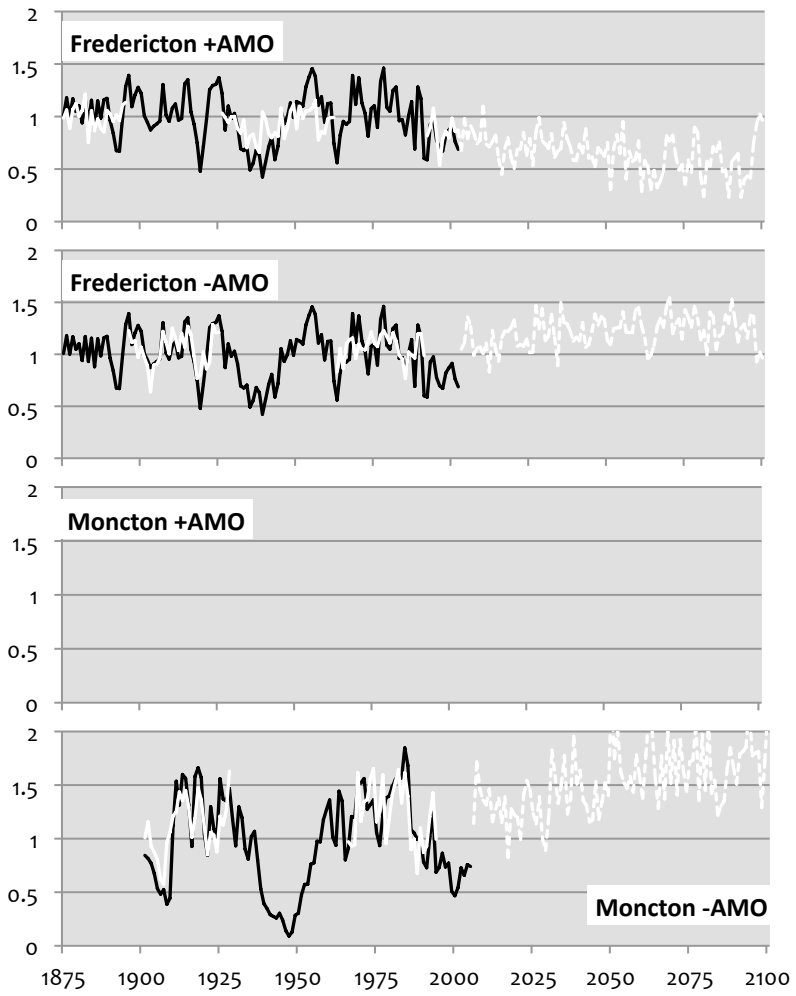

Figure 5.19. Significant **yellow birch A1b** scenario forecasts are illustrated here. Black lines are actual standardized annual ring-widths, solid white lines are model calibration period fits, dotted white lines are modeled future annual ring-widths. Y-axis is standardized ring-width index, while x-axis is the year.

5.11 Eastern Hemlock Model Interpretation for SRES B1 Scenario

The performance of the eastern hemlock regression models resulted in six of nine models passing the acceptability criteria (Table 5.12). The application of the six approved models to the CGCM3 future climate data scenario SRES B1 predicted future radial growth divergence of approximately 15% declines in Charlo, 20% decreases in Edmundston, 30% decreases in Aroostook, 30% increases in Miramichi with the positive AMO model, 20% declines in Fredericton with the positive AMO model, and 5% increases in Fredericton with the negative AMO model (Figure 5.20). These five models result in an average 39% explained variance.

Better geographic coverage, allows for more potential to interpret the future trends of eastern hemlock radial growth and it appears that more continentally distributed sites should experience a decline in radial growth from historic levels under the SRES B1 scenario. The low explained variance is a limiting factor when interpreting the patterns in the selected variables of the models and although important variables have likely been left out of these models, there is still an evident pattern of negative response in eastern hemlock to deep winter snow depths (Table 5.14). The most limiting element of climate to eastern hemlock radial growth is likely the shorter growing season imposed by a deep snow pack. At the most northern site, near the range limit, spring and summer precipitation is the largest hindrance to radial growth. Beyond those alignments among the variables, the remaining predictors exhibit a very random distribution.

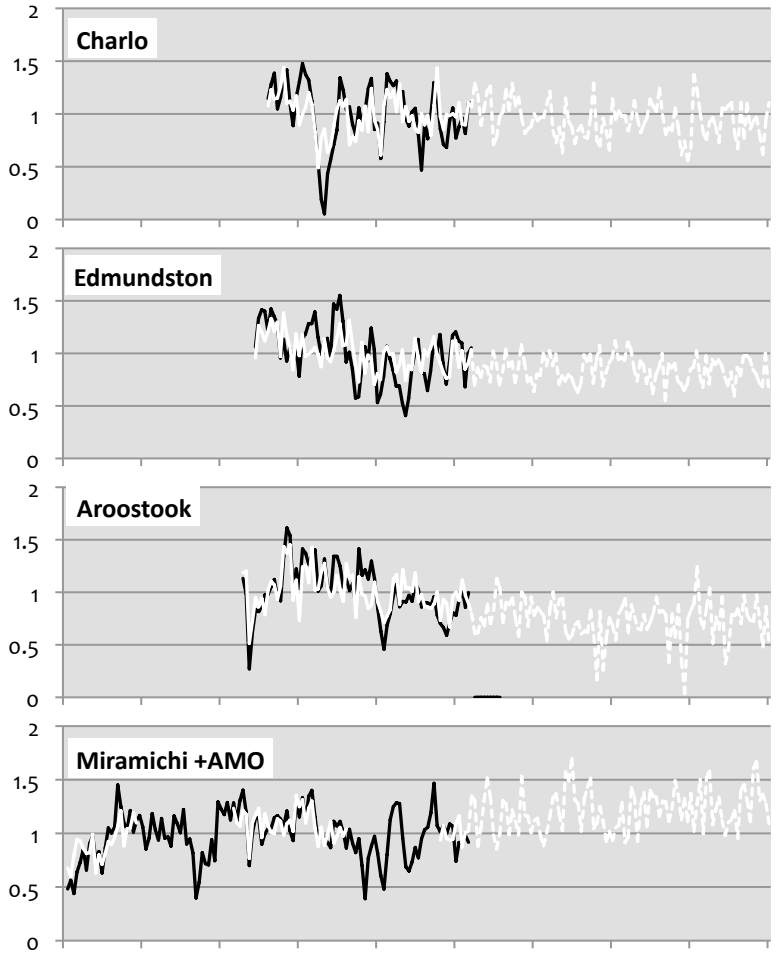
Charlo
Edmundston
Aroostook
Miramichi +AMO
2
1.5
1
0.5
0

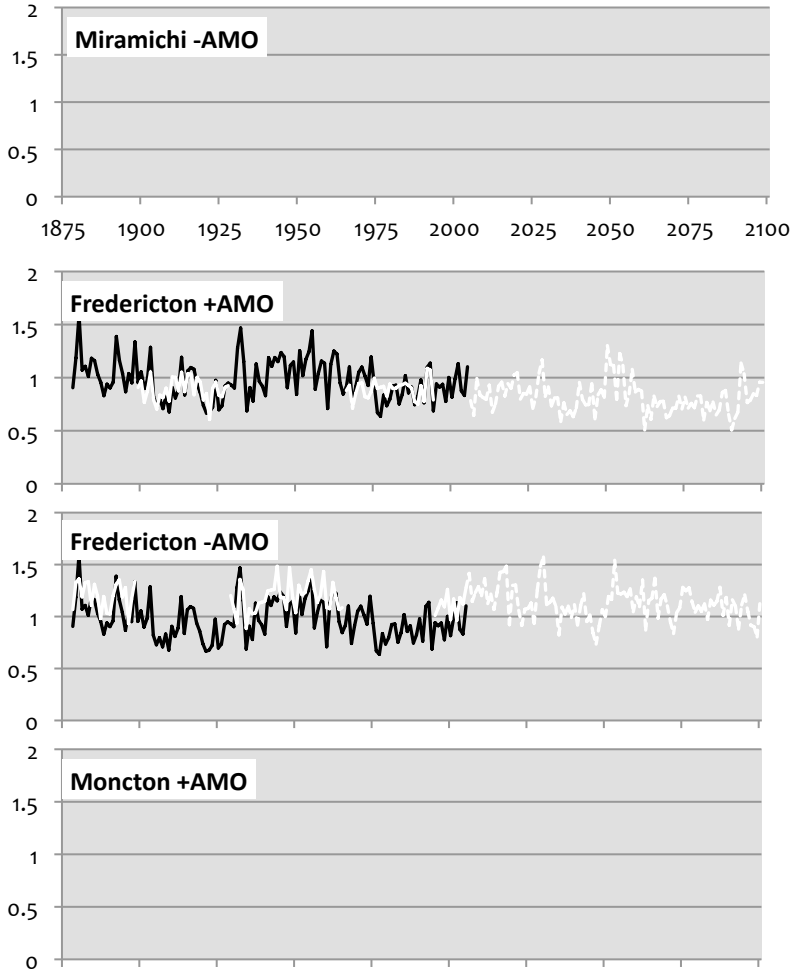
Miramichi -AMO
Fredericton +AMO
Fredericton -AMO
Moncton +AMO
2
1.5
1
0.5
0
1875
1900
1925
1950
1975
2000
2025
2050
2075
2100

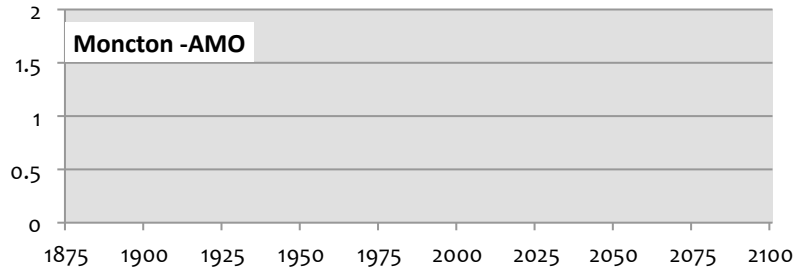

Figure 5.20. Significant **eastern hemlock B1** scenario forecasts are illustrated here. Black lines are actual standardized annual ring-widths, solid white lines are model calibration period fits, dotted white lines are modeled future annual ring-widths. Y-axis is standardized ring-width index, while x-axis is the year.

5.12 Eastern Hemlock Model Interpretation for SRES A1b Scenario

The performance of the eastern hemlock regression models resulted in six of nine models passing the acceptability criteria (Table 5.12). The application of the six approved models to the CGCM3 future climate data scenario SRES A1b predicted future radial growth divergence of approximately no change in Charlo, 20% decreases in Edmundston, 30% decreases in Aroostook, 25% increases in Miramichi with the positive AMO model, 5% increases in Fredericton with the positive AMO model, and 20% declines in Fredericton with the negative AMO model (Figure 5.21). Changes in eastern hemlock forecasts are comparably minimal under the SRES A1b scenario and a similar trend of reduced radial growth for more continentally distributed sites is evident.

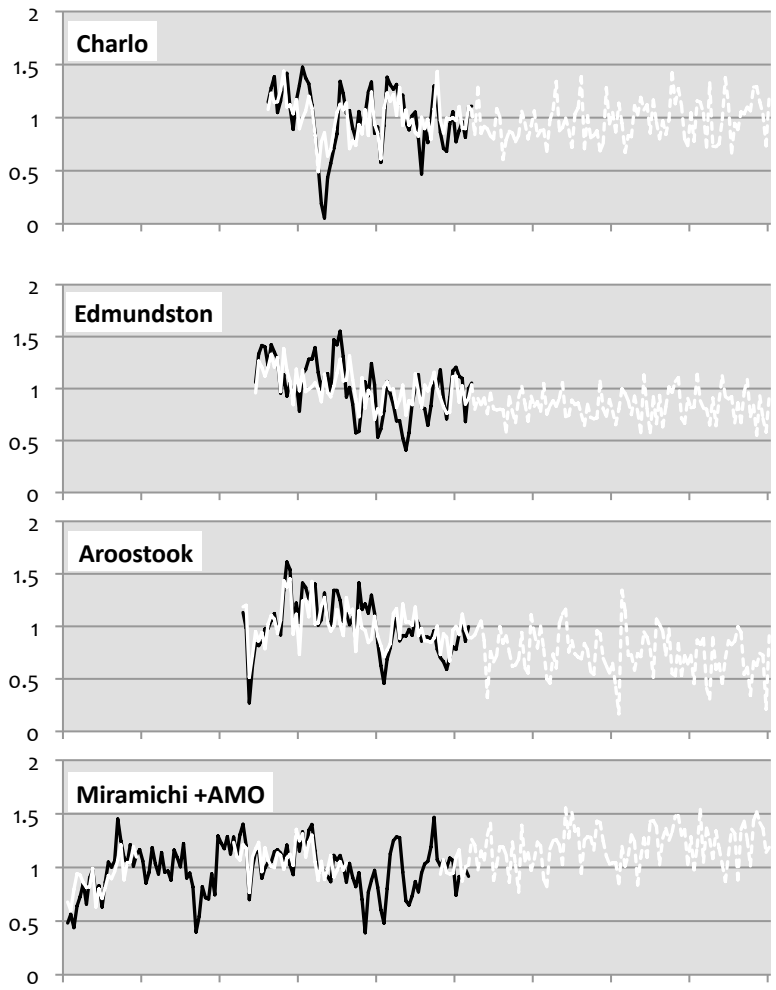
Charlo
Edmundston
Aroostook
Miramichi +AMO
2
1.5
1
0.5
0

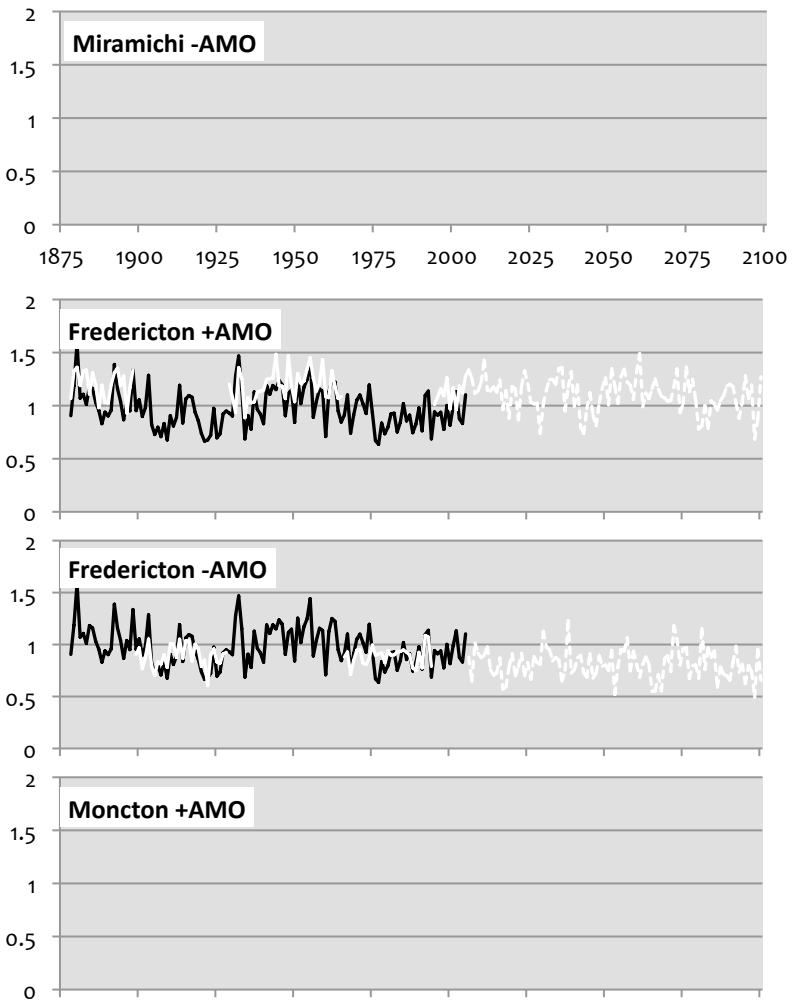
Miramichi -AMO
Fredericton +AMO
Fredericton -AMO
Moncton +AMO
2
1.5
1
0.5
0
1875
1900
1925
1950
1975
2000
2025
2050
2075
2100

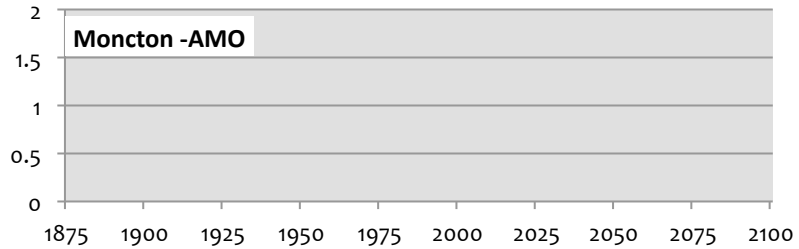

Figure 5.21. Significant **eastern hemlock A1b** scenario forecasts are illustrated here. Black lines are actual standardized annual ring-widths, solid white lines are model calibration period fits, dotted white lines are modeled future annual ring-widths. Y-axis is standardized ring-width index, while x-axis is the year.

5.13 Red Spruce Model Interpretation for SRES B1 Scenario

The performance of the red spruce regression models resulted in six of nine models passing the acceptability criteria (Table 5.12). The application of the six approved models to the CGCM3 future climate data scenario SRES B1 predicted future radial growth divergence of approximately 15% increases in Charlo, no change in Edmundston, 20% increases in Miramichi with the positive AMO model, 15% increases in Miramichi with the negative AMO model, 40% increases in Fredericton with the positive AMO model, and 25% increases in Fredericton with the negative AMO model (Figure 5.22). These six models result in an average 37% explained variance.

The geographic coverage offered by the six models, allows for some potential to interpret the future trends of red spruce radial growth and it appears that a general progression of modest increases from historic ring-width production levels should prevail under the SRES B1 scenario. The low explained variance is a limiting factor when interpreting the trends of future growth and the patterns in the selected variables of the models. Although important variables have likely been left out of these models, there is still an evident pattern of positive response in red spruce to the previous fall's precipitation (Table 5.14). Also, a positive response to the current growing season's late summer precipitation in northern sites, transitioning to early summer precipitation in the southern sites is apparent. The remaining variables do not exhibit relationships across multiple models and display random characteristics.

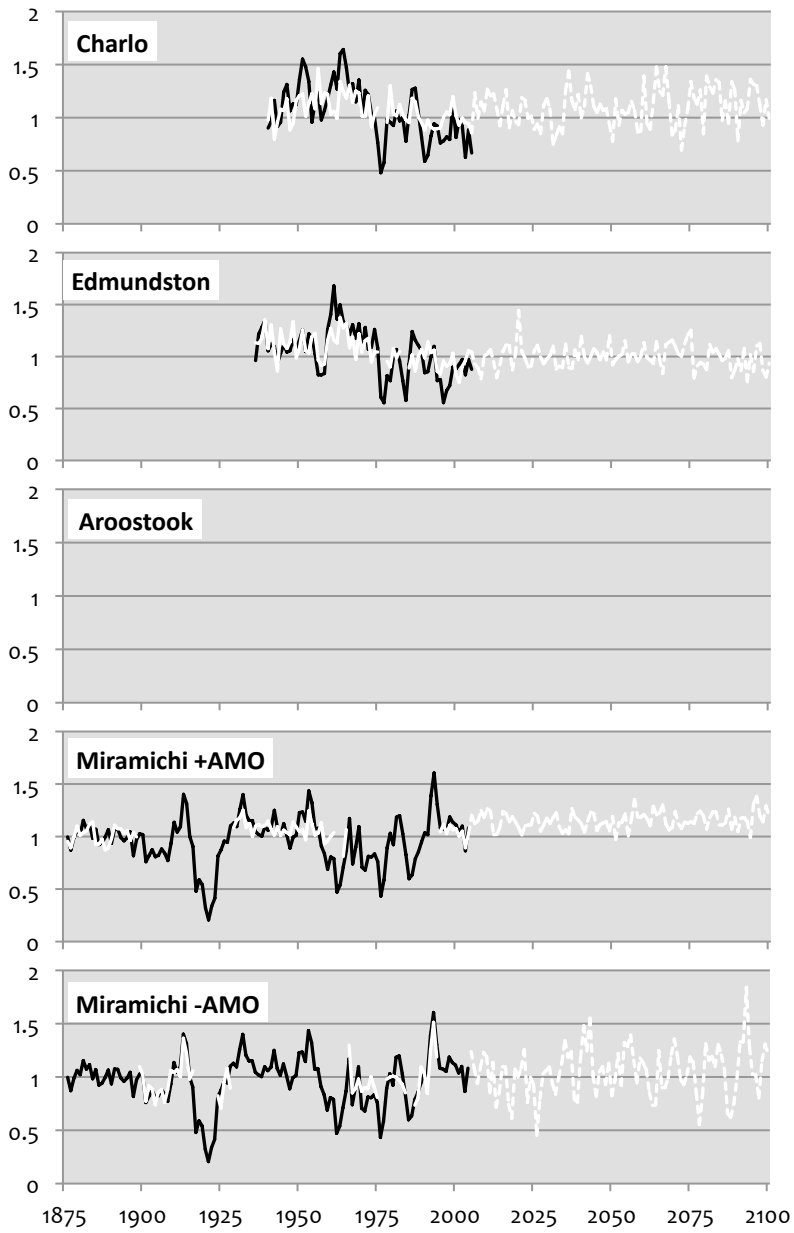

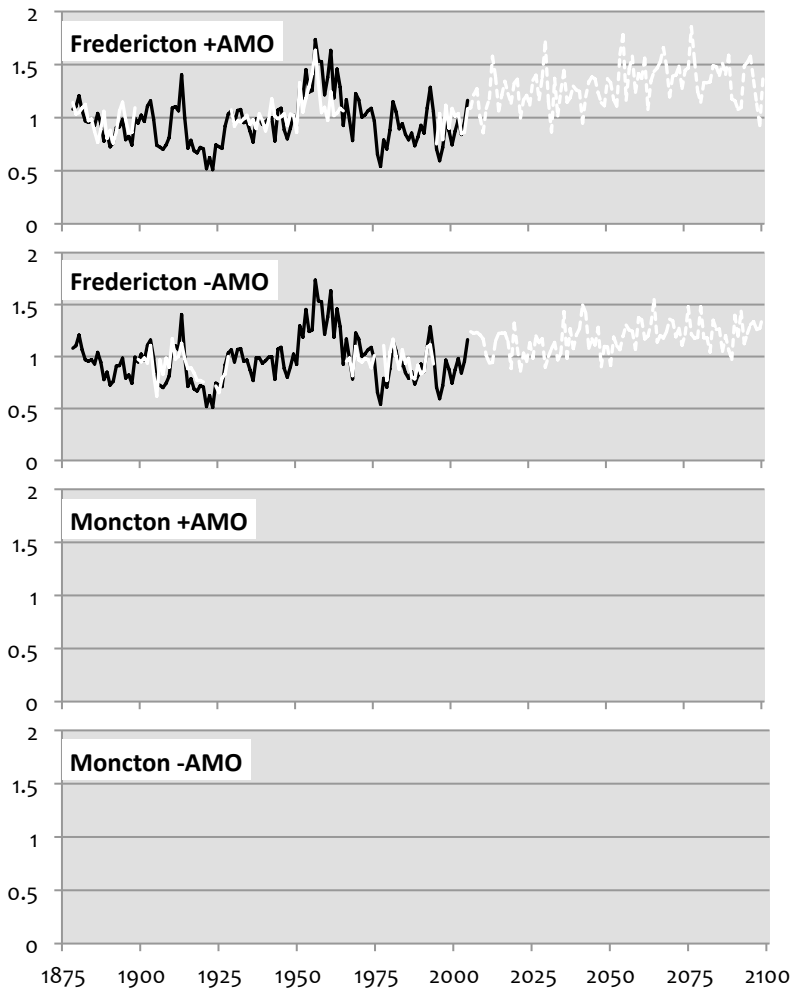

Figure 5.22. Significant **red spruce B1** scenario forecasts are illustrated here. Black lines are actual standardized annual ring-widths, solid white lines are model calibration period fits, dotted white lines are modeled future annual ring-widths. Y-axis is standardized ring-width index, while x-axis is the year.

5.14 Red Spruce Model Interpretation for SRES A1b Scenario

The performance of the red spruce regression models resulted in six of nine models passing the acceptability criteria (Table 5.12). The application of the six approved models to the CGCM3 future climate data scenario SRES A1b predicted future radial growth divergence of approximately 25% increases in Charlo, no change in Edmundston, 20% increases in Miramichi with the positive AMO model, 15% increases in Miramichi with the negative AMO model, 65% increases in Fredericton with the positive AMO model, and 45% increases in Fredericton with the negative AMO model (Figure 5.23). These results indicate slightly higher forecasted radial growth for some sites and demonstrate a possible further general progression of modest increases from historic ring-width production levels under the SRES A1b scenario.

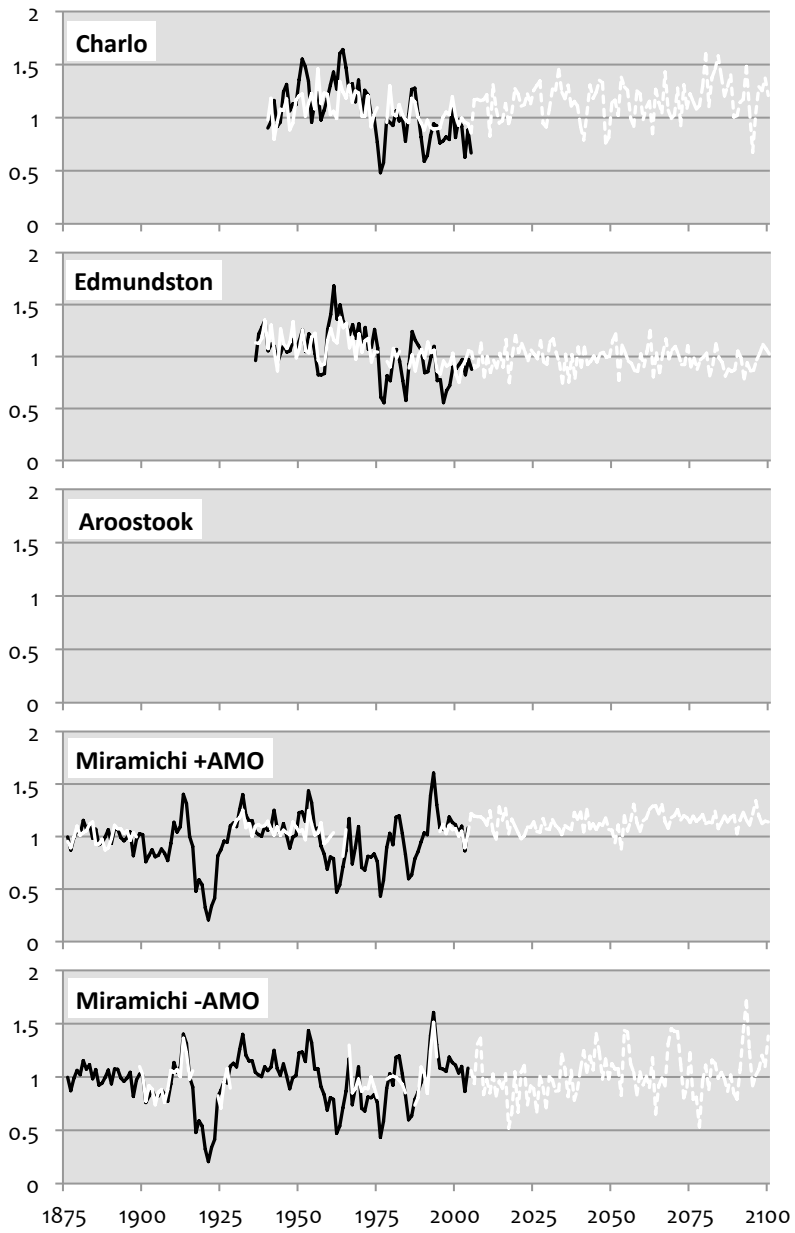

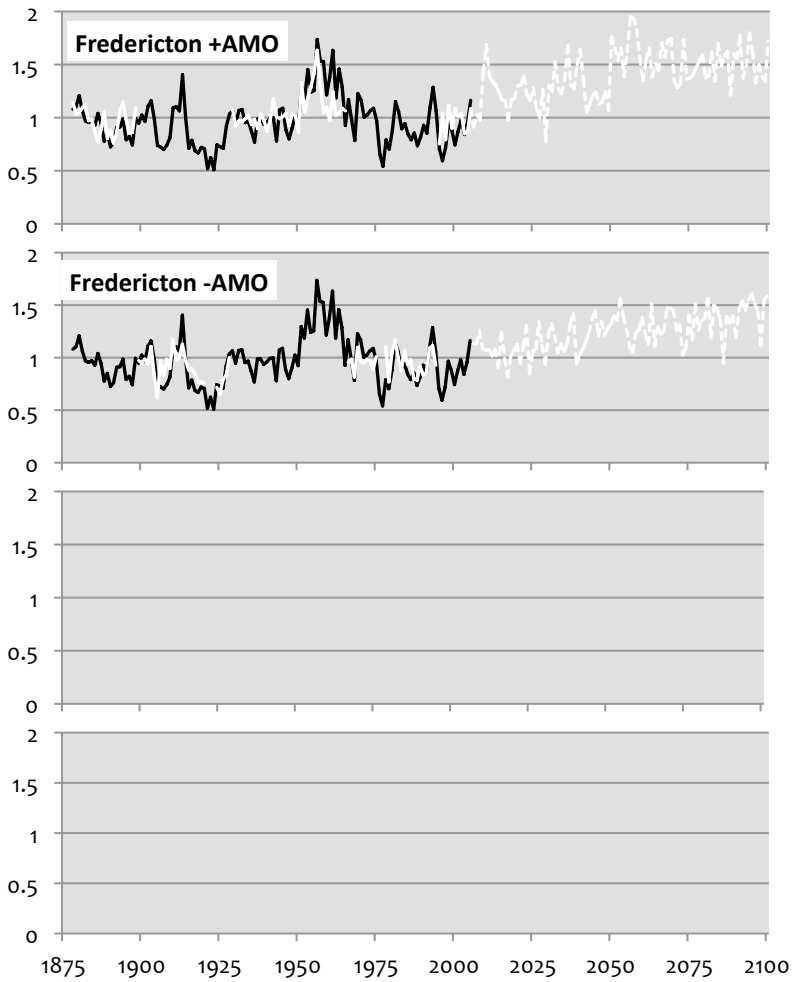

Figure 5.23. Significant **red spruce A1b** scenario forecasts are illustrated here. Black lines are actual standardized annual ring-widths, solid white lines are model calibration period fits, dotted white lines are modeled future annual ring-widths. Y-axis is standardized ring-width index, while x-axis is the year.

5.15 Eastern White Cedar Model Interpretation for SRES B1 Scenario

The performance of the eastern white cedar regression models resulted in eight of nine models passing the acceptability criteria (Table 5.12). The application of the eight approved models to the CGCM3 future climate data scenario SRES B1 predicted future radial growth divergence of approximately 20% increases in Charlo, 20% decreases in Edmundston, 15% declines in Aroostook, 30% decreases in Miramichi with the positive AMO model, no change in Fredericton with the positive AMO model, 75% increases in Fredericton with the negative AMO model, 80% decreases in Moncton with the positive AMO model, and 30% increases in Moncton with the negative AMO model (Figure 5.24). These eight models result in an average 44% explained variance.

The nearly complete geographic coverage offered by the eight models, allows for meaningful potential to interpret the future trends of eastern white cedar radial growth. The model results appear contradictory, however, when negative AMO periods are disregarded, there is a general modest radial growth decline under the SRES B1 scenario. Negative AMO models exhibit substantial increased ring-width production potential which may offset any declines. Explained variance is relatively high with the eastern white cedar models but it is still a limiting factor when interpreting the trends of future growth and the patterns in the selected variables of the models. Although important variables have likely been left out of these models, there is still an evident pattern of negative response to the warm June temperatures (Table 5.14). Also, a positive response to warm February temperatures is demonstrated across many models, as is a negative response to a high root freeze index. Remaining variables exhibit largely unsynchronized distribution patterns.

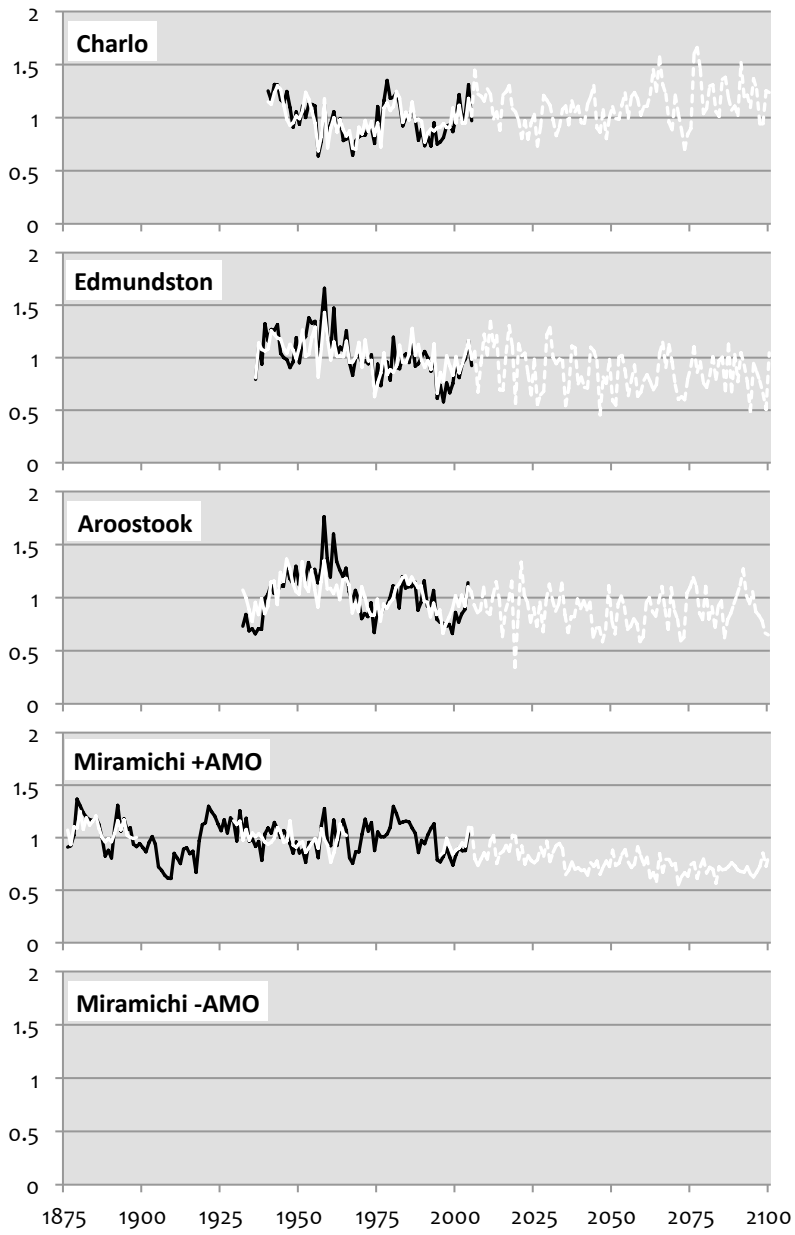

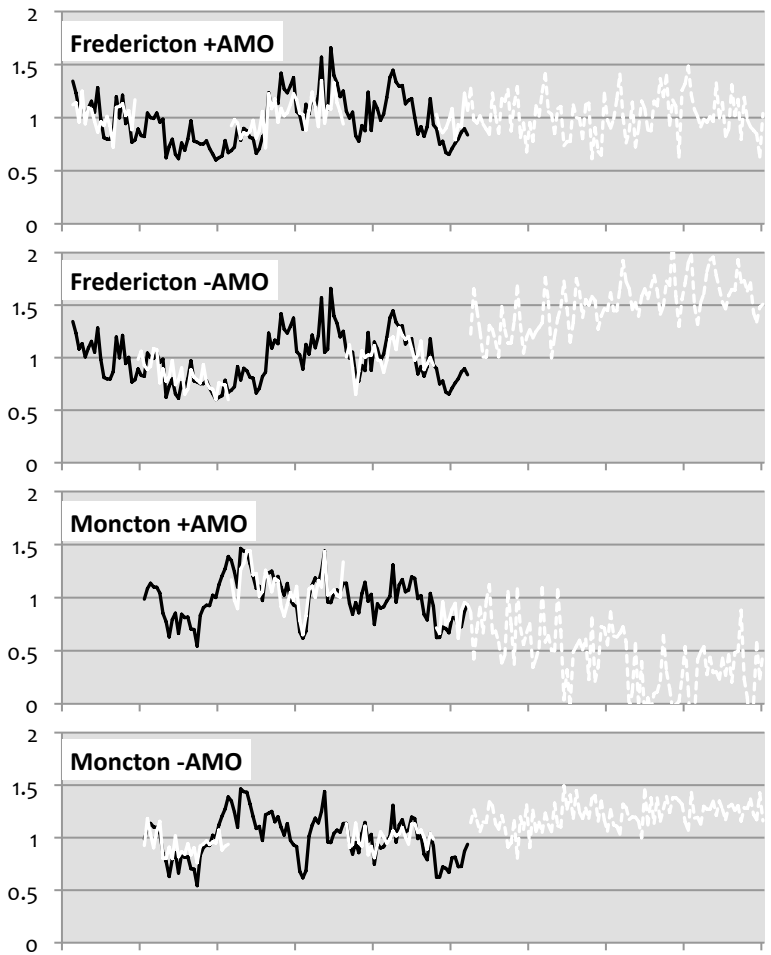

Figure 5.24. Significant **eastern white cedar B1** scenario forecasts are illustrated here. Black lines are actual standardized annual ring-widths, solid white lines are model calibration period fits, dotted white lines are modeled future annual ring-widths. Y-axis is standardized ring-width index, while x-axis is the year.

5.16 Eastern White Cedar Model Interpretation for SRES A1b Scenario

The performance of the eastern white cedar regression models resulted in eight of nine models passing the acceptability criteria (Table 5.12). The application of the eight approved models to the CGCM3 future climate data scenario SRES A1b predicted future radial growth divergence of approximately 40% increases in Charlo, 25% decreases in Edmundston, 15% declines in Aroostook, 35% decreases in Miramichi with the positive AMO model, no change in Fredericton with the positive AMO model, >100% increases in Fredericton with the negative AMO model, 100% decreases in Moncton with the positive AMO model, and 45% increases in Moncton with the negative AMO model (Figure 5.25). The results of the model forecasts under the SRES A1b scenario display similar looking contradictory outcomes and these models follow their previous radial growth directions. This can be interpreted in the same manner as was done in the SRES B1 scenario; generally decreasing ring-width production may be offset by radial growth gains during negative AMO periods.

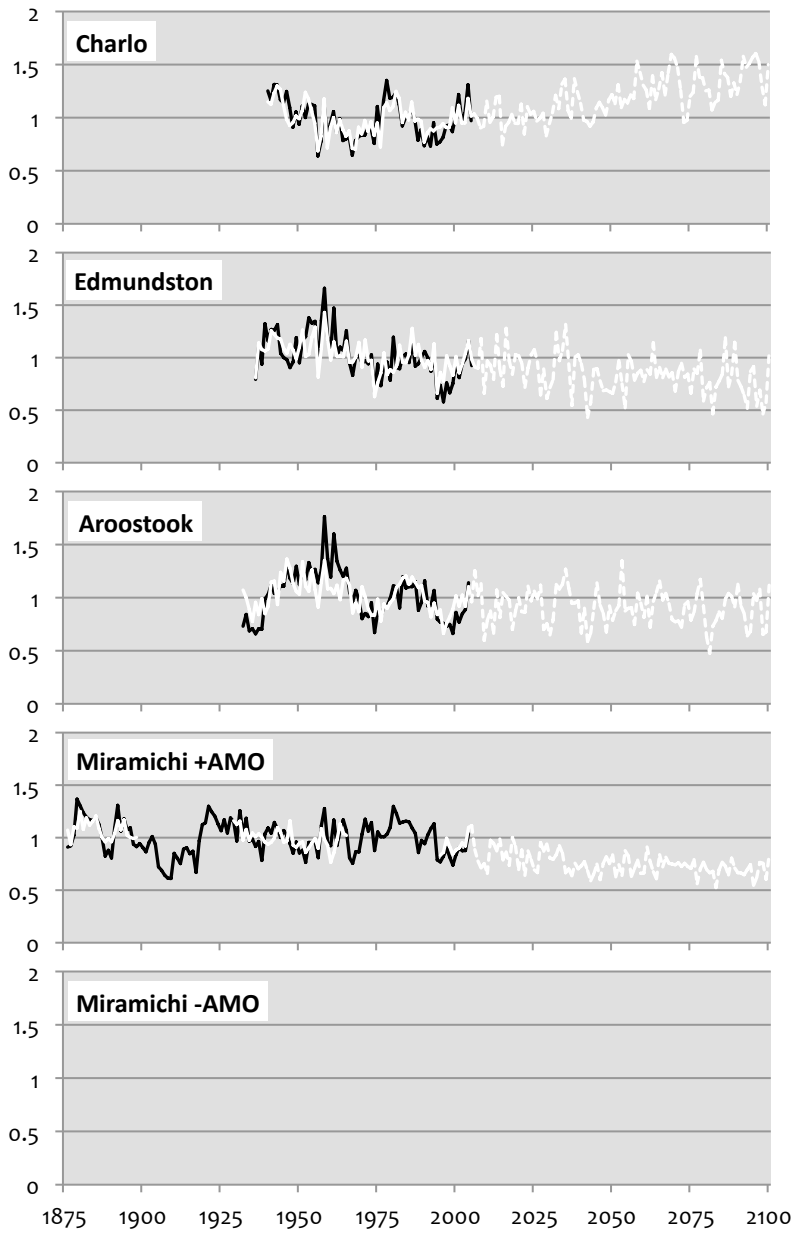

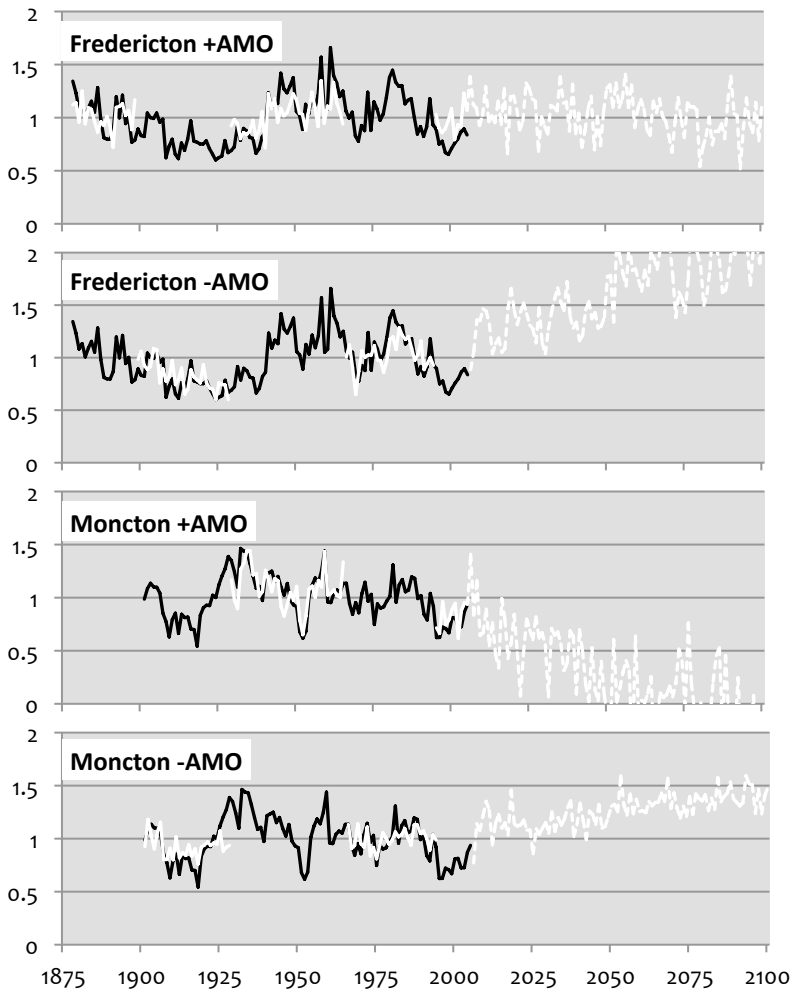

Figure 5.25. Significant **eastern white cedar A1b** scenario forecasts are illustrated here. Black lines are actual standardized annual ring-widths, solid white lines are model calibration period fits, dotted white lines are modeled future annual ring-widths. Y-axis is standardized ring-width index, while x-axis is the year.

5.17 White Pine Model Interpretation for SRES B1 Scenario

The performance of the white pine regression models resulted in five of nine models passing the acceptability criteria (Table 5.12). The application of the five approved models to the CGCM3 future climate data scenario SRES B1 predicted future radial growth divergence of approximately 20% decreases in Edmundston, 5% increases in Aroostook, 10% increases in Fredericton with the negative AMO model, 15% increases in Moncton with the positive AMO model, and no change in Moncton with the negative AMO model (Figure 5.26). These five models result in an average 49% explained variance.

The spotty geographic coverage offered by the five models, makes it difficult to assess potential change in white pine radial growth despite several relatively strong models. The models that did pass the acceptability criteria indicate little overall change in white pine radial growth. Explained variance is comparably high with the restricted number of white pine models but it is still a limiting factor when interpreting the trends of future growth and the patterns in the selected variables of the models. Although important variables have likely been left out of these models, there is still an evident pattern of positive response to wet summers (Table 5.14). Precipitation is far more inconsistent across the landscape then temperature and the reliance on this climatic pattern explains the low mean intra-species/inter-site correlation value of 0.28 among white pine sites (Table 5.2). Remaining variables exhibit largely unsynchronized distribution patterns.

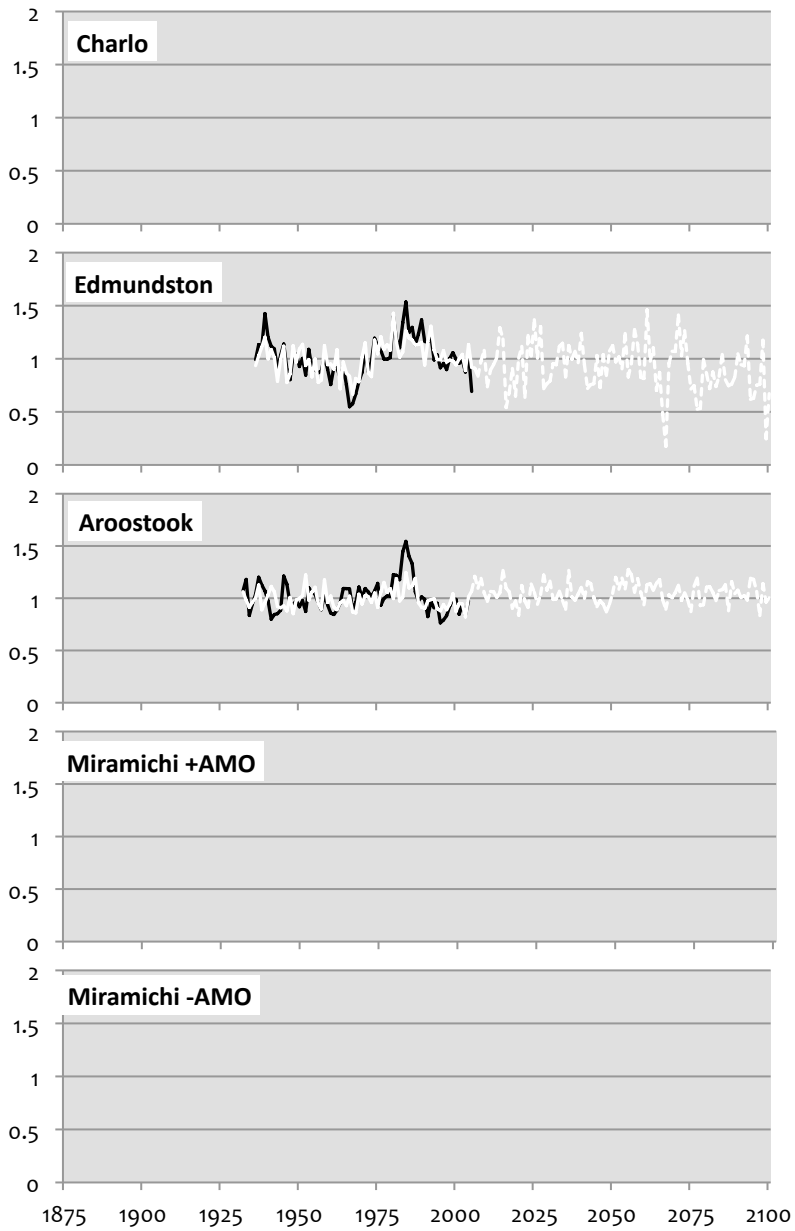

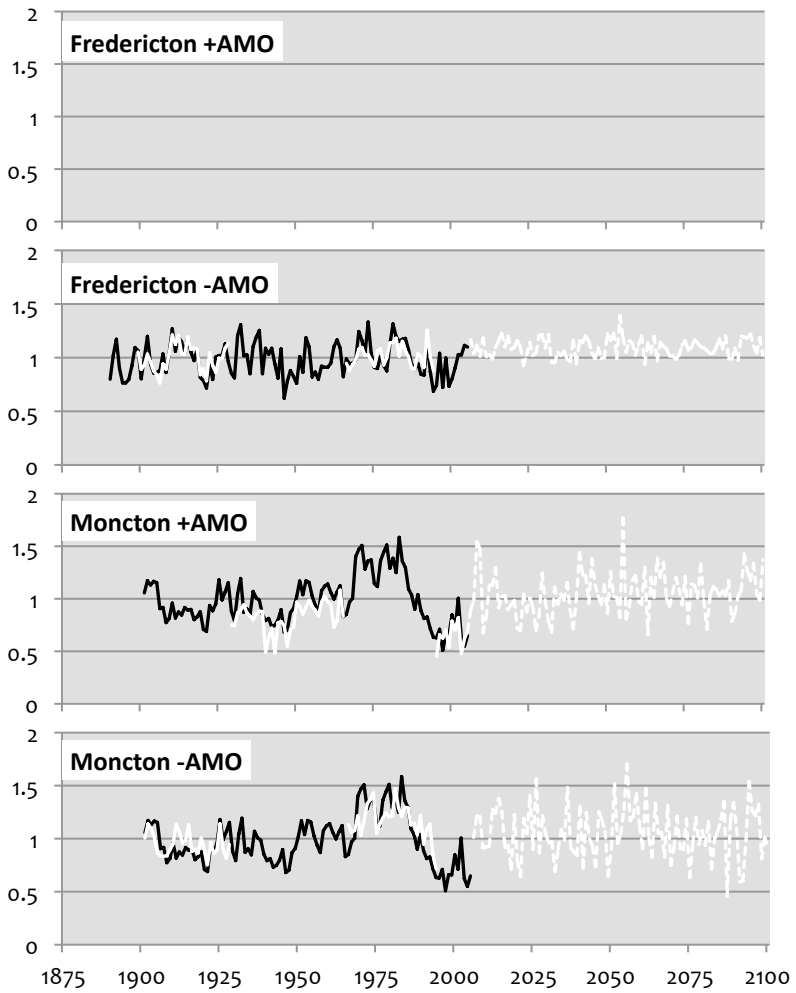

Figure 5.26. Significant **white pine B1** scenario forecasts are illustrated here. Black lines are actual standardized annual ring-widths, solid white lines are model calibration period fits, dotted white lines are modeled future annual ring-widths. Y-axis is standardized ring-width index, while x-axis is the year.

5.18 White Pine Model Interpretation for SRES A1b Scenario

The performance of the white pine regression models resulted in five of nine models passing the acceptability criteria (Table 5.12). The application of the five approved models to the CGCM3 future climate data scenario SRES A1b predicted future radial growth divergence of approximately 20% decreases in Edmundston, 20% increases in Aroostook, 20% increases in Fredericton with the negative AMO model, 35% increases in Moncton with the positive AMO model, and no change in Moncton with the negative AMO model (Figure 5.27). Although the geographic coverage of these white pine models is spotty and interpretation of the models across the landscape is difficult, a general increasing radial growth trend may result under the SRES A1b scenario for white pine.

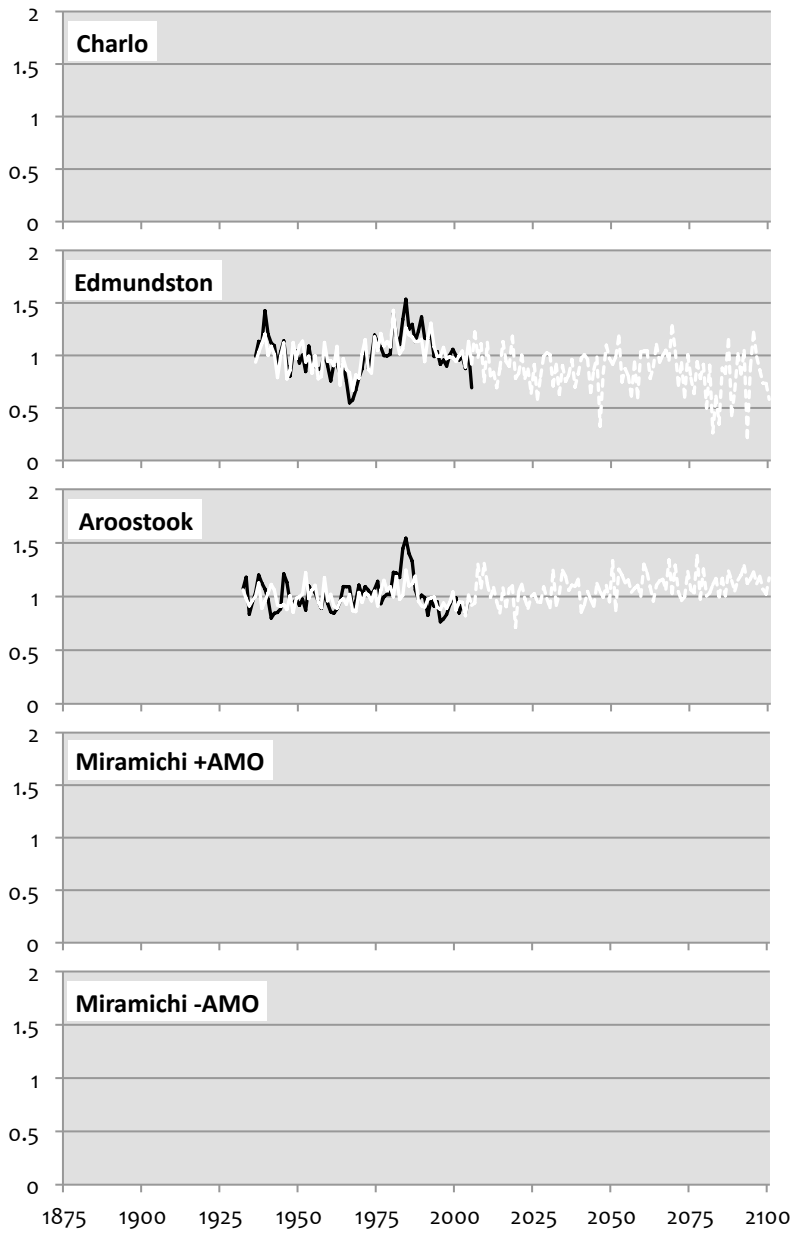

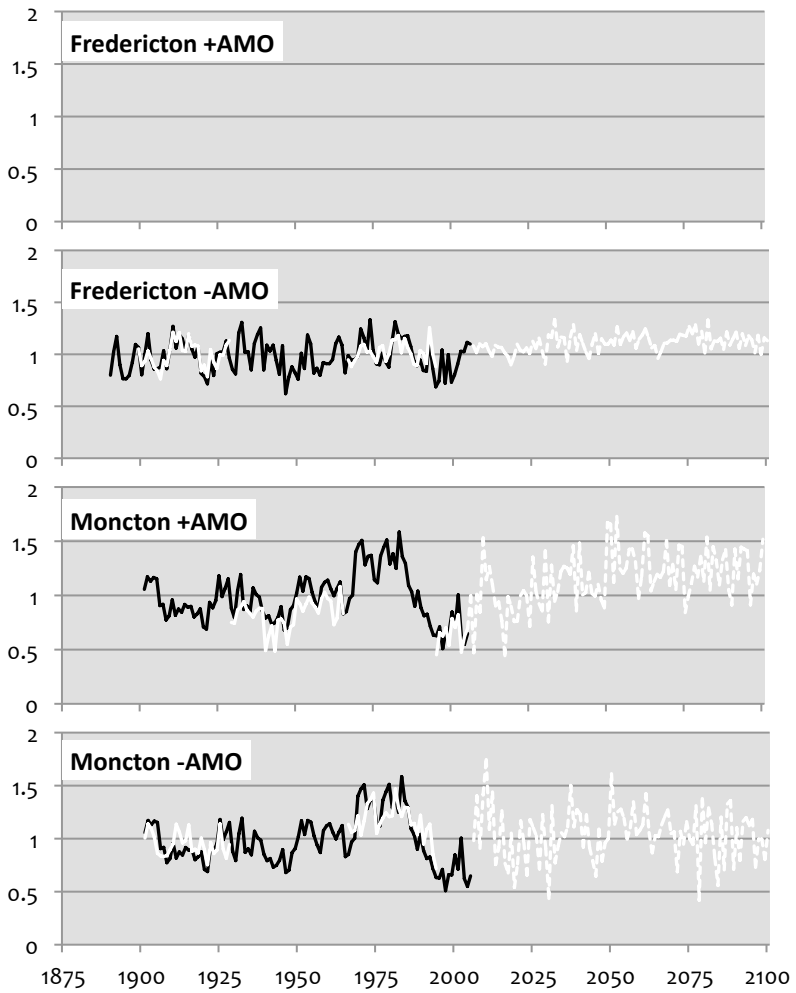

Figure 5.27. Significant **white pine A1b** scenario forecasts are illustrated here. Black lines are actual standardized annual ring-widths, solid white lines are model calibration period fits, dotted white lines are modeled future annual ring-widths. Y-axis is standardized ring-width index, while x-axis is the year.

5.19 Model Credibility

The linear regression models presented in this report feature many tree species, covering a relatively large heterogeneous geographic space, over a comparably long climatic time span. Despite some meaningful results, many of the models suffered from low explained variance and a lack of synchronization or similarities among the predictor variables selected into the optimum subset models. The future forecasts of these models also raise questions about the validity of the future Coupled Global Climate Model data. So, what are the specific problems and how may they be addressed in future studies to create more reliable predictions of future radial growth?

5.19.1 Application of Linear Models in Oscillating Climate Conditions

By reexamining the intra-species/inter-site correlation values, relatively weak relationships within the various sample sites of each species are apparent (Table 5.2). Heterogeneity of temperature and precipitation across the landscape of the study area are a likely cause of much of the weak r-values. However, it is doubtful this geographic variability of climate is completely to blame for the scarcity of synchronized predictor variables and the low explained variance across the radial tree growth models. Rather, the ability of a linear model to incorporate non-linear radial growth responses to climatic variables is the likely culprit. As the oceans stimulate the long-term climate to oscillate between extreme phases, it is highly probable that biological thresholds of various tree species are crossed numerous times over their long life spans. The result is likely that many independent variables exhibit non-linear functions such as exponential, logarithmic or polynomial, in relation to the dependent radial tree growth curves. To properly address these potential non-linear functions, curve fitting would have to be undertaken on a massive scale to either transform the problematic climate variables into linear functions for application in a linear regression

or undertake complex non-linear least squares regression models. To accomplish this task across many species and many sample sites with large independent variable sets would be labor intensive.

The time conserving approach applied in this study was to deconstruct the input variables based on the potential cause of non-linear radial growth response. This cause was perceived to be the AMO as it seemed to have widespread influence on many of the tree species studied. The variables were split into positive and negative time periods in an attempt to isolate contrasting climatic influences. Only three sites (Miramichi, Fredericton, and Moncton) had long enough recorded climate history to complete this task. This approach, although not ideal, allowed useful models to be constructed when attempts over the full time span failed to identify a significant number of influential predictor variables. Perhaps the particular deconstruction used here could have been further optimized but, a non-linear model building method would be preferable given greater time and resources.

5.19.2 Critical Exclusions in the Future Climate Data

Determining the impact of anthropogenic forcing on global climate systems over centennial timescales has been the focus of Coupled Global Climate Modelers for decades using various types of complex computer simulations (Murphy et al. 2009). The results of these endeavors are models that predict long-term, large scale, external forcing of the climate well, but do not reproduce or predict decadal climate variability (DCV) due to internal forcing (Murphy et al., 2009). An example of such models is the CGCM3 used in this study. Given the measured relationship of radial growth response of New Brunswick tree species to multidecadal, internally forced, ocean-atmosphere oscillation conditions, it is obvious that models based on predicting centennial scale, external forcing would be of limited use in forecasting radial tree growth. More specifically, in relation to North Atlantic Ocean conditions, these external forcing based, long-term models would be expected to smooth over the

multidecadal oscillations so important to New Brunswick tree species. That is to say, potential negative phases of the AMO would be forecast as warmer and potential positive phases would be forecast as cooler then would be expected in reality. This brings to question the predictions made in the radial tree growth models of this study produced for negative and positive phases of the AMO.

Recently, DCV due to internal forcing was demonstrated to be potentially predictable on inter-annual to decadal timescales (Collins et al., 2006). Also, the IPCC is planning to include experiments in their Fifth Assessment Report from the CMIP5 cluster of simulation experiments that will provide better decadal climate projections (Taylor et al., 2008). It is recognized that in shorter time scales, such as decadal ones, internal variability is of greater magnitude than external anthropogenic forcing (Murphy et al., 2009). Given the probable relationship of New Brunswick tree species to internally forced multidecadal variability, these new prediction models cannot come soon enough. That being said, anthropogenic climate change still has huge potential to impact future radial growth and forest health; and both long-term climate change and shorter-term internal variability are crucial for predicting forest response to climate.

Another concern with using one coupled global circulation model (CGCM) is the potential for error. The CGCM3 used in this study is a world class CGCM but it is one perspective on future climate. The employment of multiple CGCMs for the forecasting of radial tree growth would produce many more forecast outputs, however other models may have greater predictive accuracy regarding such climatic elements as the thaw/refreeze variables that the CGCM3 fails to precisely model. Inclusion of other CGCMs will ultimately result in larger data management requirements however. Also CGCMs with the ability to forecast down to much smaller regional scales is crucial for properly modeling radial tree growth at that local to regional level.

5.19.3 Prospective Future Biological Thresholds

The availability of past climatic situations that are analogous to future climatic scenarios is another concern. During the period over which the climate models in this study are based, there has been much climatic variability, but there are also potentially future forecast climatic extremes that are outside of the range of past climates. A prime example of this would be future winter precipitation falling as rain instead of snow, drastically changing factors relating to growth (Laroque and Smith 2003, Goldblum and Rigg 2005). The models are therefore limited in their capacity to provide a prediction of radial growth under a forecasted climatic range that is outside of what they experienced in the past.

Important ecological thresholds that relate to a tree's response to temperature or precipitation in a particular month or season may not have been reached in the past and would therefore be neglected in these forecast models. This is likely the case with some of the models produced in this study. The short time period of model calibration available in the most northern sites has limited the interval over which radial growth response could be analyzed and accounted for. The extreme negative phase of the AMO from 1899 to 1928 was not available to the models calibrated over shorter periods and thus the climatic extremes which characterized that period are unaccounted for. Also as the climate changes, new extreme climate conditions will occur that have never been experienced over the instrumental record. Consequently, as the models work their way into more extreme climate change scenarios, it is expected that their predictive capability will begin to fail, which is why more extreme SRES scenarios (A1F1, A2) are not modeled here.

The potential for a particular species to incorporate specific climatic factors differently into its radial growth response pattern as it reaches climatic thresholds remains unknown. We do know that some climate-growth relationships are age dependent (Carrer and Urbinati 2004). The degree to which physiological changes in the studied tree species have altered their response to climate inputs over the timeframe investigated is obscured by the process. How much future physiological changes will impact the radial growth response to future climates is not known and could play a large role in keeping a particular species competitive or contributing to its demise. Due to the mature trees sampled for this study the hope was this limitation to forecasting would be minimized.

5.19.4 Non-Climatic Disturbance

It should also be kept in mind that these models are only predicting radial growth response to the future climatic inputs and do not account for radial growth reductions inflicted by insect outbreaks or other pathogens. As the climate warms, trees will not be the only species to shift ranges in response to the new conditions. Other species will also have a migrational response that could differ substantially in geographical and temporal scales. Both alien and native pest and pathogen disturbance is expected to increase on the poleward margins of temperate forests as bioclimatic barriers are moved through rapid climate changes (IUFRO 2009). Therefore, it should be anticipated that future radial growth of New Brunswick tree species could be significantly affected by the influences of pests and pathogens more commonly associated with southern portions of the various tree species' ranges. This fact, and the fact that the trees are currently rooted in place compared to the ability of insects to more readily disperse, cannot be taken into account in these radial growth model forecasts.

5.20 AMO Direction and Trends

Despite all of the uncertainty surrounding the radial growth forecast models constructed for this report, including the lack of DCV in future climate data, we can make some informed speculation on the potential direction of ocean conditions and their expected impacts on New Brunswick forests over the shorter-term.

It is generally recognized that the last time the AMO shifted phases was in 1994-95. This shift was to a positive phase, which has generally resulted in increased radial growth of shade tolerant tree species in the past. It is possible however, that a shift back to a negative phase could happen earlier than anticipated due to an Atlantic thermohaline circulation slow down (Sutton and Hudson 2005). The Meridonal Overturning Circulation (MOC) is largely responsible for the transport of heat via ocean currents from equatorial regions of the Atlantic towards northerly regions (Msadek and Frankignoul 2008). Most global coupled climate models suggest a weakening of the MOC in climate change scenarios, although debate still surrounds the processes involved (Guemas and Salas-Me´lia 2008). If MOC slowdowns induced by global warming did occur in the near future, we should expect a phase reversal of the AMO and lower radial growth rates of shade tolerant tree species. Perhaps of greater use, given the current debate regarding the future of the MOC influence, is the probabilistic projection of future AMO phase changes based on long-term tree-ring reconstructions. Based on a 424 year AMO reconstruction from tree-rings completed by Gray et al. (2004), Enfield and Cid-Serrano (2005) produced a study of projected risk of future AMO phase shifting. Their results suggest we should expect a 33% chance of a phase reversal in the next 5 years, a 59% chance of reversal in 10 years, a 78% chance of reversal in 15 years, a 92% chance of reversal in the next 20 years, and finally there is near certainty of a phase reversal of the AMO within 25 years based on past activity (Enfield and Cid-Serrano 2005). Given these probabilities, it is likely that the AMO will

undergo a phase reversal between 2020 and 2030. If that situation unfolds as envisioned, the radial growth of shade tolerant tree species should slow after this point, until the AMO finishes its negative phase. If the trend of spruce budworm outbreaks occurring during negative phases of the AMO in the 20th century is not coincidental, the probability of a major spruce budworm outbreak should remain low until AMO phase reversal occurs. This probability of phase reversal of the AMO also has implications for yellow birch. If we do in fact experience another decade or more of positive phase AMO, the radial growth of yellow birch should continue to suffer as it has since the current positive phase of the AMO began. Once phase reversal occurs, yellow birch radial growth should again increase. However, until that situation unfolds, yellow birch may be more susceptible to dieback, insect outbreak, pathogen attack, or pollution.

5.21 NAO Direction and Trends

Despite much debate and theoretical positioning regarding the processes which drive the NAO, several modeling studies have linked rising green house gas concentrations with more positive phase trends in the NAO (Hurrell et al. 2003). In contrast to these modeling results are two long-term NAO reconstructions. The first is a well-verified, multiproxy tree-ring reconstruction reaching back to 1400 A.D. by Cook and D'Arrigo (2002). The second is a 218 year long NAO reconstruction from coral strontium-to-calcium ratios sampled near Bermuda by Goodkin et al. (2008). Both sets of authors show that the NAO performance is linked to hemispheric mean temperature and the magnitude of the NAO waxes and wanes as the climate warms and cools. It is proposed that green house gas emissions are forcing more extreme NAO phases and they also suggest increasing global temperatures will force a continuation of extended multidecadal NAO phase activity (Cook and D'Arrigo 2002, Goodkin et al. 2008). This they propose, will make climate forecasting more difficult

for the North Atlantic region and undermine the predictability of anthropogenic warming (Goodkin et al. 2008).

An implication from their studies for shade tolerant tree species radial growth in New Brunswick is that it will include both periods of rapid and slow growth. As we are currently ending an extended period of extreme positive phase of the NAO and seem to be transitioning toward a negative phase, shade tolerant tree species radial growth should respond favorably, especially considering we are in a warm phase of the AMO. However, if future extended positive phases of the NAO occur simultaneously with negative phases of the AMO, shade tolerant tree species could experience suppressed radial growth and extended periods of stress leading to other disturbances such as insect or disease outbreaks and ultimately increased mortality.

6.0 Conclusion

The reaction of the relatively complacent forests of New Brunswick to climate has been little studied. Through the most geographically intensive and tree species inclusive dendroclimatology study ever in New Brunswick, a new level of comprehension, regarding the past, present and potential future radial growth response of six New Brunswick tree species has been introduced. Of the six tree species studied, the four most shade tolerant and the one moderately shade tolerant, exhibited long-term fluctuations in their population level radial growth rates, which corresponded to long-term fluctuations in measurements of North Atlantic Ocean sea surface temperature and pressure. This ocean influenced, internal climate variability has likely been responsible for past widespread, population level, radial growth fluctuation. As such, the radial growth of some of New Brunswick's most important tree species appears to exhibit a much stronger internally forced climate signal, rather than an external anthropogenically forced global warming signal. These

oscillating growth responses introduce difficulty into the future modeling of radial growth rates using Coupled Global Climate Models.

In light of unreliable 100 year forecasting models, radial growth rates of New Brunswick trees can still be predicted to a lesser extent using probabilistic projection of phase reversal in ocean surface temperature based on proxy records (Enfield and Cid-Serrano 2005). This suggests with near certainty that phase reversal will occur on or before 2030, resulting in a cooler phase of the Atlantic Multidecadal Oscillation, and lowered overall radial growth after that time, of the shade tolerant tree species sugar maple, eastern hemlock, red spruce, and eastern white cedar, while increased radial growth of yellow birch should occur. Alternately the North Atlantic Oscillation, is currently diminishing into a negative phase, which in combination with the current positive phase of the AMO, should provide optimal climatic conditions for the four shade tolerant tree species of this study over the next several years. What is not yet well understood, is how exactly global warming will influence the oscillating conditions of the North Atlantic Ocean.

Increased certainty of the future climatic response of New Brunswick's forests requires two advances in knowledge. The first is the production of better coupled global climate models that have the ability to more accurately forecast fluctuating ocean conditions. The second is more complex radial growth models of New Brunswick tree species that can account for most climatic influences. Until these advances are completed, the future productivity of New Brunswick trees will have to be roughly approximated and uncertainty will remain.

References

Auclair, A. N. D., Martin, H. C., and Walker, S. L., 1990. A Case Study of Forest Decline in Western Canada and the Adjacent United States. *Water, Air and Soil Pollution 53:13-31.*

Auclair, A. N. D., 1993a. Extreme Climatic Fluctuations as a Cause of Forest Dieback in the Pacific Rim. *Water, Air, and Soil Pollution 66: 207-229.*

Auclair, A. N. D., 1993b in Luisis, N., Lerario, P., and Vannini, A. (eds.), Recent Advances in Studies on Oak Decline, pp. 139-148. Proc, IUFRO Conference, September 1992, Seva di Fasano, Italy.

Auclair, A. N. D., Lill, J. T., and Revenga, C., 1996. The Role of Climate Variability and Global Warming in the Dieback of Northern Hardwoods. *Water, Air, and Soil Pollution 91: 163-186.*

Auclair, A. N. D., 2005. Patterns and General Characteristics of Severe Forest Dieback from 1950 to 1995 in the Northeastern United States. *Canadian Journal of Forest Research 35: 1342-1355.*

Bauce, E., and Allen, D. C., 1991. Etiology of a Sugar Maple Decline. *Canadian Journal of Forest Research 21:686-693.*

Beier, C. M., Sink, S. E., Hennon, P. E., D'Amore, D. V., and Juday, G. P., 2008. Twentieth-Century Warming and the Dendroclimatology of Declining Yellow-Cedar Forests in Southeastern Alaska. *Canadian Journal of Forest Research 38: 1319-1334.*

Bergeron, N., and Sedjo, R., 1999. The Impact of El Niño on Northeastern Forests: A Case Study on Maple Syrup Production. *Discussion Paper Rff:99-43.*

Bourque, C. P.-A., Cox, R. M., Allen, D. J., Arp, P. A., and Meng, F. R., 2005. Spatial Extent of Winter Thaw Events in Eastern North America: Historical Weather Records in Relation to Yellow Birch Decline. *Global Change Biology 11: 1477-1492.*

Brown, D. R., and Braaten, O. R., 1998. Spatial and Temporal Variability of Canadian Monthly Snow Depths, 1946-1995. *Atmosphere-Ocean 36:37-54.*

Burnham, K. P., and D. R. Anderson. 1998. *Model Selection and Inference: A Practical Iinformation-Theoretic Approach.* Springer-Verlag, New York, New York, USA.

Burnham, P., K., 2002. *Model Selection and Multi-Model Inference: A Practical Information-Theoretic Approach* (2nd Edition). Secaucus, NJ, USA: Springer-Verlag New York, Inc.

Carrer, M., and Urbinati, C., 2004. Age-Dependent Tree-Ring Growth Responses to Climate in *Larix decidua* and *Pinus cembra. Ecology 85(3):730-740.*

Campbell, J. L., Mitchell, M. J., Groffman, P. M., Christenson, L. M., and Hardy, J. P., 2005. Winter in Northeastern North America: a Critical Period for Ecological Processes. *Frontiers in Ecology and the Environment 3(6):314-322.*

Clayden, S. R., 2000. History, Physical Setting, and Regional Variation of the Flora. In Hinds, H. R., *Flora of New Brunswick* (pp 35-73). Fredericton, NB: Biology Department, University of New Brunswick.

Collins, M., Botzet, M., Carril, A. F., Drange, H., Jouzeau, A., Latif, M., Masina, S., Otteraa, O. H., Pohlmann, H., Sortberg, A., Sutton, R., and Terray, L., 2006. Interannual to Decadal Climate Predictability in the North Atlantic: A Multimodel-Ensemble Study. *American Meterological Society vol. 19:1195-1203*

Cook , E., R., 1985. A Time Series Analysis Approach to Tree-Ring Standardization. Ph.D. dissertation. The University of Arizona, Tuscson, Arizona, USA.

Cook, E. R. and D'Arrigo, R. D., 2002. A Well-Verified, Multiproxy Reconstruction of the Winter North Atlantic Oscillation Index since A.D. 1400. *Journal of Climate 15(13):1754-1764.*

Cox, M., R., and Zhu, B., X., 2003. Effects of Simulated Thaw on Xylem Cavitation, Residual Embolism, Spring Dieback and Shoot Growth in Yellow Birch. *Tree Physiology 23:615-624.*

Diaz-Nieto, J., and Wilby, L., R., 2005. A Comparison of Statistical Downscaling and Climate Change Factor Methods: Impacts on Low Flows in the River Thames, United Kingdom. *Climatic Change 69: 245–268.*

Enfield, D.B., Mestas-Nuñez, A.M., and Trimble, P.J., 2001. The Atlantic Multidecadal Oscillation and its Relation to Rainfall and River Flows in the Continental U.S. *Geophysical Research Letters 28:2077-2080.*

Enfield, D. B., and Cid-Serrano, L., 2005. The Probabilistic Projection of Climate Risk. *US Clivar 3(3):10, 12-1.*

Fritts, H.C., 1976. Tree Rings and Climate. Academic Press, London.

Giraridin, P., M., Raulier, F., Bernier, Y., P., and Tardiff, C., J., 2008. Response of Tree Growth to a Changing Climate in Boreal Central Canada: A Comparison of Empirical, Process-Based, and Hybrid Modeling Approaches. *Ecological Modeling 213:209-228.*

Goldblum, D., and Rigg, L., S., 2005. Tree Growth Response to Climate Change at the Deciduous-Boreal Forest Ecotone, Ontario, Canada. *Canadian Journal of Forest Research 35:2709-2718.*

Goodkin, N. F., Hughen, K. A., Doney, S. C., and Curry, W. B., 2008. Increased Multidecadal Variability of the North Atlantic Oscillation since 1781. *Nature Geoscience 1:844-848.*

Graumlich, L. J., 1993. Response of Tree Growth to Climatic Variation in the mixed Conifer and Deciduous Forests of the Upper Great Lakes Region. *Canadian Journal of Forest Research 23:133-143.*

Gray, S. T., Graumlich, L. J., Betancourt, J. L., and Pederson, G. T., 2004. A Tree-Ring Based Reconstruction of the Atlantic Multidecadal Oscillation since 1567 A.D. *Geophysical Research Letters 31:L12205.*

Grissino-Mayer, H. D., 2001. Evaluating Crossdating Accuracy: A Manual and Tutorial for the Computer Program COFECHA. *Tree-Ring Research 57:205-221.*

Guemas, V., and Salas-Me´lia, D., 2008. Simulation of the Atlantic Meridional Overturning Circulation in an Atmosphere-Ocean Global Coupled Model. Part II: Weakening in a Climate Change Experiment: A Feedback Mechanism. *Climate Dynamics 30-831-844.*

Hacke, U. G., and Sauter, J. J., 1996. Xylem Dysfunction During Winter and Recovery of Hydraulic Conductivity in Diffuse-Porous and Ring-Porous Trees. *Oecologia 105: 435-439.*

Hacke, U. G., and Sperry, J. S., 2001. Functional and Ecological Xylem Anatomy. *Perspectives in Plant Ecology, Evolution and Systematics 4(2): 97-115.*

Hartmann, H., and Messier C., 2008. The Role of Forest Tent Caterpillar Defoliations and Partial Harvest in the Decline and Death of Sugar Maple. *Annals of Botany 102:377-387.*

Holmes, R. L., 1992. Dendrochronology Program Library, Version 1992-1 Edition. *Laboratory of Tree-Ring Research, University of Arizona, Tuscson.*

Hurrell, J., Kushnir, Y., Ottersen, G., and Visbeck, M., 2003. An Overview of the North Atlantic Oscillation. The North Atlantic Oscillation: Climatic Significance and Environmental Impact. *Geophysical Monograph 134 35p.*

[IUFRO] International Union of Forest Research Organizations, 2009. Adaptation of Forests and People to Climate Change. A Global Assessment Report. Seppälä, R., Buck, A., and Katila, P., (eds.). IUFRO World Series Volume 22. Helsinki. 224 p.

Iverson, L. R., Prasad, A. M., Matthews, S. N., and Peters, M., 2008. Estimating Potential Habitat for 134 Eastern US Tree Species Under Six Climate Scenarios. *Forest Ecology and Management. 254:390-406.*

Kaplan, A., Crane, M., Kushnir, Y., Clemetn, A., Blumenthal, B., and Rajagopalan, B., 1998. Analyses of Global Sea Surface Temperature 1856-1991. *Journal of Geophysical Research 103:18567-18589.*

Lane, C. J., Reed, D. D., Mroz, G. D., and Liechty, H. O., 1993. Width of Sugar Maple (*Acer saccharum*) Tree Rings as Affected by Climate. *Canadian Journal of Forest Research 23:2370-2375.*

Laroque, C.P. and Smith, D.J. 2003. Radial-Growth Forecasts for Five High-Elevation Conifer Species on Vancouver Island, British Columbia. *Forest Ecology and Management 183:313-325.*

Loo, J., and Ives, N., 2003. The Acadian Forest: Historical Condition and Human Impacts. *The Forestry Chronicle 79(3):462-474.*

Mantua, N.J., Hare, S.R., Zhang, Y., Wallace, J.M., and Francis, R.C., 1997. A Pacific Interdecadal Climate Oscillation with Impacts on Salmon Production. *Bulletin of the American Meteorological Society 78:1069-1079.*

McKenney, D. W., Pedlar, J. H., Lawrence, K., Campbell, K., and Hutchinson, M. F., 2007. Potential Impacts of Climate Change on the Distribution of North American Trees. *Bioscience 57(11):939-948.*

Millers, I., Shriner, D. S., and Rizzo, D., 1989. History of Hardwood Decline in the Eastern United States. *General Technical Report NE-126. U.S. Department of Agriculture, Forest Service, Northeastern Forest Experiment Station, Radnor, Pennsylvania, U.S.A., 75 p.*

Mosseler, A., Lynds, J. A., Major, J. E., 2003. Old-Growth Forests of the Acadian Forest Region. *Environmental Review 11:S47-S77.*

Msadek, R. and Frankignoul, C., 2008. Atlantic Multidecadal Oceanic Variability and its Influence on the Atmosphere in a Climate Model. *Climate Dynamics, published online August 08*

Murphy, J., Kattsov, V., Keenlyside, N., Kimoto, M., Meehl, G., Mehta, V., Pohlmann, H., Scaife, A., and Smith, D., 2009. Towards Prediction of Decadal Climate Variability and Change. World Climate Research Program. *WCC-3 Decadal Climate Variability Session: White Paper.*

Payette, S., Fortin, M-J., and Morneau, C., 1996. The Recent Sugar Maple Decline in Southern Quebec: Probable Causes Deduced from Tree Rings. *Canadian Journal of Forest Research 26:1069-1078.*

Pitelka, L. E., and Raynal, D. J., 1989. Forest Decline and Acidic Deposition. *Ecology 70(1):2-10.*

Phillips David, 1990. The Climates of Canada. Environment Canada. Canadian Government Publishing Centre (Ottawa).

Phillips, B. E., and Laroque, C. P., 2007. Future Radial Growth Forecast for Six Coniferous Species In Southeastern New Brunswick. MAD Lab Report 2007-02. Available at http://www.mta.ca/madlab/2007-02.pdf

Phillips, B. E., and Laroque, C. P., 2008. Expanding on Radial Growth Forecasting: The Potential Future Response of Three Southeastern New Brunswick Tree Species. MAD Lab Report 2008-04. Available at http://www.mta.ca/madlab/2008-04.pdf

Phillips, B. E., and Laroque, C. P., 2009a. Reducing Uncertainty: Acadian Forest Radial Growth Forecasting at a Multi-level Scope. MAD Lab Report 2009-03. Available at http://www.mta.ca/madlab/2009-03.pdf

Phillips, B. E., and Laroque, C. P., 2009b. Climatic Stress Events and Radial Growth Forecasting of *Acer saccharum* Across New Brunswick and Central Nova Scotia, Canada. MAD Lab Report 2009-04. Available at http://www.mta.ca/madlab/2009-04.pdf

Robitaille, G., Boutin, R., and Lachance, D., 1995. Effects of Soil Freezing Stress on Sap Flow and Sugar Content of Mature Sugar Maples (*Acer saccharum*). *Canadian Journal of Forest Research 25:577-587.*

Sperry, J. S., Donnelly, J. R., and Tyree, M. T., 1988. Seasonal Occurrence of Xylem Embolism in Sugar Maple (*Acer saccharum*). *American Journal of Botany 75(8):1212-1218.*

Stokes, M. A., and Smiley, T. L., 1968. An Introduction to Tree-Ring Dating. University of Arizona Press, Tucson.

St.Clair, S. B., Sharpe, W. E., and Lynch, J. P., 2008. Key Interactions between Nutrient Limitation and Climatic Factors in Temperate Forests: a Synthesis of the Sugar Maple Literature. *Canadian Journal of Forest Research 38:401-414.*

Sutton , R. T., and Hodson, D. L. R., 2005. Atlantic Ocean forcing of North American and European summer climate. *Science 309:115–118.*

Tardif, J., Brisson, J., and Bergeron, Y., 2001. Dendroclimatic Analysis of *Acer saccharum*, *Fagus grandifolia*, and *Tsuga canadensis* from an Old-growth Forest, Southwestern Quebec. *Canadian Journal of Forest Research 31:1491-1501.*

Taylor, K. E., Stouffer, R. J., and Meehl, G. A., 2008. A Summary of the CIMP5 Experiment Design. 12th Session of the JSC/CLIVAR Working Group on Coupled Modelling

Walker, S. L., Auclair, A. N. D., and Marin, H. C., 1990. History of Crown Dieback and Deterioration Symptoms of Hardwoods in Eastern Canada, Parts I, II and III. *Environment Canada,*

Atmospheric Environment Service, Federal LRTAP Liaison Office. Downsview, Ontario, Canada, 561 p.

Williams, C.N., Jr., Menne, M.J., Vose, R.S., and Easterling, D.R., 2006. United States Historical Climatology Network Daily Temperature, Precipitation, and Snow Data. ORNL/CDIAC-118, NDP-070. Available on-line [http://cdiac.ornl.gov/epubs/ndp/ushcn/usa.html] from the Carbon Dioxide Information Analysis Center, Oak Ridge National Laboratory, U.S. Department of Energy, Oak Ridge, Tennessee.

van Mantgem, P.J., Stephenson, N.L., Byrne, J.C., Daniels, L.D., Franklin, J.F., Fulé, P.Z., Harmon, M.E., Larson, A.J., Smith, J.M., Taylor, A.H., and Veblen T.T., 2009. Widespread Increase of Tree Mortality Rates in the Western United States. *Science 323:521-524.*

Vasseur, L., and Catto, N., 2008. Atlantic Canada; *in* From Impacts to Adaptation: Canada in a Changing Climate 2007. *Edited by* D.S. Lemmen, F.J. Warren, J. Lacroiz and E. Bush; Government of Canada, Ottawa, ON, p. 119-170.

Vincent, L.A., and Gullett, D.W., 1999. Canadian Historical and Homogeneous Temperature datasets for climate change analyses. *International Journal of Climatology 19:1375-1388.*

Vincent, L.A., and Gullett, D.W., 2002. Homogenization of Daily Temperatures over Canada. *Journal of climate 15:1322-1334.*

Yin, X., and Arp, P. A., 1994. Tree-Ring Based Growth Analysis for a Sugar Maple Stand: Relations to Local Climate and Transient Soil Properties. *Canadian Journal of Forestry Research 24:1567-1574.*

Zelazny, V. F., Martin, G. L., Toner, M., Gorman, M., Colpitts, M., Veen, H., Godin, B., McInnis, B., Steeves, C., Wuest, L., and Roberts, M. R., 2003. Out Landscape Heritage: the Story of Ecological Land Classification in New Brunswick. *Ecosystem Classification Working Group. New Brunswick Dept. of Natural Resources.*

Zhu, X. B., Cox, R. M., Bourque, C.-P. A., and Arp, P. A., 2002. Thaw Effects on Cold-Hardiness Parameters in Yellow Birch. *Canadian Journal of Botany 80: 390-398.*